UNITED NATIONS UNIVERSITY

UNU-GTP
Geothermal Training Programme

ORKUSTOFNUN

Blési hot spring at Geysir geothermal field

Peter Kiranga Mbia

SUB-SURFACE GEOLOGY, PETROLOGY AND HYDROTHERMAL ALTERATION OF MENENGAI GEOTHERMAL FIELD, KENYA

Report 1
December 2014

UNITED NATIONS UNIVERSITY
UNU-GTP
Geothermal Training Programme

GEOTHERMAL TRAINING PROGRAMME
Orkustofnun, Grensásvegur 9,
IS-108 Reykjavík, Iceland

Reports 2014
Number 1

SUB-SURFACE GEOLOGY, PETROLOGY AND HYDROTHERMAL ALTERATION OF MENENGAI GEOTHERMAL FIELD, KENYA

MSc thesis
School of Engineering and Natural Sciences
Faculty of Earth Sciences
University of Iceland

by

Peter Kiranga Mbia
Geothermal Development Company Ltd. - GDC
P.O. Box 17700-20100
Nakuru
KENYA
pmbia@gdc.co.ke, mbiapeter@gmail.com

United Nations University
Geothermal Training Programme
Reykjavík, Iceland
Published in April 2014

ISBN 978-9979-68-339-1
ISSN 1670-7427

This MSc thesis has also been published in April 2014 by the
School of Engineering and Natural Sciences, Faculty of Earth Sciences
University of Iceland

INTRODUCTION

The Geothermal Training Programme of the United Nations University (UNU) has operated in Iceland since 1979 with six month annual courses for professionals from developing countries. The aim is to assist developing countries with significant geothermal potential to build up groups of specialists that cover most aspects of geothermal exploration and development. During 1979-2014, 583 scientists and engineers from 58 developing countries have completed the six month courses, or similar. They have come from Asia (37%), Africa (36%), Central America (15%), Europe (11%), and Oceania (1%) There is a steady flow of requests from all over the world for the six-month training and we can only meet a portion of the requests. Most of the trainees are awarded UNU Fellowships financed by the Government of Iceland.

Candidates for the six-month specialized training must have at least a BSc degree and a minimum of one year practical experience in geothermal work in their home countries prior to the training. Many of our trainees have already completed their MSc or PhD degrees when they come to Iceland, but several excellent students who have only BSc degrees have made requests to come again to Iceland for a higher academic degree. From 1999 UNU Fellows have also been given the chance to continue their studies and study for MSc degrees in geothermal science or engineering in co-operation with the University of Iceland. An agreement to this effect was signed with the University of Iceland. The six-month studies at the UNU Geothermal Training Programme form a part of the graduate programme.

It is a pleasure to introduce the 36th UNU Fellow to complete the MSc studies at the University of Iceland under the co-operation agreement. Peter Kiranga Mbia, BSc in Geology, from Geothermal Development Company - GDC, completed the six-month specialized training in Borehole Geology at the UNU Geothermal Training Programme in October 2010. His research report was entitled: *Borehole geology and hydrothermal alterations of well HE-39, Hellisheidi geothermal field, SW-Iceland.* After two years of geothermal research work in Kenya, he came back to Iceland for MSc studies at Faculty of Earth Sciences in August 2012. In April 2014, he defended his MSc thesis presented here, entitled *Sub-surface geology, petrology and hydrothermal alteration of Menengai geothermal field, Kenya*. His studies in Iceland were financed by the Government of Iceland through a UNU-GTP Fellowship from the UNU Geothermal Training Programme. We congratulate him on his achievements and wish him all the best for the future. We thank the Faculty of Earth Sciences at the School of Engineering and Natural Sciences of the University of Iceland for the co-operation, and his supervisors for the dedication.

Finally, I would like to mention that Peter´s MSc thesis with the figures in colour is available for downloading on our website *www.unugtp.is*, under publications.

With warmest greetings from Iceland,

Ludvik S. Georgsson, director
United Nations University
Geothermal Training Programme

ACKNOWLEDGEMENTS

I sincerely thank the United Nations University, Geothermal Training Programme (UNU-GTP) for providing me with full scholarship of this study, my employer Geothermal Development Company (GDC), for granting leave to undertake this study and allowing me to use data from wells. I would also like to thank the University of Iceland and Iceland GeoSurvey (ÍSOR) for providing me with the necessary access to facilities and training required for successful completion of this study.

I'm particularly indebted to my advisors: Anette K. Mortensen, Björn S. Hardarson and Níels Óskarsson, for their enthusiasm, encouragement, numerous valuable discussions, input, critical comments and guidance during the study period. Special thanks also go to Hjalti Franzson for his helpful suggestions and discussion on various aspects of this work. I would like to thank the entire UNU-GTP and ÍSOR GeoSurvey staff, special thanks go to the Director, Mr. Lúdvik S. Georgsson, Ingimar, María, Thórhildur, Málfríður, Markús, Rósa, Steinthór, Signý and Sigurdur, for their personal and technical support. I am grateful to my colleagues at Geothermal Development Company for their effort during data collection and the support they have given me all along. I'm also grateful to my fellow master students for the quality time we spent together during my study.

Finally I'm indebted to my wife Julie, my daughter Lynette and my two sons, Lewis and Alpha, for enduring my absence, love, encouragement and prayers during this session. God made all this possible, glory to His holy name.

DEDICATION

This work is dedicated to my wife Julie, for her tolerance and accepting to be the mother and the father of my children during the course of my studies.

ABSTRACT

Menengai is a trachytic central caldera volcano in the Kenya rift valley with abundant high-temperature geothermal activity. The field is currently in its initial stages of development for geothermal energy in Kenya following Olkaria and Eburru fields. Regional surface geology of Menengai is largely composed of late Quaternary volcanics. The building of a 200,000 year old trachyte shield volcano was followed by piecemeal subsidence through two paroxysmal eruptions 29,000 and 8,000 B.P to produce a caldera of about 84 km^2 in size that has subsequently been largely filled by recent trachyte lavas. Twenty four exploration and production wells, some of them hotter than 390°C, have been drilled in Menengai caldera by Geothermal Development Company (GDC). The aim of this study is to reveal the evolutionary history of the Menengai volcano and to describe its igneous lithostratigraphy and secondary mineralization in order to characterize hydrothermal processes within the field. Analytical methods used include binocular microscope analysis, petrographic analysis, X-ray diffractometer analysis and inductively coupled plasma (ICP-ES) analysis. Studies of drill cutting from wells MW-02, MW-04, MW-06 and MW-07 have provided information on the stratigraphy, hydrothermal alteration and present state of the geothermal system. Petrochemistry of these wells revealed subsurface lithostratigraphy that includes, consolidated pyroclastic tuff, pyroclastics, basalt, trachybasalt, phonolite, trachy-andesite, syenitic intrusive units, while trachyte constitutes over 90% of the total.

Reaction of geothermal fluids with the host rocks has resulted in a progressive hydrothermal alteration with increasing depth. A number of studies have recognized characteristic alteration zones at Menengai based on distribution of key index alteration minerals. These zones, in order of increasing alteration grade, are zeolite-smectite, quartz-illite and wollastonite-actinolite zone. The study reveals that Menengai evolved a complex compositional variation with time as a result of magma fractionation, possibly in combination with crustal contamination and hydrothermal activities en route to the surface. The study defines the geology of the Menengai into, post-caldera, syn-caldera, upper and lower pre-caldera volcanics. Petrography and mineral chemistry of the basaltic and trachytic end members of the Menengai rocks indicate that two or more distinct magma types were involved in the formation of the volcano.

This study reveals that magma exists beneath the caldera floor, at depth slightly over 2000 m within the summit area. This is evidenced by fresh glassy, quenched cuttings at these depths in wells MW-04 and MW-06. This implies that the thickness of the geothermal reservoir above the magma-containing domain may be no more than 1.5 km from the hydrostatic surface at ~400 m.

TABLE OF CONTENTS

Page

Page

LIST OF FIGURES

LIST OF TABLES

ABBREVIATIONS

GDC	Geothermal Development Company
EARS	East African Rift System
TVA	Tectono-volcanic axis
KRVS	Kenya Rift Valley System
ISOR	Iceland GeoSurvey
ICP-ES	Inductively Coupled Plasma - Emission Spectrometry
XRD	X-ray diffraction analysis
Ppm	Parts per million

1. INTRODUCTION

Menengai caldera volcano (centre at 35° 04'E, 0° 12'S) is located on the floor of the Kenya rift valley (Figures 1 and 2). It is one of seven late Quaternary caldera volcanoes in the inner trough of the Kenya rift valley, which are associated with a high thermal gradient as a result of shallow intrusions (Figure 1). Other volcanoes within the rift, from north to south include Barrier, Emuruangogolak, Silali, Paka, Korosi, Longonot and Suswa; all of which are associated with geothermal activity.

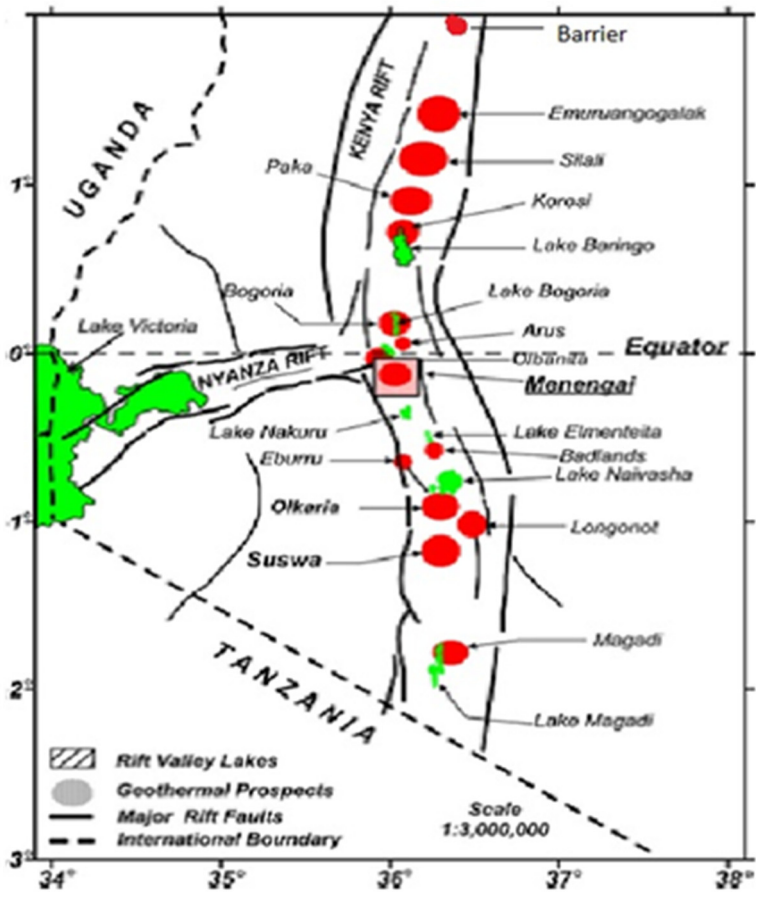

FIGURE 1: Location of the Menengai geothermal prospect and other prospects along the Kenya Rift Valley (GDC, 2010)

Menengai volcano is located some 24 km south of Equator and about 10 km north of Nakuru town. The caldera is a prominent geographical feature on the rift floor and its presence was noted as early as 1894 by travellers but first studied in details by McCall (1957a, b, 1964, 1967). The caldera is partially filled by young rugged lava flows. Nakuru area lies at elevations between 1560 m and 2260 m above sea level and is characterized by rather flat topography, as a result of filling of the rift by volcanic rocks, and flattening topography by ignimbrites and other pyroclastic deposits locally covering faulting and differential uplift (e.g. KRISP working group, 1987; Leat, 1991). The eastern shoulder of the inner trough rises some 600 m higher and forms the Bahati platform and the western shoulder forms the Mau plateau.

The Menengai volcano is young and was formed about 200,000 years ago with the growth of 30 km^3 volume lava shield (Leat, 1983). It forms part of the central Kenya peralkaline province, which is characterised by its unique assemblage of peralkaline salic magmatic systems (e.g. Macdonald and Baginski, 2009; Macdonald and Scaillet, 2006). The building of a trachyte shield volcano was followed by piecemeal subsidence to produce, about 84 km^2 large caldera. Menengai caldera has been largely filled by younger-well preserved trachyte lavas, of post-caldera time (Jones and Lippard, 1979; Leat, 1983).

Menengai volcano is currently in its initial stages of development for geothermal energy in Kenya by Geothermal Development Company - GDC. This is the third geothermal field to be developed in Kenya following Olkaria and Eburru fields, which have been developed by KenGen. Geothermal Development Company (GDC), began drilling in the Menengai in early 2011, and by April 2014, 24 wells have been completed although, several wells were temporally abandoned without reaching target depths due to drilling problems. The drilling is on-going at the time of research with four GDC drill rigs. The original drilling design of the Menengai wells by Geothermal Development Company (GDC) was to reach depths of 3000 m in all wells, but that has not been possible due to shallow magma proximity and unstable conditions in the central part of the field, which has caused the drill-bits to become stuck and has constricted most wells at ~2100-2200 m depth. In the upper sections of the wells, fresh, fractured and

hard post-caldera lava have caused many drilling problems such as rig vibration and time needed to heal fluid losses with concrete plugs.

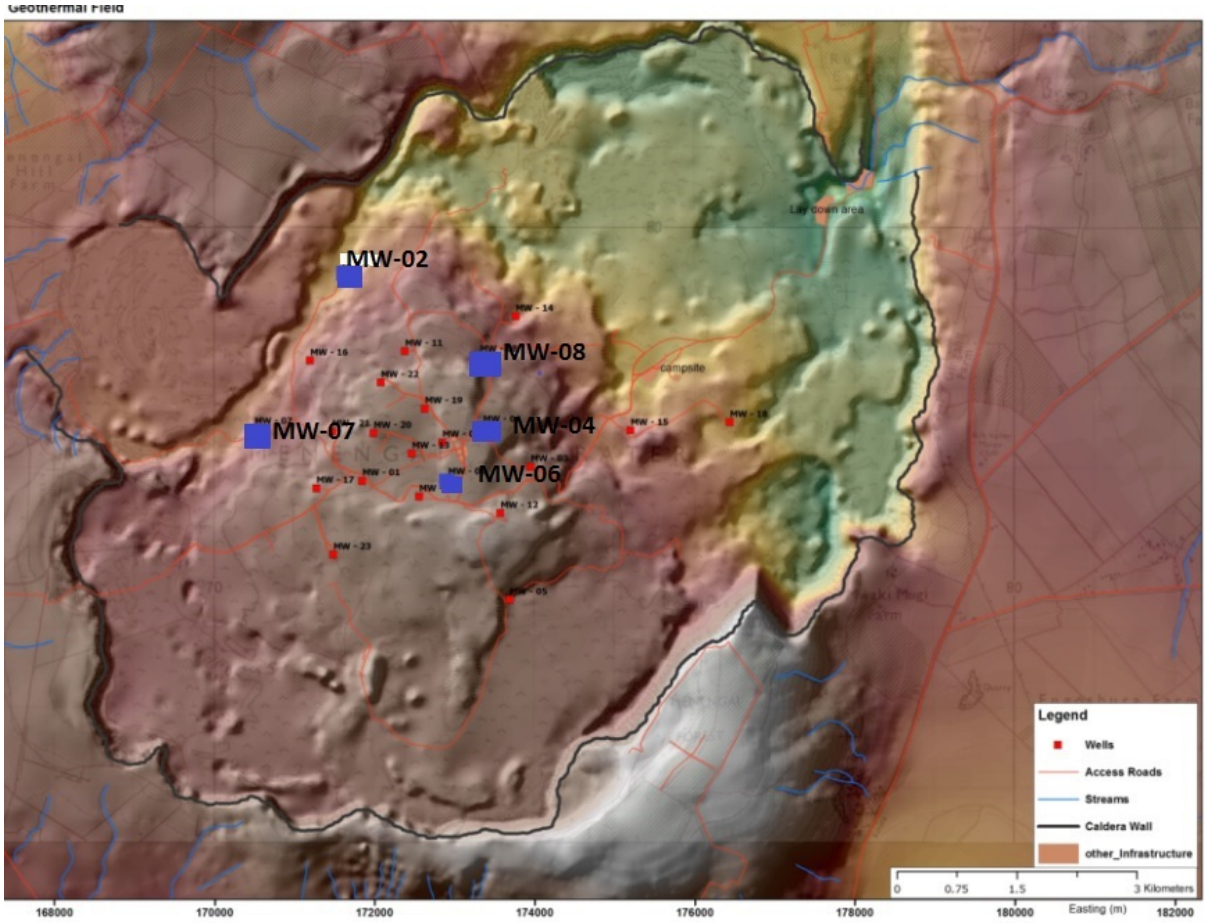

FIGURE 2: Menengai caldera showing study wells as blue and other drilled wells in red (GDC, 2013)

The geothermal system in the Menengai provides good opportunities for studying high-temperature fluid-rock interaction in a hydrothermal system. In this study four wells, MW-02, MW-04, MW-06 and MW-07, in the Menengai geothermal field, were used to study the extent of hydrothermal processes within different strata of the wells. However, selected samples from well MW-08 were also used for petrological studies. Leat (1983) in his PhD work, studied the structural and geochemical evolution of the Menengai caldera using surface data. The current geothermal wells make it possible to study the petrology and hydrothermal history at depth using the cuttings from these wells with the aim of defining the subsurface conditions and evolution of the Menengai caldera.

In investigating the geochemical characteristics of the Menengai rocks, the fundamental objectives were to outline the petrogenesis of the primary magma group and also outline differentiation in the primary magma. The study aimed at describing lithostratigraphy within and below the caldera filling and define the hydrothermal processes that created the secondary mineralization within the Menengai field. The study also aim at updating the geological conceptual model of the Menengai field based on the findings of this research.

2. GEOLOGY

Menengai is, largely composed of silica-saturated, peralkaline trachyte, which were believed to be erupted in recent times within the caldera. Leat (1984) divided the exposed rock units in the Menengai into pre-caldera, syn-caldera and post-caldera volcanics (Figure 3). Tectonically, Menengai is divided into two systems; the Ol'rongai, which has north-northwest trending faults and is older than the north-northeast trending Solai system (Figures 3 and 4).

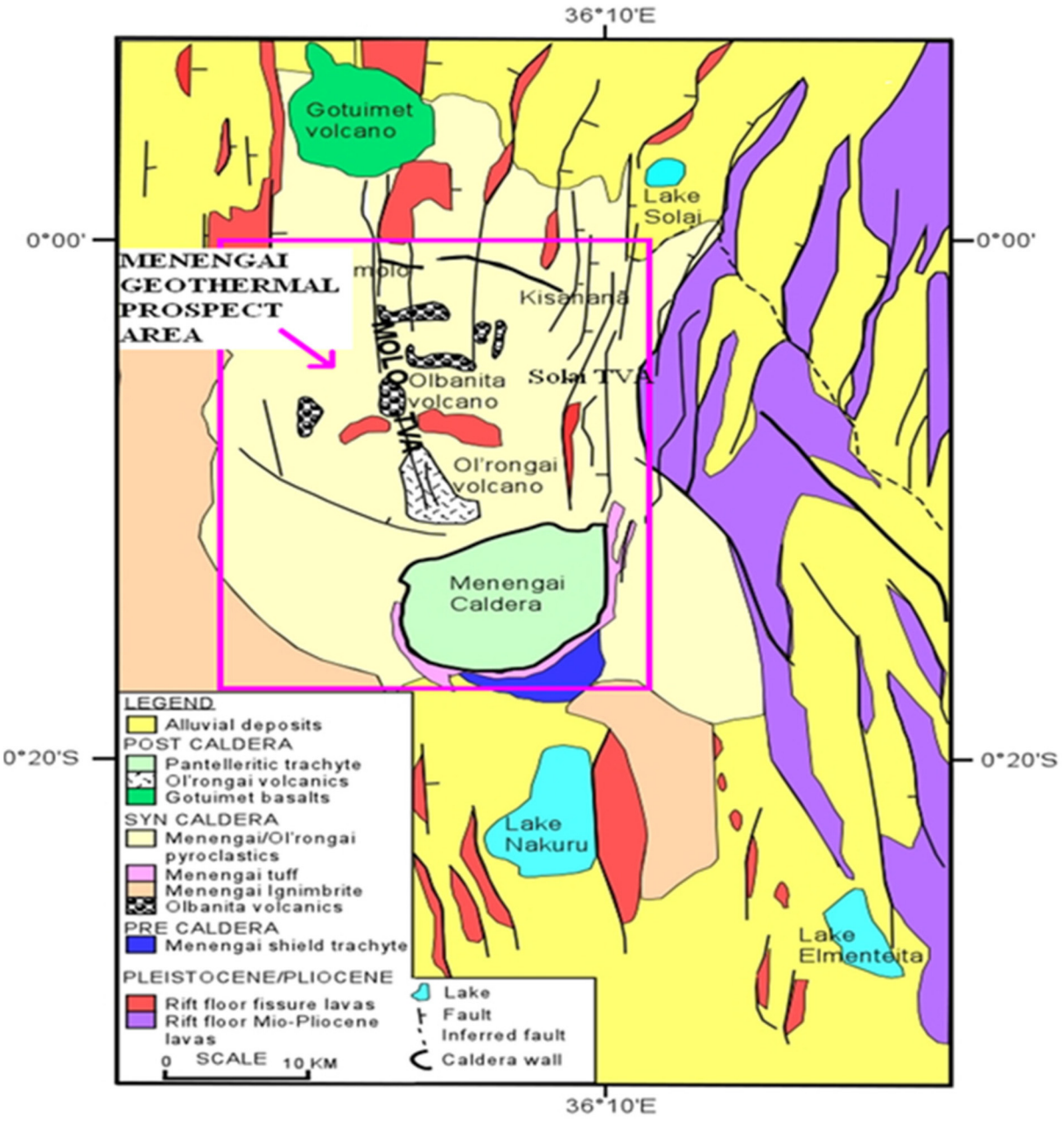

FIGURE 3: Geological map of the Menengai area and surroundings (GDC, 2010)

In his surface geological mapping of the entire area, Leat (1984) recognized that post-caldera lavas are located on the floor of the Menengai caldera. Doming at the caldera centre was assigned to on-going magmatic intrusive activity at depth. It has been argued that the caldera collapse occurred as piecemeal, or Krakatau-style and the Menengai is regarded as one of the best preserved Krakatau-style calderas in the world (Leat, 1983, 1984; Macdonald et al., 2011; McCall, 1967). The only major post-caldera modification has been the eruption of lavas on the caldera floor. Two periods of caldera collapse have been recognized, with each accompanied by the eruption of an ash-flow tuff, preceded by air-fall pumices, and both emplaced as single flow units (e.g. Leat, 1984; Macdonald, 1974).

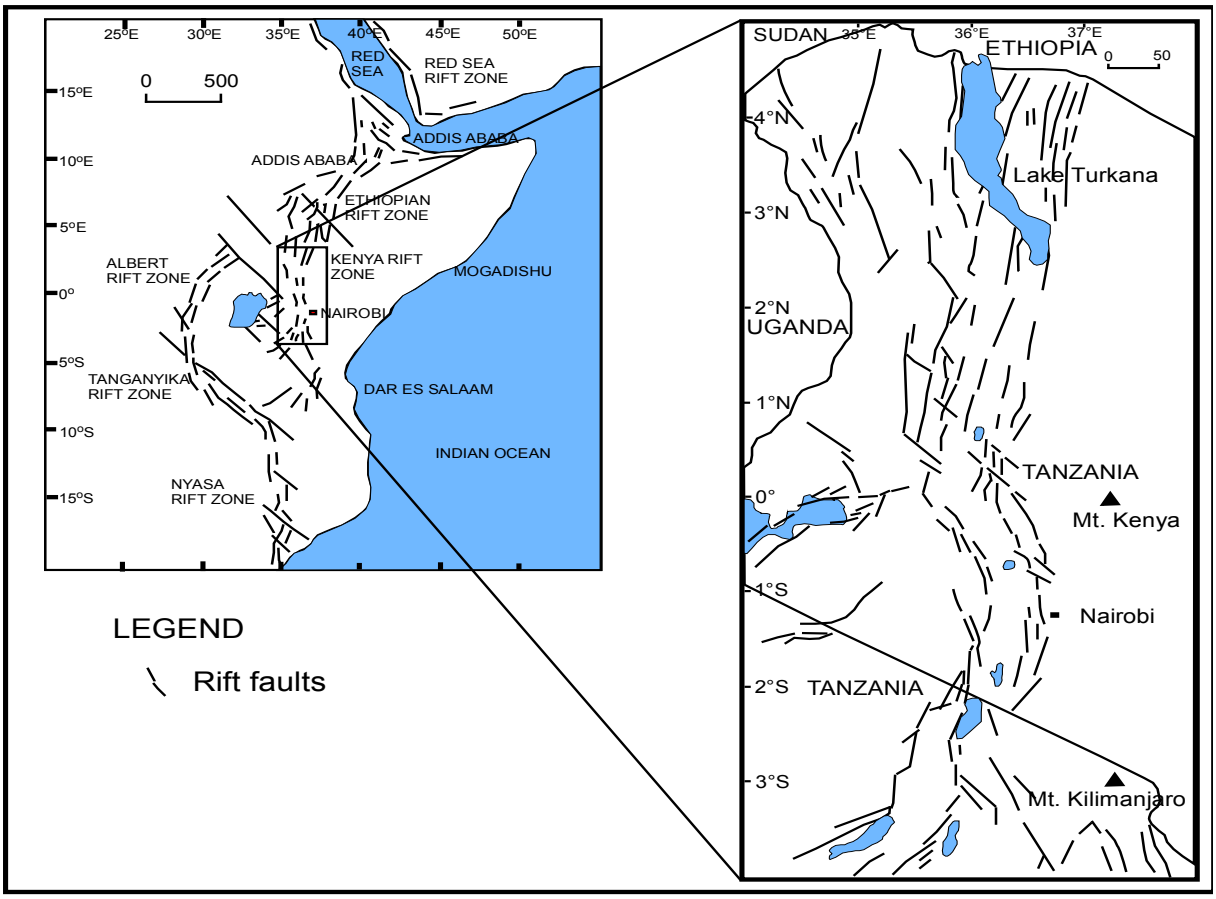

FIGURE 4: Map showing the Kenya rift zone within the East African Rift System (modified from Dunkley et al., 1993)

2.1 Geological setting

2.1.1 Regional geology

The regional surface geology of the Menengai is largely composed of late Quaternary volcanics, which are associated with the development of the Kenya Rift (Figures 1 and 3). The area north of the Menengai is characterized by lavas from N-S trending fissures (e.g. Macdonald et al., 2011; Leat, 1984). These lavas are trachytic and trachy-phonolitic in composition and mainly observed to be exposed in the scarp walls beyond the Olbanita swamps, Lomolo and Kisanana areas (e.g. GDC, 2010; Jones, 1985; Leat, 1983) (see Figure 3). They underlie ignimbrites and pyroclastics probably originating from the Menengai eruptions to the south.

The Pliocene eruptions that followed the Miocene volcanics and the subsequent faulting are divided into four principal phases (Baker et al., 1988). These phases were coupled with faulting episodes, during which time most of the structural features of Menengai evolved. The first phase was the wide-spread Mau-Kinangop tuff/ ash flows, (3.7-3.4 Ma). Major faulting occurred following the ignimbrite (tuff/ash) eruptions, which converted an earlier half graben to a graben. The second phase was the eruption of the Limuru flood trachytes (2.0-1.8 Ma), which was initiated by the progressive inward migration of the fault zones. This migration resulted in the formation of step-faulted platforms (Mau escarpments) and the fissure eruptions of the Limuru trachyte flood lavas (Baker et al., 1988). Basalt and basaltic trachy-andesite form the third and fourth phases, respectively (1.65-0.9 Ma). These last two phases were triggered by faulting that followed the eruption of the Limuru flood trachytes. The faulting was triggered by a hotspot resulted in the uplift of the region, opening up fractures, which served as conduits for Quaternary volcanic activity and the development of many large shield volcanoes of silicic composition along the axis of the rift (Baker et al., 1988).

2.1.2 Tectonic and geological setting of the East African rift valley

The East African Rift System (EARS) is undoubtedly the largest, presently active, intracontinental rift, with significantly greater volumes of volcanic products than any other recently active rifts of similar nature. It forms a divergent plate boundary, where the African plate is splitting into the Nubian and Somali protoplates and has undergone massive volcanism from the Late Tertiary to Recent (Figure 5). It extends more than 5,000 km from the Gulf of Aden to Mozambique (Leat, 1983; Macdonald, 2002; Omenda, 1997) and is in the process of splitting the African plate into two at a rate of about 6-7 mm annually in the north. The rate decreases to south, to about 1.9 mm annually (Fernandes et al., 2004).

FIGURE 5: Location of the Menengai caldera volcano within the central Kenya peralkaline province. Menengai, Longonot and Suswa are trachytic caldera volcanoes, whereas Eburru and Olkaria are rhyolitic dome fields. The Akira Plains Field contain peralkaline rhyolites and trachytes in addition to basalt (from Macdonald et al., 2011).

The Kenyan rift is a volcano-tectonic feature that transects the country extending from Lake Turkana in the north to Lake Natron in the south (Rogers et al., 2000). It forms a classic graben structure, which is on average 40-80 km in width. Mohr (1982) estimated that the volume of volcanic rocks in the East African Rift in Kenya and Ethiopia alone to be 500,000 km^3, compared to 12,000 km^3, in the Rio Grande Rift of western USA and 5,000 km^3 in the Baikal rift. Volcanism in the rift started 35-30 Ma in the Turkana region of northern Kenya. This was followed by normal faulting and extension, estimated currently to be 35-40 km (e.g. Rogers et al., 2000). Since its inception, magmatism has subsequently propagated southwards with time, reaching northern Tanzania at 5-8 Ma (Macdonald, 2002). The spreading of the Rift valley resulted in thinning of the crust and is associated with several episodes of lava eruptions and tectonic activities. Structure-controlled evolution of the East African Rift system, involves faults exploiting the weak collision zones at the contact between the Archean Tanzania craton and the Proterozoic Orogenic belt (Smith and Mosley, 1993). According to Rogers et al. (2000), magma volumes and geochemistry of mafic volcanic rocks imply that magmatism has resulted from interaction of lithosphere with melts and/ or fluids from one or more mantle plumes.

The volcanic and structural development of the Kenya Rift has been studied for many years using chronologic and litho-stratigraphic correlation methods (e.g. Baker et al., 1972; Baker and Wohlenberg,

1971; Chorowiz, 2005; Dunkley et al., 1993; Fairhead, 1976; Nick et al., 2000; Omenda, 2012, 1993; Omenda et al., 1993; Riaroh and Okoth, 1994; Smith and Bailey, 1968; Thompson and Dodson, 1963). Fairhead (1976) supported the idea that the rift system is a tensional feature probably representing an initial stage of continental break-up. The E-W tensional forces, which characterize the Kenya Rift, resulted in block faulting, which includes tilted blocks as evidenced in both the floor and escarpments of the rift. All these studies have confirmed that the rift-related activities started during the early Miocene with extensive basaltic and phonolitic volcanism on the crest of an uplifted dome (Figure 4).

The voluminous magmatism in the rift implies the presence of either elevated asthenospheric temperatures or easily fusible mantle lithosphere or both (Omenda, 1997; Simiyu et al., 1997). The African plate has migrated steadily north-eastwards over the past 50 Ma, relative to the hot spot reference frame (Rogers et al., 2000). However, the temporal migration of magmatism from north to south is probably more easily reconciled with the slow northward drift of the African plate over the Kenyan plume (Corti, 2011; Rogers et al., 2000). The anomalous uplift and the occurrence of local widespread volcanism prior to rift initiation indicates that the rifting in East Africa is associated with the thermal and dynamic consequences of mantle plumes acting at the base of the lithosphere (Corti, 2011).

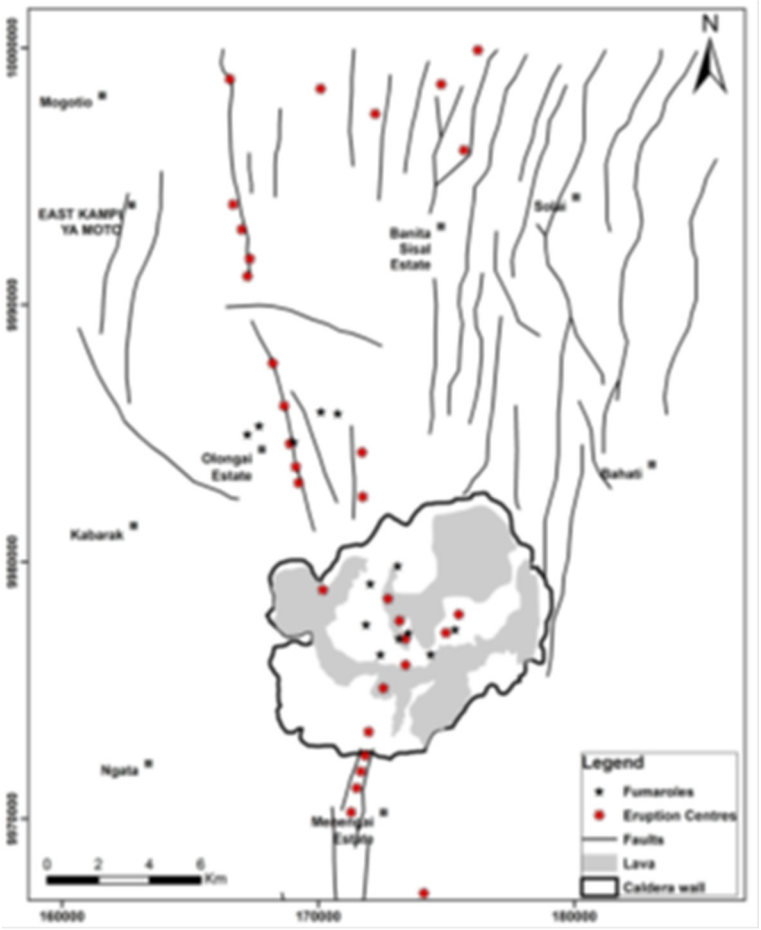

FIGURE 6: Location of fumaroles and eruption centres in the Menengai geothermal field (GDC 2010).

During the Quaternary, eruptions of transitional basalts, trachytes, and rhyolites have been the most common along the rift axis, and they are associated with central volcanoes (Figure 6). The distribution of the Quaternary lavas associated with rifting have been used to infer the tectonic evolution of the Kenya Rift (Omenda, 1997).

2.1.3 Local geology

Rocks exposed at the surrounding of the Menengai area are mainly the Menengai massif building lavas (pre-caldera formations), the pyroclastics that accompanied the caldera collapse (syn-caldera) and glassy lavas that erupted after the collapse (post-caldera) (e.g. GDC, 2010; Leat, 1984). The pre-caldera volcanics are mainly exposed beneath the caldera cliff and comprise several layers of lava flows. Leat (1983) estimated that, around the Lion Hill cliff, at the southeast caldera rim, layers of lava flows totalling a thickness of over 300 m are exposed. These lavas are mainly trachytic with over 95% of them containing sanidine crystallites with riebeckite/arfvedsonite in small amounts. Large (up to a meter) and small lithic inclusion of syenitic rocks are common. The pre-caldera lavas have been dated to be about 0.18±0.01 Ma (Leat, 1983).

The syn-caldera rocks are spread around the Menengai caldera and comprise ignimbrite and pumice/ash deposits. The ignimbrite is exposed both at the upper parts of the caldera rim (eastern and northern rim), where it resembles agglomerate deposits rich in poorly sorted angular lithic and glassy/semi-pumiceous material that shows rheomorphic texture indicative of pyroclastic flow emplacement (e.g. Macdonald et al., 2011). This is the proximal phase indicating that the source was at the Menengai caldera and its rim.

Other exposures away from caldera rim include extensive mantling of the ground in the north and west (Kampi ya moto, El bonwala and Ol'rongai areas (Figure 3). According to Leat (1983), the syn-caldera ignimbrite deposits formed through two caldera forming eruptions. The first eruption took place about 29,000 years ago and produced a large caldera. The second period of collapse occurred at ~8,000 years ago, with the formation an 11.5x7.5 km present-day summit caldera associated with a huge amount of compositionally zoned per alkaline trachyte and the second fall-ash flow tuff sequence. The tuff represented some 30 km^3 of magma.

The stratigraphy of the fall-ash flow tuff deposits was described by Leat, (1985, 1984). Macdonald et al., (1994) describe details of thickness, degree of welding, clasts content, and distribution of the ash. Like the first ash flow tuff, the younger tuff is inferred to have been erupted from a compositionally zoned magma chamber, with strong roof-ward enrichment in Mn, Fe, Na and depletion in Al, Mg, Ca, K, Ti, P and Ba, corresponding to pantelleritic trachyte at the top, grading down through comenditic trachyte to more primitive, Ba-rich trachyte which corresponds with upper pre-caldera volcanics (Figure 18).

Leat (1984) suggested that, the growth of the lava shield was truncated, at about 29 ka, by a period of caldera collapse, accompanied by the eruption of an ash flow tuff, preceded by pumice falls. The ash flow tuff had a volume of 20 km^3 and was erupted as a single flow unit. Leat et al., (1984) further argued that this ash tuff was compositionally zoned; the earliest erupted products were pantelleritic trachyte.

Post-caldera strata are mainly composed of lavas on the caldera floor in addition to minor eruption centres to the southwest of the volcano. The post-caldera eruptions may have been preceded by explosive episodes producing ash and pumice products found in the caldera floor. This episode probably occurred both inside the caldera and at Ol'rongai simultaneously (e.g. Leat and Macdonald, 1984). These lavas have built a thick pile inside the caldera rising to 2160 m a.s.l. More than 70 post-caldera lava flows cover the caldera floor, the youngest being only a few hundred years old (Leat, 1984). The dated post caldera lavas gave an age of 1,400 years BP (Jones and Lippard, 1979), though the youngest might be assumed to be a few hundred years old according to their pristine nature (e.g. Leat, 1984). The lavas are dark holocrystalline or glassy vesicular rocks. The ropy flow texture is still intact, indicating the young age and the low viscosity of the lavas. Mineral composition is mainly composed of sanidine feldspar with occasional riebeckite (Jones, 1981).

Intra-caldera lake sediments of diatomaceous earth and well bedded pumiceous sands with rounded pebbles in the north-eastern part of the caldera floor are probably indicative of prehistoric existence of shallow fresh water lakes. Leat (1984) suggested, that they were formed as a result of overflow from the 'Gamblian' lake into the caldera through the SE graben and partly through underground channels, along joints and through tephra and soil horizons, but the lake sediments are estimated to be formed between 10,300 to 8,300 years BP.

2.1.4 Subsurface geology

Studies of drill cutting from the Menengai have provided important information on the stratigraphy, hydrothermal alteration and state of the geothermal system (e.g. Kipchumba, 2013; Lopeyok, 2013; Mibei, 2012; Omondi, 2011). Chemical analyses of the present study have revealed that the subsurface lithostratigraphy include trachytes, trachy-phonolites, tuff, pyroclastics, basalt, trachybasalt, phonolites, trachy-andesites and syenitic intrusives. Reaction of geothermal fluids with the host rocks in Menengai has resulted in a progressive hydrothermal alteration sequence with increasing depth. Previous studies have recognized characteristic alteration zones at the Menengai based on distribution of key index minerals. Post-, syn- and pre-caldera volcanics and lake sediments completely cover the contact between the volcanics of the Menengai and its underlying basement formations.

2.1.5 Geothermal manifestations

The apparent signatures of geothermal potential include the young volcanism represented by numerous recent eruptions both inside and outside the caldera, the caldera collapse and intense tectonics movements resulting in the intense faults marking the area north of the Menengai caldera. Other geothermal surface manifestations in the Menengai and its surroundings occur as hot grounds,

fumaroles, warm temperature boreholes and altered grounds. These manifestations are confined within the caldera, along the tectonovolcanic axes and other faults (Mungania, 2004). Several vents and most fumaroles are scattered on the caldera floor in apparently random fashion (Figure 6). These vents are probably sited on fractures which cut across the cauldron block. The fractures were probably formed during caldera collapse and indicate that during caldera collapse, the cauldron block broke into many smaller blocks, separated by faults.

The two groups of fumaroles in the central and western parts of the caldera floor are located within a fresh lava flows and close to eruption centres (Figure 6). The other group of fumaroles, located in the central eastern part of the caldera floor, is found at the young lava/pumice contact and has extensively altered the pumiceous formation. The structural control for these groups of fumaroles appears to be related to the eruption craters which may be the source of the pyroclastic deposits.

2.2 Structural geology of Menengai

Structurally, Menengai is a pre-caldera low-angle volcanic shield, which has almost vertical embayed caldera walls up to 300 m high (Leat, 1983; Macdonald, 2002). The floor of the area depicts extensional tectonics with spatial variation in the stress field, indicated by two main orientations of fault systems. Leat (1984), found that the structures associated with Ol'rongai Tectono-volcanic axis are oriented to the NNW-SSE and are related to the NW-SE pre-caldera orientation. However faults associated with the Solai TVA system have NNE-SSW orientation, which corresponds to the orientation of the Menengai caldera.

2.2.1 The Menengai caldera and ring faults

The Menengai caldera is an elliptical depression with major and minor axes measuring about 11.5 km and 7.5 km respectively (e.g. GDC, 2010; Leat, 1983). The circular rim of the caldera ring fault is well preserved with vertical cliff. The ring structure has only been disturbed by the Solai graben faults at the northeast end of the caldera and at the south-southwest end (Figure 7).

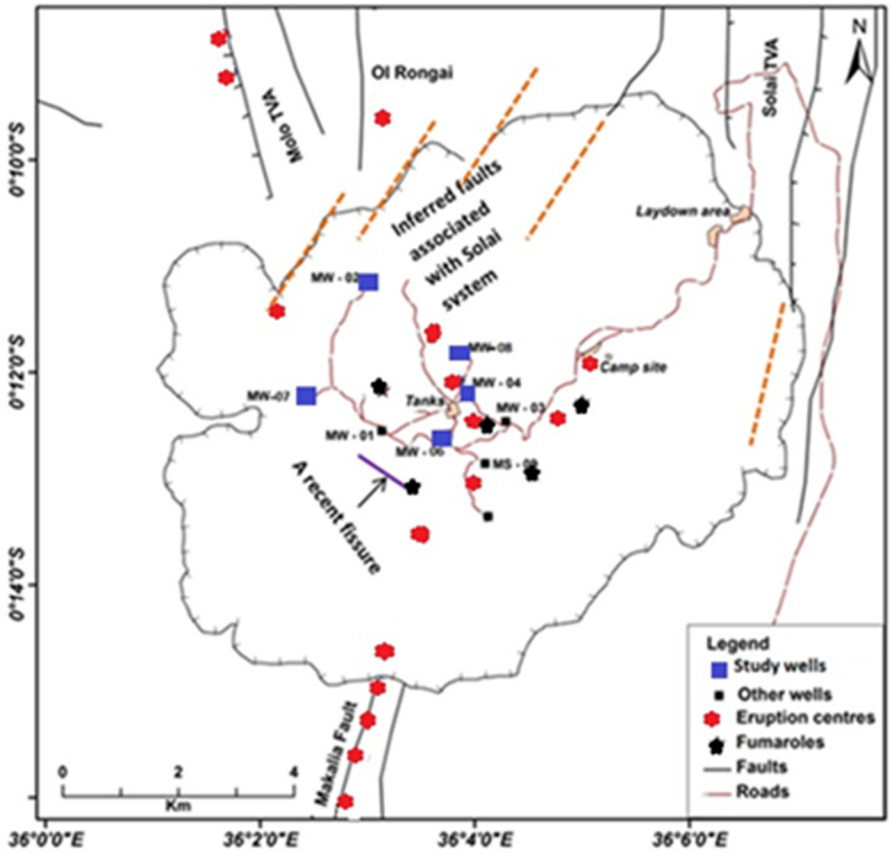

FIGURE 7: Structural map of the Menengai area (modified from GDC, 2010)

The caldera floor is covered with lavas such that it is not possible to estimate the collapse depth or any structures that may be marking the caldera floor. Several vents are situated close to the caldera wall. The position of these vents was probably controlled by the ring fracture of the caldera; the magma came up through the caldera fault. Ring fracture volcanism is a common feature of caldera for example, in Longonot caldera, few km south of the Menengai caldera (Leat, 1983).

2.2.2 The Ol'rongai and Molo tectono-volcanic axis (TVA)

The Molo tectono-volcanic axis (TVA) is a prominent volcano-structural feature, represented on the surface by a zone concentrated with faults and fractures along which volcanic eruptions took place in the early Pleistocene. (Geotermica Italiana, 1987). The Ol'rongai structural system (Figure 7) represents a part of the larger Molo TVA that has experienced significant volcanic activity, which resulted in a build-up of a NNW-SSE trending ridge referred to as the Ol'rongai volcanoes. In the Ol'rongai area, the structure is marked by intense volcanic activity including an explosive crater. The surface expression of this volcano has been significantly eroded, possibly by ponding of volcanic materials from Menengai volcano, erosion and sedimentation. However, gravity highs are present in this area and could reveal the roots or plugs that are remnants of an old magma chamber (Simiyu and Keller, 1997). Leat (1984) argued that the Menengai pre-caldera shield had the same orientation as the NNW-SSE structures and was influences by these faults. The Ol'rongai faults are therefore older than the Solai system which cut the caldera. On a regional scale, the Ol'rongai system extends northwards through Lomolo and past the Gotuimet volcanic centre (Leat, 1983) (Figure 3).

2.2.3 The Solai graben (TVA)

The Solai tectonic axis is a narrow graben averaging 4 km in width and striking N-S to NNE-SSW from the eastern end of the Menengai caldera through Solai (Figure 7). It comprises numerous faults/fractures, all trending NNE-SSW. This is the only system that has cut the Menengai pyroclastics at the northern end of the caldera (e.g. Leat, 1991). The southern extension under the Menengai volcanic pile is an important hydrogeological domain that possibly favours permeability within brittle lava formations underlying the Menengai eruptives (e.g. Leat, 1984, 1983). These structures probably extend into the Menengai caldera system and beyond giving rise to the Makalia fault system, which passes through the western part of Nakuru town. The Ol'rongai and the Solai TVA seem to converge beneath the caldera and this has enhanced the permeability of the geothermal system within the caldera (Leat, 1991).

2.3 Hydrogeology

The Menengai caldera lies on the floor of the Rift valley and is bounded by the Bahati escarpment, Rusinga and Marmanent-Olarabe Rift cliffs to the east and Mau escarpment with the Pekerra River and Kilombe volcano to the west (Figure 8). The surface drainage system is largely from the east and the western scarps. On the rift floor, the drainage is mainly from Menengai caldera northwards with the exception of the drainage from the southern rim or slopes of the Menengai caldera into Lake Nakuru (Mungania, 2004).

The permanent rivers in the area are Molo and Rongai in the NW area. Rivers Rongai and Molo flow north across the Rongai plain from the Mau range and then flow towards Lake Baringo, some 40 km north of the equator. The perennial rivers are the Crater and Olbanita streams in the eastern parts. The Crater stream originate from the Bahati forest and flows into the Menengai caldera. Rivers Njoro and Lamuriak are semi-permanent and flow from the Mau Hills into Lake Nakuru. The main rock types encountered in this area are brittle lava flows, dominating much of the northern surface and also forming bulk of the pre-caldera deposits. Welded pyroclastics and related ash falls cover the central area around the caldera. Lacustrine deposits are also present and are quite dominant at Lake Nakuru south of the caldera. However, recent tectonic activity associated with Solai TVA has modified the fracture patterns and created regions of enhanced permeability enabling meteoric recharge into the geothermal system. Intense fracturing of the brittle rocks create a closely spaced fault/fracture network, which provide hydraulic conduits into the subsurface.

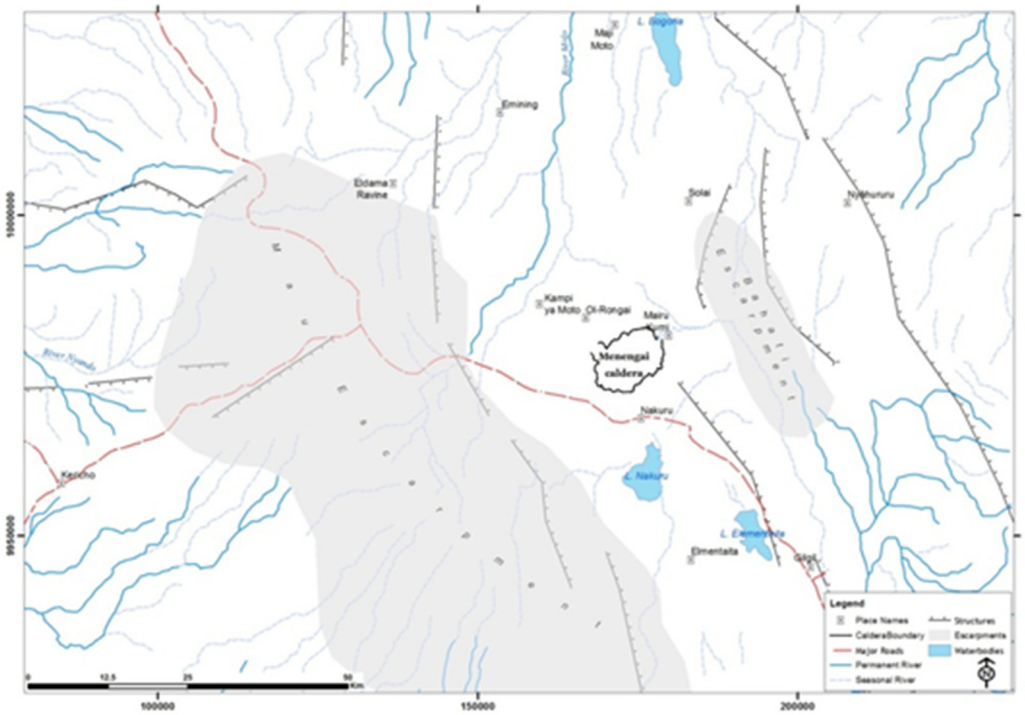

FIGURE 8: Regional hydrogeological map of the Menengai area (from GDC, 2010)

2.4 Geophysics

Geophysical studies such as seismic, gravity, resistivity (i.e. Transient Electromagnetic (TEM) and Magneto Telluric (MT) surveys have been done in the Menengai geothermal field. Gravity survey (Simiyu and Keller, 2001), shows a N-S trending anomaly, which reaches a maximum in the Molo TVA, but is less prominent within the Solai TVA. Recent gravity studies done by GDC (2013), covering both the caldera and the surounding areas include a total of 1635 stations. The results show a NNW-SSE elongated gravity high, with the maximum values of 18 mGal attained in the Olrongai Hills and the gravity high seems to continue southwards. Within this general pattern, the Menengai caldera, show a positive anomaly of about 6 mGal. Within the Menengai caldera, the map shows a gravity high at the caldera summit, confined by gravity lows to the north, east, and southern sections along the caldera rim (GDC, 2013).

Most rock forming minerals are electrical insulators in their natural state. Conductivity or resistivity of materials is controlled by charge carriers (Keller and Frischnecht, 1966). Electrons are the charge carriers in solid rocks while ions are the charge carriers in solutions. Therefore, the concentration and mobility of charge carriers determines the resistivity or conductivity of different rocks (Hersir and Björnsson, 1991). The electrical resistivity in rocks therefore depends on, porosity and pore structure of the rock, salinity of the water, amount of water, alteration minerals, temperature and pressure (Hersir and Björnsson, 1991).

A resistivity cross-section through at 1800 m a.s.l. in the Menengai caldera show a thin high resitivity (>70 ohm-m) top layer underlain by a thick low resistivity (<20 ohm-m) layer) (GDC, 2013). At sea level (Figure 9); high resistivity dominates almost the entire caldera, which could be attributed to alteration due to high temperature alteration minerals which are resistive. To the south of the map an N-S elongated low resistivity anomaly is evident, probably associated with either low temperatures or a fracture zone. Gichira (2012) interpreted a low-resistivity anomaly seen at 4000 m below the surface of Menengai caldera as a deep conductor which was suggested to be a shallow heat source beneath the caldera.

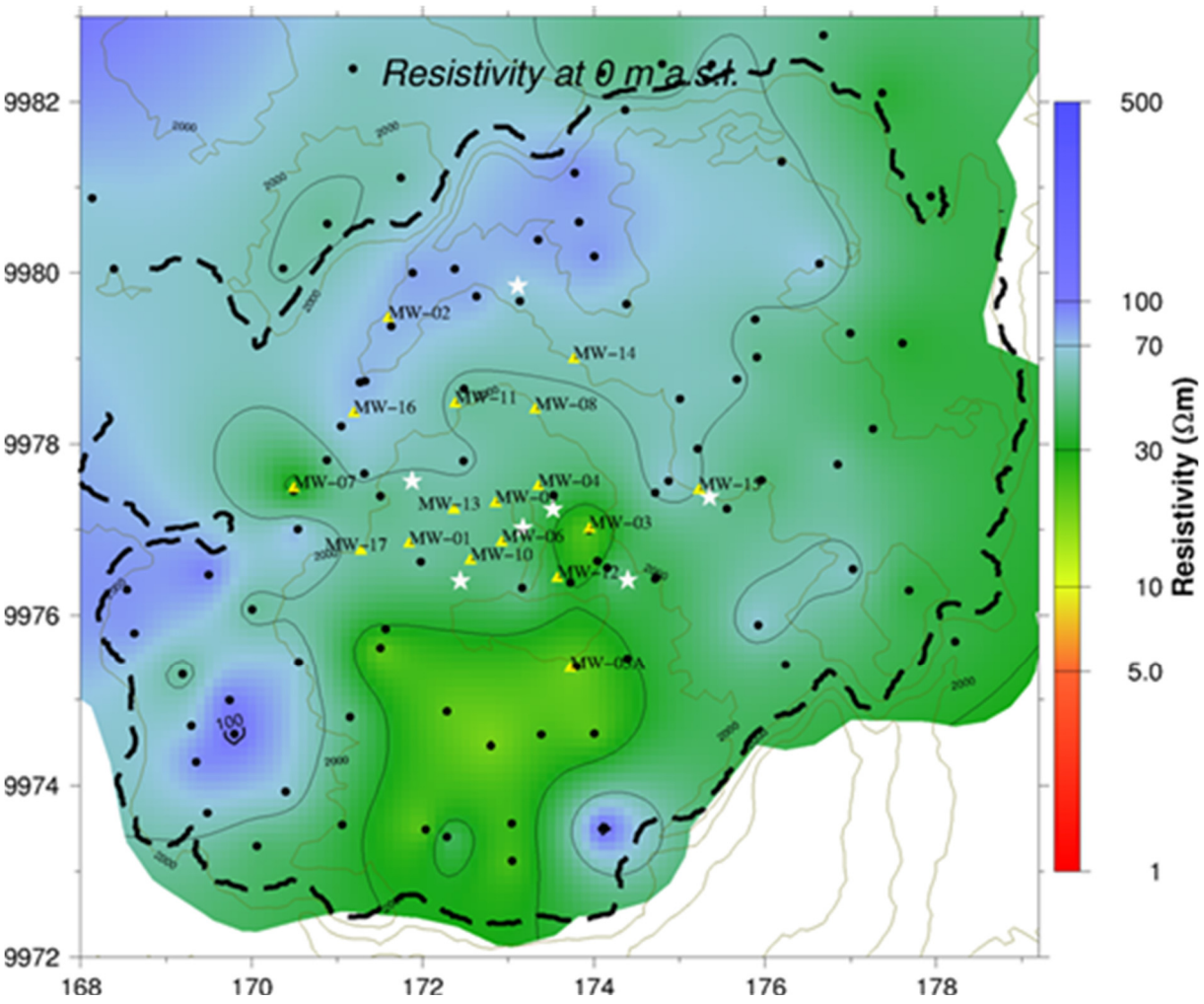

FIGURE 9: Resistivity distribution at sea level in the Menengai caldera (GDC, 2013)

2.5 Fluid and gas chemistry of the Menengai field

Seven wells have so far been discharging at the time of this study. The fluids encountered in the wells, are of sodium bicarbonate type with HCO_3 concentrations as high as 8,200 ppm (calculated as CO_2) and average ~5,000 ppm (GAB, 2013). Quartz equilibrium and Na/K geothermometer temperatures are around 200°C indicating that the water is from relatively cold feed zones and therefore inferred to be shallow (GAB, 2013). Carbon dioxide is by far the most abundant gas in the steam phase. The high CO_2 in the Menengai wells is mainly magmatic. By volume its concentration ranges from 1.2-5.7 % of the weight (GAB, 2013). These high gas pressures considerably lower the boiling point of the rising hot water, reflecting lower boiling temperatures for the measured total pressures in the wells (Kipng'ok, 2011). The pH of deeper fluids of MW-04 aquifers are near neutral (6.9), while the surface discharge fluid is alkaline with an average pH of 9.2 (GDC, 2013). Chloride values (>400 mg/kg), make this anion the second most abundant after bicarbonate, as was reported from the Menengai wells fluids (GDC, 2013). The Cl and SiO_2 values are indicative of hot geothermal fluids entry into the wells. H_2S (over 30 mmol/kg) was recorded from wells MW-04, MW-06, MW-09, MW-10 and MW-12, which was inferred to be from the shallow degassing magma heat source around the caldera summit area (GDC, 2013). Low calcium concentrations noted in discharged water from the Menengai wells was interpreted to be as a result of removal of calcite from the aquifer solution by calcite precipitation (Kipng'ok, 2011).

3. METHODOLOGY

3.1 Sampling

In this study, drill cuttings from wells MW-02, MW-04, MW-06, MW-07 and MW-08 were analysed, all from the Menengai geothermal field. Cuttings from these wells were collected at 2 m intervals for lithological logging during drilling. Samples for whole rock chemistry were selected according to lithological change with depth but even sample distribution was also considered to detect chemical variation with depth if any. The studied wells (Table 1) were drilled between 28th February 2011 and 1st June 2012 by Geothermal Development Company (GDC) as exploration and production wells.

TABLE 1: Data of wells MW-02, MW-04, MW-06, MW-07 and MW-08 of the Menengai geothermal field

Well ID	Eastings	Northings	Elevation	Depth (TD m)	Production casing (m)	Liners shoe (m)
MW-02	171598	9979482	1894	3189	791	3189
MW-04	173351	9977500	2104.82	2106	1092	2085
MW-06	172921	9976850	2103.58	2192	1088	2171
MW-07	170495	9977480	1947.64	2125	1168	2107
MW-08	1733231.3	9978225.3	2015	2345	917	2263

3.2 Analytical techniques

With the aim of characterizing the evolutionary history and the hydrothermal alteration sequence of the Menengai caldera, several analytical methods were used in this study to accommodate various objectives. These include; binocular microscope analysis, petrographic analysis, X-ray Diffractometer analysis (XRD) and ICP-ES analysis (Appendices A and B). All these analytical techniques are described in more detail below.

3.2.1 Binocular microscope analysis

Preliminary analysis of the sample cuttings was done using Wild Heerbrugg binocular microscope at ISOR, the Icelandic GeoSurvey laboratory, with the aim of identifying lithological units, secondary minerals, intensity of alteration and subsurface structures like, fractures, veins and feed zones. Binocular analysis is a visual method for preliminary analysis and a semi quantitative form of describing rock and pore characteristics from drill cuttings. Unlike core samples, interpretation of cuttings is far more difficult as there are several complications regarding the collection of cuttings, which have to be accounted for. For instance, the composition of the cutting samples may not represent the actual rock penetrated as drilling softer, more brittle, more readily cleaved, or fine-grained minerals may result in their depletion in a sample or a previously drilled unit may be incorporated into the sample (e.g. Low, 1977; Mbia, 2010). Sometimes the grain size of minerals may be larger than the cutting chips and it is often difficult to identify rocks from small samples. Mixing of the cuttings during transportation to the surface is also a challenge while interpreting the lithology. Interpretation becomes even more difficult as the cutting size decreases with increasing depth. In comparison to cores, the cuttings represent fragmented rocks and thus detailed features and geological relationships are lost. Time lag between the time the cuttings are produced and when they reach the surface and collected is a problem especially for samples from greater depth. Consequently cuttings are derived from a shallower depth than that indicated when collected at the surface. Representative samples from the penetrated lithological units were selected for further analysis by other analytical techniques.

3.2.2 Petrographic microscope analysis

Sixty-two polished thin sections (62), representing cutting samples from the wells, were analysed for this study using Leitz Wetzler petrographic microscope at ISOR, Icelandic GeoSurvey laboratories. This

analysis aimed at describing the texture, main component of the rock, confirming the rock type, intensity of rock alteration, secondary minerals present, which were not identified during binocular analysis and for identifying the evolution of alteration mineral sequences.

In Petrographic analysis minerals are identified through their different properties in plane-and cross polarized light, including their birefringence, pleochroism, twinning as well as interference properties with conoscopic lens. A summary of the results together, with previously published results, were incorporated and the data was presented with the aid of Log Plot software (Rock Ware, 2007). In addition, petrographic findings are included in the lithological descriptions of the four wells in Appendices C, D, E and F.

3.2.3 X-ray diffraction analysis

Ninety-seven (97) samples were selected for this study to cover the gradual increase in alteration with depth as well as in intervals where alteration becomes more intense. Samples were also selected in areas where more analysis was deemed necessary. The cuttings were crushed by an agate mortar rock crusher and the finely grounded rocks were then mixed with water to form a paste, which was mounted on a glass slide. The analyses were done using Bruker AXS, D8 Focus Diffractometer at ISOR, Icelandic GeoSurvey. Crystalline solids produced patterns of reflected X-rays. These crystals at certain specific wavelengths and incidence angles produced intense peaks of reflected radiation (known as Bragg peaks). Bragg diffraction occurs, when electromagnetic radiation or subatomic particle waves with wavelength comparable to atomic spacing are incident upon a crystalline sample, and undergo constructive interference in accordance to Bragg's law (Putnis, 1992). For a crystalline solid, the waves are scattered from lattice planes separated by the interplanar distance d. Where the scattered waves interfere constructively, they remain in phase and the path length of each wave, is equal to an integer multiple of the wavelength. The path difference between two waves undergoing constructive interference is given by $2d\sin\theta$, where θ is the scattering angle (Putnis, 1992). However, the procedure of preparing samples for XRD analysis is described in Appendix B and some examples are shown in Appendix G.

3.2.4 Inductively coupled plasma (ICP-ES) analysis

One hundred and one samples (101) were selected from top to the bottom of the four wells and analysed for bulk rock chemistry using Spectro Ciros inductively coupled plasma (ICP) emission spectrometry at the University of Iceland. The samples were analysed along with international standards and calibrated. ICP emission spectrometry is a plasma technique with a plasma temperature in the range 6000-10,000 K. The sample solution was passed as an aerosol from a nebulizer into argon plasma. The ICP is a stream of argon atoms, heated by the inductive heating of a radio-frequency coil and ignited by a high-frequency Tesla spark (Rollinson, 1993). The sample dissociates in the argon plasma and a large number of atomic and ionic spectral lines are excited. The spectral lines are detected simultaneously by a range of detectors, they are compared with calibration lines, and their intensities are converted into concentrations (Rollinson, 1993).

Major and trace elements were analysed from the study wells. The use of cuttings for geochemical and petrologic work presents a number of difficulties as cuttings may not be strictly representative of bulk rock down-hole, as the drilling process can be fairly destructive to delicate minerals. It is important to be clear in mind that mixing of the samples with cuttings from shallower depth as the wells progress can mask the pristine chemical composition of the analysed samples. Hydrothermal effects such as, element mobility, secondary mineral deposition and depletion (leaching) was considered during chemical data interpretation. In order to minimize these drawbacks, the geochemical samples were selected from rock cuttings with homogeneous grain population and minimal signs of alteration. Another problem is that samples may reflect a broader sampling interval than the indicated depth, as circulation rates may be variable during drilling. All the analyses have been normalized to 100% to allow direct comparison with fresh rocks. Details of rock crushing procedure and preparation of glass flux samples are described in Appendix B. The major elements analysed include Si, Ti, Fe, Al, Mn, Mg, Ca, Na, K, and P; which were recalculated as oxides. Trace elements analysed include, Sr, Ba, Zr, Y, Zn, Ni, Cu, Cr, Co, V, Sc, Rb, and La, presented as ppm.

4. RESULTS

4.1 Introduction

Geothermal system in the Menengai caldera provides an opportunity for studying the nature of high temperature fluid-rock interaction in a hydrothermal system. The reaction of geothermal fluids with the Menengai rocks has resulted in a progressive hydrothermal alteration sequence with increasing depth that was observed throughout the Menengai field. Samples from wells, MW-02, MW-04, MW-06 and MW-07, provided the source material for the study of petrology and alteration in the geothermal system. Selected samples from well MW-08 were also analysed for total chemistry. The selected samples for whole-rock chemistry were based on lithological change in depth and also on evenly distribution with depth in order to have representable samples in all sections. Bed rock stratigraphy, hydrothermal alteration mineralogy, whole-rock analyses and aquifers of the Menengai geothermal field are presented below.

4.2 Bed rock stratigraphy

Six distinct volcanic units were defined in the study wells. The post-caldera volcanics occupies the upper 300 m to 400 m of the wells. These volcanics are separated from syn-caldera volcanics, by tuff horizon (Tuff horizon 2, in Figure 10), which has varying thickness from well to well, and approximating about 30 to 40 m in thickness. Syn-caldera volcanics, which ranges from about 300-450 m depth, was recognized as the third unit and was separated from the upper pre-caldera volcanics by a tuff and pyroclastic layer (tuff horizon 1, in Figure 10). Lower pre-caldera volcanics which has different chemical characteristic from the upper pre-caldera volcanic occupies the lower section of the wells from about 1200 m to the bottom. However, well MW-02 shows distinct chemical characteristics compared to the other studied wells and was not used for stratigraphical correlation purpose, though its results were compared with other wells for interpretation purpose.

Binocular, petrographic and ICP analyses show that the dominant rock unit from the study wells is trachyte, which constitutes over 90% of the total rocks and is intercalated by minor tuff layers. Minor phonolite and rhyolitic rocks were also noted, probably formed by fractional crystallization of trachytic magma. Basalt occurs as minor intrusions at deeper zones. For the purpose of outlining different eruption episodes recorded within the Menengai caldera, trachyte was classified into three varieties based on their texture, where variety one has abundant large feldspar phenocryst in a fine grained matrix, classified as medium grained trachyte. Variety two are fine grained trachytes with smaller feldspar phenocryst, the distinction being in the quantity of phenocrysts. Third variety consist of fresh intrusions of trachytic lava, which were classified as syenite (coarse grained, holocrystalline trachyte), indicating that there were episodes of magma rejuvenation during and after the Menengai shield formation process (Figure 10). Wells MW-04 and MW-06 were drilled into magma, resulting in fresh quenched glassy cuttings at 2080 and 2172 m depth, respectively, suggesting a shallow heat source most likely a magma intrusion below the caldera summit. A summary account of major rocks types found in the study wells is given below, though the full description of all these is given in Appendices C, D, E and F.

Trachyte

The post-caldera trachyte occurs as young frothy lava pile forming a dome that has partially filled the caldera. Generally trachyte occurs as grey, brownish-grey to light grey rock. They are generally flow banded and porphyritic. Different varieties of trachyte are generally differentiated from each other by their texture; fine grained, medium grained and coarse grained types. Their variability in the mineralogical and textural properties indicates that these trachytes are not from single large volume flow, though the eruptions could have occurred within a short period of time. They are porphyritic with large phenocryst of alkali feldspar (mainly sanidine), pyroxenes and Fe-Ti oxides. The phenocrysts are set in a fine grained matrix with flow texture. On the surface to about 300-400 m depth, generally fresh, unaltered trachyte lava was noted. Minor fractures and oxidized cutting however were found as described later in the Appendices C, D, E and F. Trachyte at varying depths, for example on fractured areas and along the lithological boundaries are highly altered. Aquifers correlate with highly altered

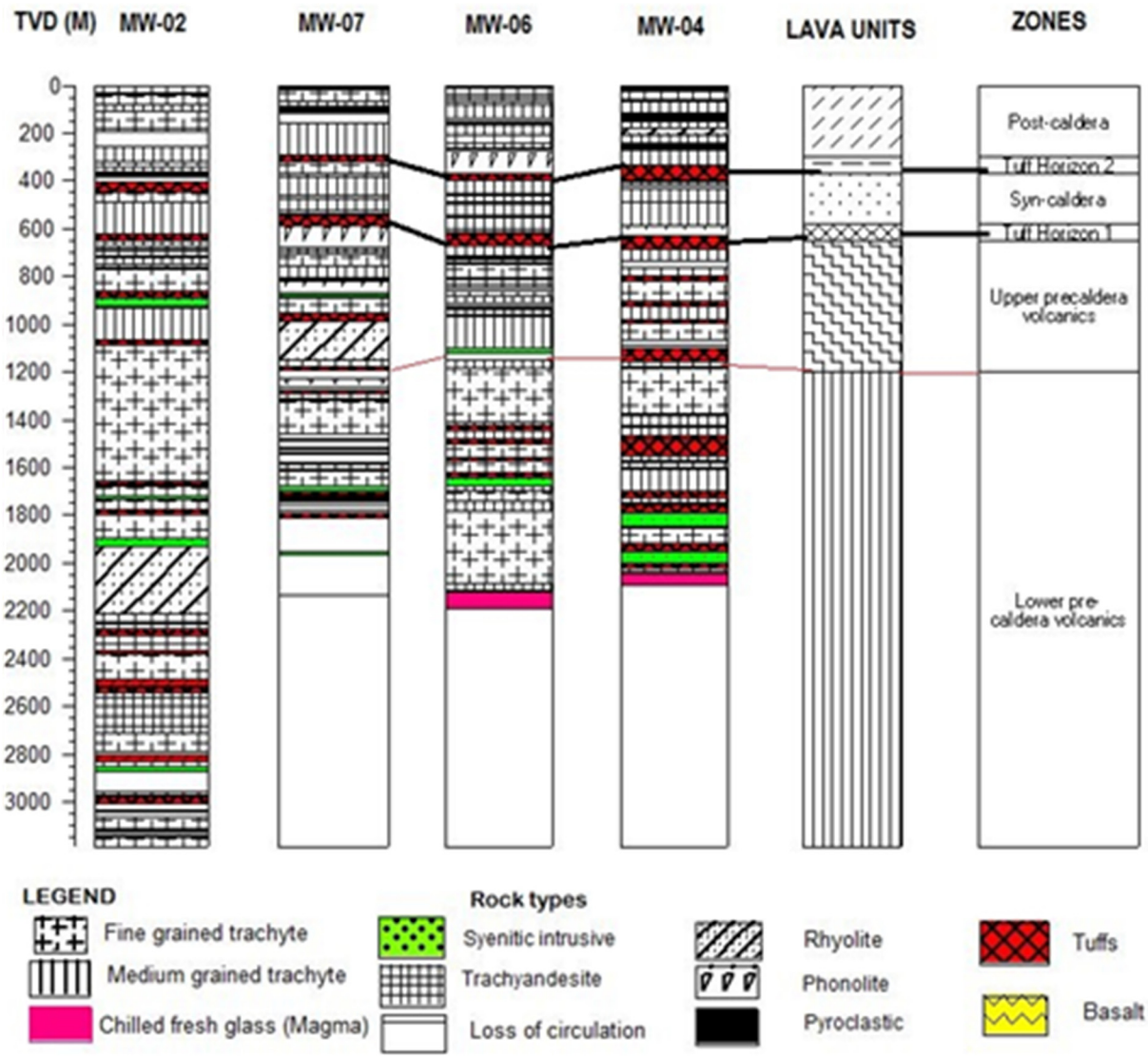

FIGURE 10: Lithostratigraphical correlation and volcanic units of wells MW-02, MW-04, MW-06 and MW-07

lithological boundaries as a result of water-rock interaction. Feldspar phenocrysts (mainly sanidine) in some cuttings are extensively altered. Where the rock is fractured, the feldspar phenocrysts show dissolution. The compositions among different varieties of the trachytes are slightly different, which leads to the conclusion that eruptions took place in several episodes.

Pyroclastics

Pyroclastic fragments are found on the surface and occasionally as highly oxidized thin layers intercalating the lavas. They generally appear as brownish to grey, loose unconsolidated deposits composed of ash, vesicular and pumiceous fragments. Their frequent intercalation as thin lenses between lavas implies that several eruptions occurred within the Menengai caldera (Figure 10). With increased depth pyroclastic alters to clays.

Tuff

Tuffs occur as thin beds and also as intercalations between lava flows. They are generally reddish brown, commonly composed of non-welded, poorly crystalline and vitrified volcanic ash with glassy texture. The tuffs are often highly altered to clays along contact boundaries. They contain poorly crystalline lithic fragments, which are vesicular in nature. Two major tuff marker horizons were recognized in the study wells, which define the post, syn- and upper pre-caldera volcanics. These tuffs marker horizons were found at 332-394 m and between 626 and 688 m depth in well MW-04. In well MW-06, the upper and the lower tuff marker horizon were noted at 366-400 and 618-670 m depth, respectively. These two

marker horizons were found from 290 to 322 m and between 546 and 588 m in well MW-07 respectively. Tuffs are important units for correlation since they are intersected by all the wells and were used to demarcate different eruption episodes within the Menengai volcano (post-, syn- and pre-caldera formations).

Phonolite

Based on chemical composition, some of the rock cuttings belong to the phonolitic group (see Figure 20 later), which is assumed to be derived from fractional crystallization of trachytic magma. From binocular analysis, it was difficult to resolve phonolite from trachyte, especially due to high degree of hydrothermal alteration. Phonolite was only recognized in well MW-04, MW-06 and MW-07, but was not found in well MW-02. In well MW-04, phonolite was found at 588-626, 732-766 and 1068-1076 m depth. In well MW-06, this lava was only found between 268 and 334 m depth, intercalating pyroclastic ash. They generally occurs as grey, brownish grey to light grey rock. In well MW-07, phonolite was found at 588-680 m and between 820 and 866 m depths. Phonolite found in the study wells has a texture ranging from aphanitic (fine grained) to porphyritic (seriate coarse-grained). Sanidine occurs as the main phenocrysts and also as the bulk of the groundmass. Nepheline occurs either interstitially or as euhedral microphenocrysts while pyroxene occurs characteristically as slender needles, often abundant enough to colour the rock green. The principal dark-coloured minerals are pyroxene, aegirine-augite.

Rhyolite

Rhyolite occurs as spherulitic white bands of volcanic glass enriched with quartz and feldspar crystals. Generally the rock is light grey, porphyritic with quartz and sanidine in fine grained groundmass. The groundmass is dominated by quartz and sanidine matrix. Rhyolite was identified from 192-204 m and between 988 and 1148 m depths in well MW-04 and MW-07, respectively. However, no rhyolite was identified in well MW-02 and MW-06 as described in Appendices C, D, E and F.

Basalt

Basalt occur as thin intrusive rocks in Menengai and are separated by thin layers of tuff and minor trachyte in wells MW-02 and MW-08 at several depths. No basalt was identified in wells MW-04, MW-06 and in MW-07. The basalts are generally dark grey, fine grained and porphyritic, with the main phenocrysts being augite, plagioclase and olivine. In well MW-02, basalt was found at 2342-2370, 2484-2514 and 2806-2828 m depth whereas in well MW-08 they occur at 1688-1728 and 1756-1810 m (Kipchumba, 2013). The basalts consist of groundmass containing abundant ferromagnesium minerals showing alteration mainly to epidote and clays.

Syenite (intrusives)

Tectonically, Menengai is located within the rift whereby spreading occurs and fresh magma pulses from the main magma chamber are being injected into the overlying formations, forming dykes and other intrusions. Generally the syenite occurs as relatively fresh, coarse grained and massive rocks, which are leucocratic, but with dark green spots by mafic minerals. The major difference between the syenitic samples and those termed trachyte is the grain size; syenite being coarse and relatively fresh. In well MW-02, several syenitic intrusive occur at 654-670, 892-922, 1722-1736, 1896-1930, 2684-2708, 2850-2876, 3034-3042 and 3140-3148 m depth. In well MW-04, intrusives occur at 1746-1756, 1788-1790, 1802-1830, 1952-1980, 1986-1992 and 1998-2000 m. In well MW-06, the intrusives occur at 884-886, 1104-1124 and 1644-1678 m depth. In well MW-07, the intrusives occur at 866-872, 1314-1322, 1678-1696, 1728-1734 and 1950-1964 m depth. The intrusives were probably formed as a result of magma being injected into the overlying formation. Their coarse texture is attributed to slow cooling as dykes and other intrusives. They also show oxidation as a result of reaction with steam that evaporated from the surrounding host rocks during intrusion. All syenitic intrusive rocks analysed in the Menengai classify as trachyte in the TAS diagram (see Figure 20 later).

Trachy-basalt

Trachy-basalts are rare in the Menengai and are found in well MW-02 at 2484-2514 m depth and at 1558-1728 m in well MW-08. Generally trachy-basalt is, fine grained, dark grey to brownish grey rock with plagioclase and sanidine phenocrysts resembling fine grained trachyte but they are slightly darker

in colour. Trachy-basalts with a composition between basalt and trachyte were only confirmed by their chemical composition.

Phonotephrite
Phonotephrite was only identified from selected samples from well MW-08 at 1558-1728 m depth by the total rock composition. However, in the field or in binocular analyses, the rocks are dark fine grained and relatively fresh and resemble basalt. They are porphyritic with mainly feldspar phenocrysts, though, some samples being vesicular and vesicles filled mainly by calcite and clays.

Trachy-andesite
This lava occurs as brownish grey, fine grained feldspar porphyritic lava and resembles trachyte in cutting samples and was only found in well MW-02 at 2586-2684 m depth (see Figure 20 later). These samples are assumed to be derived from a less fractionated magma.

Trachy-dacite
Trachy-dacite occurs in well MW-07 at 1224-1264 m depth. It occurs as a brownish grey to grey, fine grained sanidine porphyritic rock. Trachy-dacite is an acidic rock with chemistry between dacite and trachyte. The phenocrysts are mainly sanidine and clinopyroxenes.

Quenched fresh volcanic glass
Wells MW-04 and MW-06, which are located near the centre of the Menengai caldera, both yielded quenched glassy cuttings from 2080 m and 2172 m depths respectively. This is interpreted as a shallow magma intrusion. These zones were characterized by anomalous high temperatures, over 350^0C. Glass is highly susceptible to alteration and in a high temperature geothermal system like the Menengai; the glass would have been completely altered unless it was a very recent intrusion. These depths were characterized with drilling challenges like sticking of the drill string and shearing of the bit due to high temperature. All the chilled glassy samples classify as trachytes in the TAS diagram (Figure 10).

Palaeo-soils (sediments)
Baked, reddish brown highly altered and oxidized thin beds composed mainly of rock debris, ash and sediments were noted in well MW-06 from 1614-1644 m depth. These baked sediment beds were interpreted to imply dormant time episodes between different eruption episodes. Leat (1984) observed these types of sediments separating lava sequences at the Lions cliff where the pre-caldera lavas are exposed.

4.3 Stratigraphic correlation

A geological cross-section across wells MW-02, MW-04, MW-06 and MW-07 of the Menengai geothermal field is shown later. However, for stratigraphical correlation, well MW-02 (Figure 11) was not included as will be discussed in Chapter 4.6. Therefore, only wells MW-04, MW-06 and MW-07 (Figures 12-14) were used for stratigraphic correlation within the caldera fillings. However, well MW-02 may give valuable information on the strata below the caldera fillings as these layers appear to be part of the regional lava pile as will be discussed further in Chapter 4.6.

The post caldera volcanics in wells MW-04, MW-06 and MW-07 correlate well and these volcanics are dominated by medium-grained trachyte lava, though at the surface fine-grained thin lava were found in all wells (Figure 10). The uppermost zone is characterized by unaltered lava, intercalated by thin pyroclastics layers and it extends from the 0-386, 0-444 and 0-430 m depth in wells MW-07, MW-06 and MW-04, respectively.

Syn-caldera volcanics was dominated by medium grained trachyte lava, which extends from about 350 m to about 700 m depth. This volcanic unit was separated from post-caldera volcanics by a tuff layer (tuff marker horizon 2, in Figure 10) and below by tuff marker horizon 1. The lava sequence within this zone correlates well though with minor variation in depth and thickness. The pre-caldera volcanics, are

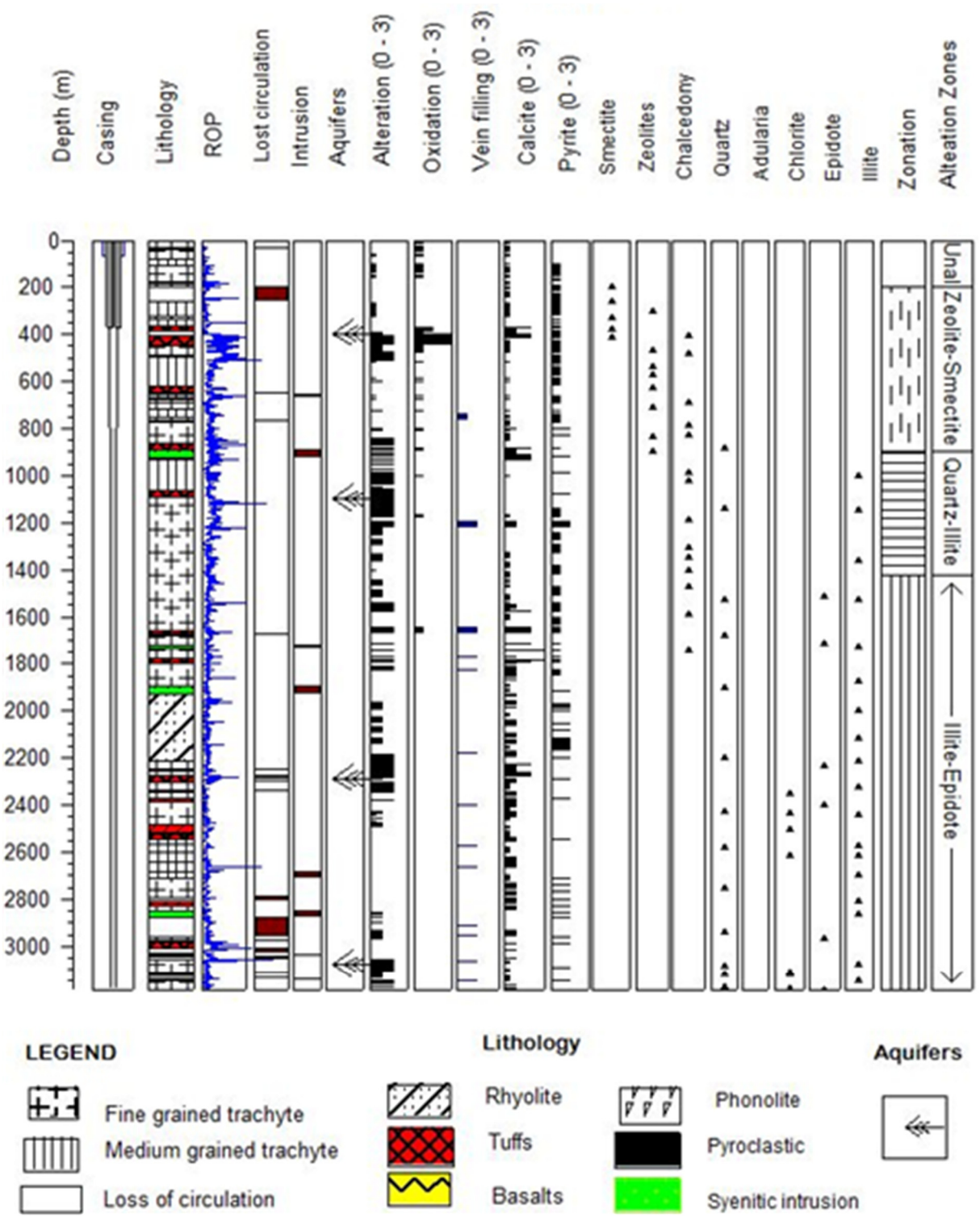

FIGURE 111: Lithostratigraphy, alteration zones and distribution of secondary minerals with depth in well MW-02. Feed points are inferred from loss of circulation, penetration rates and temperature logs

dominated by fine-grained trachyte and medium grained. The trachytes are intercalated by thin tuff and pyroclastic layers. The pre-caldera volcanics sequence is characterized by scarce syenitic dykes.

Lateral continuity of the structures of the Menengai caldera filling is complicated by faults and fractures causing displacement of rock-blocks which resulted in variation with depth within volcanic units from well to well. Slight vertical displacement of rock units may block horizontal permeable layers but the fault system assures abundant vertical aquifers within fractured stratigraphic units. Subsurface faults,

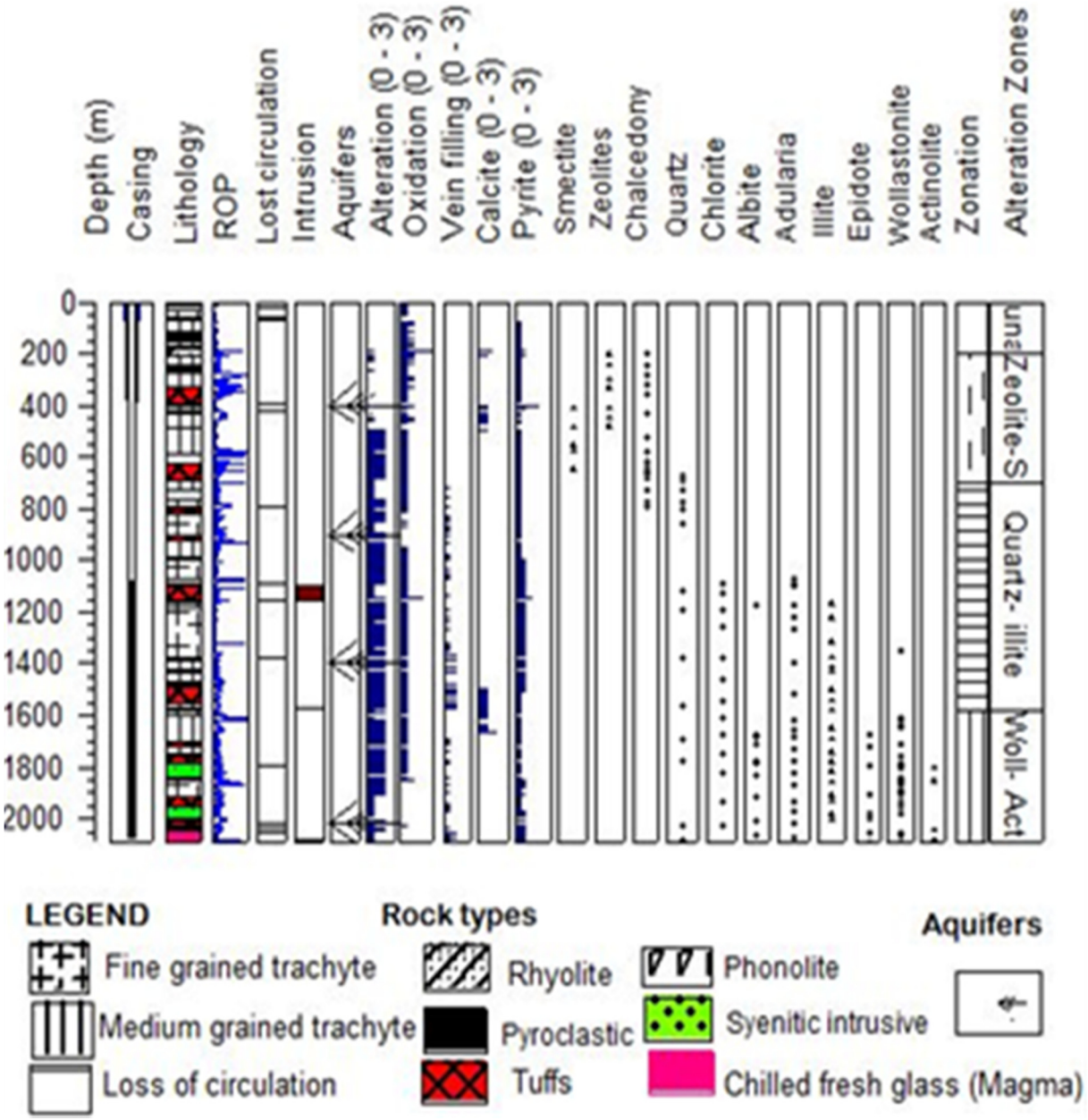

FIGURE 12: Lithostratigraphy, alteration zones and distribution of secondary minerals with depth in well MW-04. Feed points are inferred from loss of circulation and temperature logs

which were interpreted from fractured cuttings, are associated with Molo and Solai TVAs, and favour the flow of thermal fluids making the Menengai field a highly permeable and good production field. These faults are, however, not obvious on the surface within the caldera due to the Holocene post caldera lavas, tuff and pyroclastics that form the uppermost 300 m of the caldera filling. The age of the marker horizon 1 is 12,500 years (Leat, 1991). The lower pre-caldera sequence starts from about 1200 m depth to the bottom of the study wells.

4.4 Alteration mineralogy

Hydrothermal fluids carry metals and anions close to equilibrium with the secondary minerals. The source of hydrothermal fluids is mainly meteoric water (or seawater) since the low water content of magmas is insignificant in geothermal system. Magma degassing and leaching of intrusive rocks are the principal sources of anions in hydrothermal system within active volcanic centres. According to Ármannsson (2012), excess water circulates through the surrounding rocks and may scavenge and

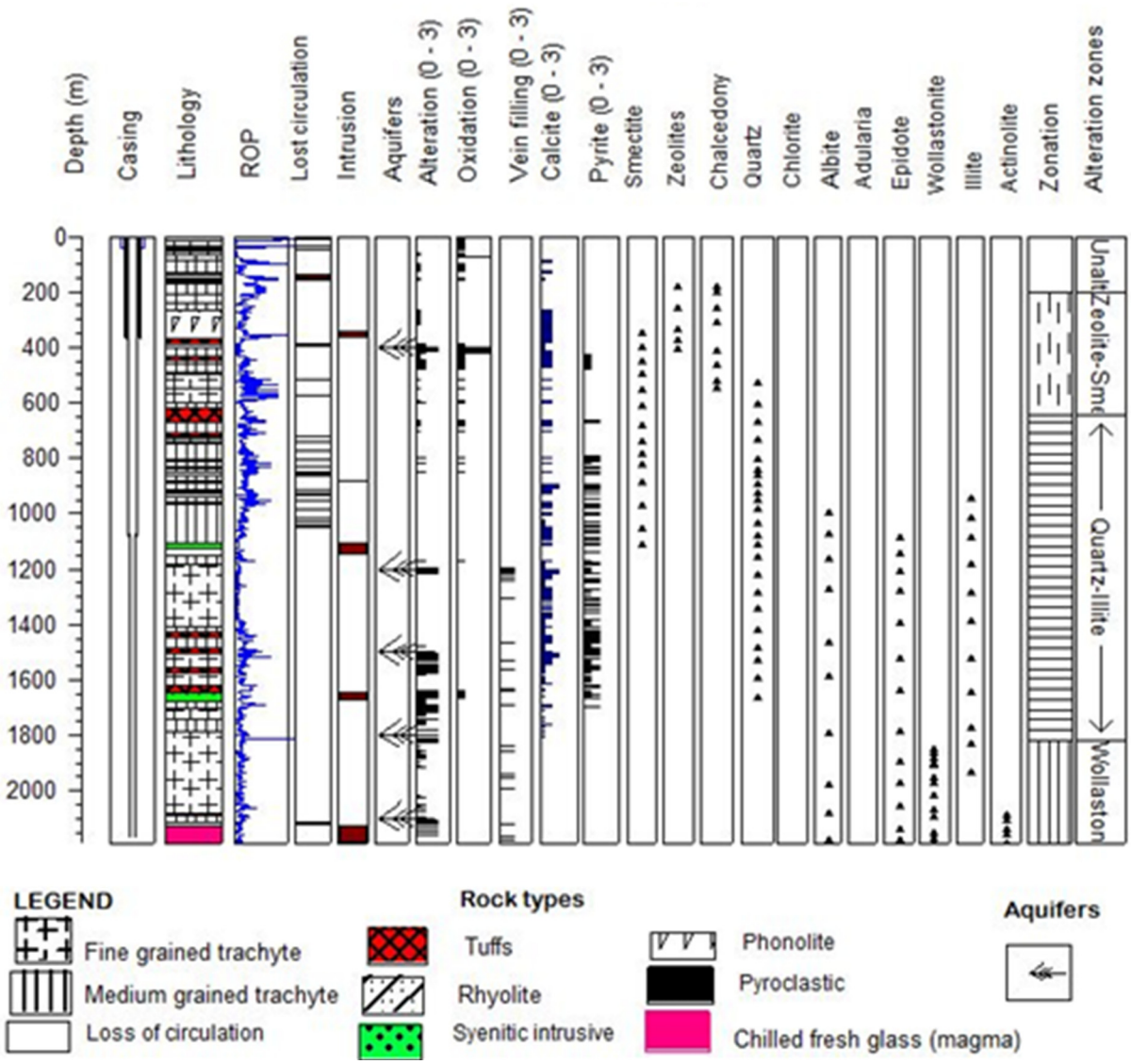

FIGURE 13: Lithostratigraphy, alteration zones and distribution of secondary minerals with depth in well MW-06. Feed points are inferred from loss of circulation, penetration rates and temperature logs

transport metals to sites where they can be precipitated as ore minerals. Hydrothermal fluids also circulate along fractures and faults. A formation which has a well-developed fracture system, may serve as an excellent host rock for hydrothermal alteration. Fluids that flow through open space fractures may precipitate secondary minerals along the walls of the fracture, eventually filling it completely (Ármannsson, 2012; Browne, 1984; Fridleifsson, 1991, 1983).

The drill cuttings from the Menengai geothermal field which include lavas, intrusions and tuffaceous fragments, show distinct alteration characteristics. Tuffs and pyroclastics fragments are typically highly altered as compared with the insignificantly altered hard-rock cuttings from the same depth interval. Lavas and intrusives are generally more resistant to alteration and hence less altered. Hydrothermal alteration progresses at different rates in the aquifer rocks. At a given pressure and temperature the rate is dependent on lithology and permeability as well as salinity and volatile content of the fluid (e.g. Browne and Ellis, 1970; Franzson, 2010; Marks et al., 2010).

In well MW-04, calcite, pyrite, smectite, zeolites, chalcedony, quartz, chlorite, albite, epidote, wollastonite, illite and actinolite occurs as the main alteration minerals (Figure 12). Zeolite was noted from 200 m depth and it disappears at about 450 m depth. Zeolite presence in a geothermal system indicates formation temperature between 40°C and 120°C (Franzson, 1998). Smectite was noted from

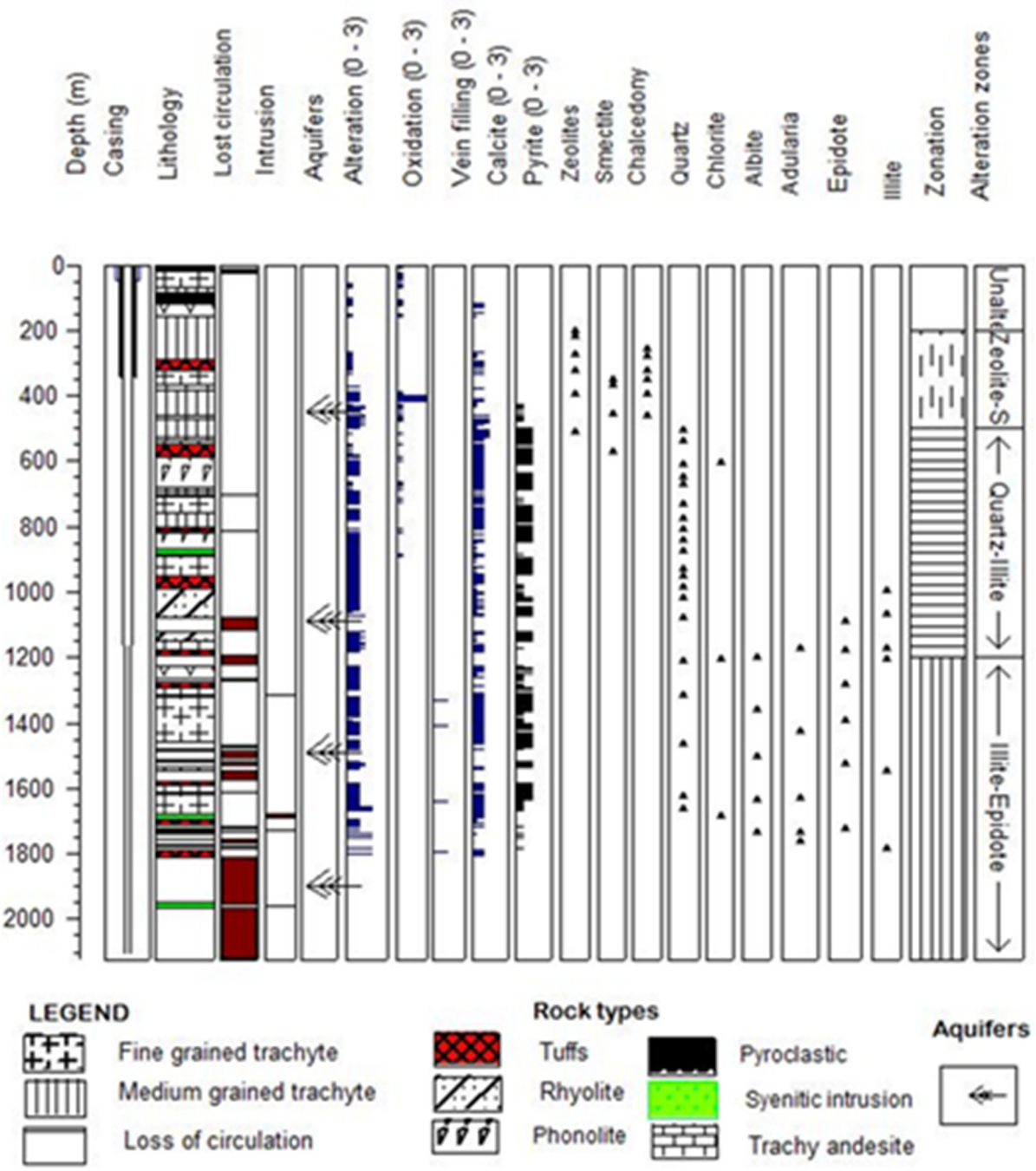

FIGURE 14: Lithostratigraphy, alteration zones and distribution of secondary minerals with depth in well MW-07. Feed points are inferred from loss of circulation and temperature logs

398 m and disappears after 650 m depth. Secondary quartz was first noted at 740 m depth and persisted to the bottom of the well. Its presence indicates formation temperature of above 180°C. Actinolite was first noted from 1880 m depth to the bottom of the well. Adularia, Illite, albite, wollastonite and actinolite were first noted at 1100, 1200, 1412 and 1880 m, respectively (Figure 12). All these hydrothermal minerals are mainly present in veins, vugs, and vesicles and as replacement of primary minerals in volcanic rocks. These minerals form when circulating fluids and reservoir rocks react resulting in a compositional change of both the solid and the fluid (e.g. Ármannsson, 2012; Browne, 1984; Larsson et al., 2001). This reaction normally involves dissolution of major rock-forming minerals and precipitation of hydrated secondary silicates, carbonates, sulphates and sulphides.

Browne (1984) suggested that the products of geothermal alteration are controlled by temperature, original rock composition, reaction time, flow, chemical composition of water (e.g. CO_2, H_2S),

permeability, and these products in turn control the chemical composition of the fluid. Pressure also plays a role in hydrothermal alteration though variation within geothermal reservoir rarely exceed 200 bars, which is a small change though has an impact on the boiling zone of the fluid and minerals solubility (e.g. Ármannsson, 2012; Lagat, 1995). High alteration intensity and deposition of secondary minerals were noted more in aquifer zones compared to fresh or unaltered shallow section of the wells.

Figure 11 shows distribution of alteration minerals in well MW-02. The well shows less high-temperature alteration minerals compared with the other study wells. Minerals like actinolite, wollastonite, and adularia were conspicuous missing suggesting less or little water-rock interaction in this well.

4.4.1 Alteration of primary mineral assemblages

Primary rock forming minerals are unstable when subjected to low temperature and pressure conditions and will be replaced by secondary minerals which are stable at those conditions (Browne, 1984). The secondary minerals formed depend on the original rock chemistry, fluid chemistry and permeability status of the rock (e.g. Browne, 1984; Reyes, 1990 (Table 2)). In Menengai, main primary minerals include olivine, feldspars (mostly sanidine), quartz, pyroxene and amphiboles.

Volcanic glass is found in pyroclastic deposits or cooling margins of intrusions. Volcanic glass is highly susceptible to alteration and will readily alter when exposed to geothermal conditions.

Olivine found in mafic rocks as primary minerals is very susceptible to alteration. It is distinguished in thin section by its high birefringence, distinctive irregular fracture pattern, lack of cleavage, and alteration products, usually clays, along fractures. At depth it is usually replaced by calcite or with clays.

TABLE 2: Primary minerals and their replacement and alteration products in the Menengai wells (modified from Reyes, 1990)

Primary mineral	Alteration mineral products
Volcanics glass	Zeolites, quartz, clays, calcite
Plagioclase	Albite, calcite, epidote
Olivine	Clays minerals, calcite, actinolite, hematite
Pyroxene, amphiboles	pyrite, actinolite, calcite, chlorite, epidote
Fe-Ti oxides	Titanite, pyrite, hematite
Sanidine, orthoclase, microcline	Adularia, illite

Pyroxene occurs mostly as a groundmass mineral and occasionally as phenocrysts varying from aegirine to augite. In thin sections pyroxenes are identified by two perpendicular cleavage orientations, inclined extinction. Pyroxene was observed to alter to clays as well as to actinolite at higher temperatures.

Feldspars in the Menengai rocks are generally plagioclase in mafic rocks and sanidine in felsic rocks. Sanidine and plagioclase occur as the major groundmass mineral as well as phenocrysts. In thin sections, the sanidine occurs as fine grained and elongated crystals showing typical trachytic texture. It also occurs both in the groundmass and as phenocrysts in rocks exhibiting porphyritic textures. The sanidine phenocrysts were readily identified by its low relief and simple twinning. At shallow depths, the feldspars are relatively unaltered but become altered progressively with depth into albite, adularia and occasionally to clays or calcite. Epidote sometimes replaces dissolved feldspar, presumably due to the local availability of Al and Ca that react with ferric iron to form minerals of the epidote-clinozoizite series.

Fe-Ti oxides and other opaque minerals occur sparely distributed in all wells and usually show high resistance to alteration. The main opaque and oxides present in the Menengai are ilmenite and magnetite, which usually become altered into pyrite and titanite.

4.4.2 Distribution and description of hydrothermal alteration minerals

Oxides Fe-oxides are distributed broadly especially on fractured cuttings and occurs mainly as hematite. At depth, oxidation is mainly associated with baked contacts between syenitic intrusions and host rocks. It was also noted between pyroclastics layers intercalating the lavas which were inferred as a period between eruption episodes. Calcite is abundant and occurs within almost all lithologies in all wells below 200 m but diminishes at temperatures above 280°C. In binocular analysis, calcite was identified using dilute hydrochloric acid. Furthermore, calcite crystals have obvious cleavage. In the Menengai, calcite occurs as a replacement of rock forming mineral and volcanic glass and as platy crystals infilling voids. This carbon dioxide can dissolve calcite in the rocks and convert it to calcium ions (Ca^{++}) and bicarbonate ions (HCO_3^-) according to the chemical equation:

$$CaCO_3 + H_2O + CO_2 => Ca^{++} + 2HCO_3^-$$

The greater the amount of CO_2 dissolved in the geothermal water, the greater the amount of calcite that can be dissolved. Calcite in the reservoir will dissolve in the geothermal liquid until a chemical equilibrium is reached (e.g. Giggenbach, 1980, 1984; Garrels and Christ, 1965). Geothermal fluids in the deep reservoir inevitably contain dissolved carbon dioxide (CO_2) under pressure (Ármannsson, 2012). As geothermal fluids rise from depth, it loses its carbon dioxide due to boiling (Ellis, 1963; Simmons et al., 1994). Table 3 shows temperature implications of some temperature dependent minerals.

Clays in Menengai appear sparsely scattered throughout the lithological sequence. Low-temperature clays such as smectite form at temperatures as low as 50°C and can persist to temperatures of about 200°C. On the other hand, high temperature clays such as chlorite and illite form at temperatures of above 230°C and 220°C, respectively.

Smectite were only detected in minor amounts by XRD analysis. It is a swelling clay and swells from 12.93-13.94 to 15-16 Å in responding to glycol treatment (e.g. Putnis, 1992). Minor smectite were detected from 190 to 720 m in well MW-06, from 350 to 1100 m in well MW-06 though not identified in wells MW-02 and MW-07 as illustrated in Figures 11-14). Smectite are shallow low temperature stable minerals and their presence in a geothermal field indicates temperature in the range 50-200°C.

Zeolites are low temperature stable hydrothermal minerals, which are thermodynamically metastable at about <110°C. The zeolites found in Menengai are scolecite/mesolite and cowlescite, which occurs generally as vesicle infillings in shallow depths. Zeolites were first detected from 180 m depth in well MW-06 and their deepest occurrence is in well MW-07 at about 500 m depth (Figure 14).

Chlorite in the Menengai occurs in association with epidote, calcite and quartz mainly as a replacement of low temperatures clays. Chlorite occurs at temperature over 230°C (Franzson, 1998). In the studied wells, it first occurs below 950 m depth in well MW-04.

TABLE 3: Some temperature dependent minerals in the Menengai geothermal field and their temperature implications (Modified from Reyes, 2000; Kristmannsdóttir, 1979; Franzson, 1998)

Minerals	Min. temp. (°C)	Max. temp. (°C)
Zeolite	40	120
Smectite	30	<200
Calcite	50-100	280-300
Quartz	180	>300
Albite	180	>300
Adularia	180	>300
Illite	220	>300
Epidote	230	>300
Chlorite	230	>300
Wollastonite	270	>300
Actinolite	280	>300

Illite occurs as replacement of K-feldspars and occurs in veins and vesicles in the Menengai field. It was identified in XRD analysis with its distinct peak at 10 Å, but the dominating illite-clay occurrence is in interlayered illite-vermiculite. Illite occurrence depict temperatures >220^{o}C in active geothermal field. Illite occurs in association with albite, calcite, pyrite and quartz in study wells. Illite was generally the most abundant clay found in all wells as shown in Tables 4-7.

TABLE 4: Results of XRD analysis of clay minerals from well MW-02

Sample no.	Depth (m)	d(001) UNT	d(001) GLY	d(001) HIT	Mineral	Remarks
#1	100	12.5	-	-	MLC	Illite-chlorite
#2	418	12.5	-	-	Amphiboles, feldspars	No clays
#3	580	9.3, 6.4	-	-	Amphiboles, feldspars	Illite-chlorite
#4	840	-	-	-	-	Illite
#5	1030	10.4, 8.7	-	-	Illite, Amphiboles,	Illite
#6	1236	10.3, 8.6, 6.4	-	-	Illite, Amphiboles Feldspars	Illite
#7	1546	10.3, 7.1, 6.5, 6.4	-	-	Illite, feldspars	Minor illite
#8	1786	10.3, 8.6	-	-	Illite, amphiboles	Illite
#9	2140	17.8, 12.1, 10.3, 7.2, 6.4	-	-	Illite, feldspar	Illite
#10	2354	12.4, 10.3	12.4, 10.3	12.4, 10.3	Illite Feldspars	Illite
#11	2436	12.4, 10.3	12.4, 10.3	12.4, 10.3	Chlorite, illite.	Illite-chlorite
#12	2502	14.15, 10.3, 7.13	14.15, 10.3, 7.13	14.1=0, 7.13=0	Illite, vermiculate.	Illite
#13	2614	14.65, 10.44, 10.19,7.2	14.65, 10.44, 10.19,7.2	7.2=0 14,6=0	Chlorite, illite.	Chlorite , Illite
#14	2700	10.4, 10.2	10.4, 10.2	10.4, 10.2	Illite	Illite
#15	2808	10,38, 10,17	10,38, 10,17	10,38, 10,17	Illite	Illite
#16	2860	10.26, 6.44	10.26, 6.44	10.26, 6.44	Feldspars, Illite	Illite
#17	2980	10.3, 10.1, 8.6, 6.4	10.3, 10.1, 8.6, 6.4	10.3, 10.1, 8.6, 6.4	Illite, amphiboles, feldspars	Illite, amphiboles
#18	3080	10.3, 10.1, 6.4	10.3, 10.1, 6.4	10.3, 10.1, 6.4	Illite, amphiboles, feldspars	Illite, amphiboles
#19	3146	10.3, 10.2, 8.6, 6.4	10.3, 10.2, 8.6, 6.4	10.3, 10.2, 8.6, 6.4	Illite, amphiboles, feldspars	Illite, amphiboles

Pyrite is abundant throughout most cuttings intervals in all four wells and usually indicates the degree of permeability in geothermal systems. In the Menengai wells, pyrite appears as shiny yellowish gold cubic crystals and sometimes disseminated on the rock surface as well as vein deposits. Pyrite persisted from the surface to the bottom of virtually all wells as indicated in Figures 11-14).

Chalcedony is low temperature silica compound which is normally white, massive and extremely fine grained and usually transforms into quartz at higher temperatures. It appears bluish and semi-transparent or translucent under the binocular microscope. They are cryptocrystalline and range from colourless, white, or bluish-grey in colour and are usually deposited in vesicles, fracture and also as veins in all wells. In the studied wells chalcedony occurs at shallow depth to about 800 m and thereafter occurring rarely to about 900 m. In the deeper sections of the wells the apparent chalcedony is most probably a cryptocrystalline aggregate of alpha quartz. Chalcedony indicates temperatures below 180°C.

Quartz: Secondary quartz occurs as replacement of chalcedony at depth and was found deposited mainly in veins and vesicles. It´s presence in a geothermal system indicates temperatures of above 180^{0}C (Franzson, 1998). Secondary quartz was identified in cuttings by its typical euhedral shape. Generally it occurs as colourless and occasionally as white euhedral to subhedral crystals.

Epidote is a product of hydrothermal alteration of various minerals (feldspar, mica, pyroxene, amphiboles, clays, etc.) in igneous rocks. The presence of epidote as a hydrothermal alteration mineral is always a good sign as it indicates temperatures of over 230^{0}C (Table 3). Epidote is rare in the Menengai as expected due to low iron content of the rocks and reducing condition that may arise from

volcanic emanations (hydrogen, hydrogen sulphide) that favours the formation of Fe (2^+) minerals such as pyrite. Since epidote is essentially the host mineral for Fe (3^+), it requires oxidized environment. In systems with low total iron the Fe (3^+) also resides in magnetite and specially hematite making epidote less probable secondary mineral. Also, in Na-rich surroundings, the Al_2O_3 component is preferentially taken up in the ever-present stable albite molecule. Epidote was first encountered at 1090 m in well MW-06 though found in sparse amounts. Where it occurs, it fills fractures and vesicles and occurs as a replacement of primary plagioclase and pyroxene. In thin section, it appears as yellowish green in colour has prismatic crystals. Good cleavage was visible in some crystals.

TABLE 5: Results of XRD analysis of clay minerals from well MW-04

Sample no.	Depth (m)	d(001) UNT	d(001) GLY	d(001) HIT	Mineral	Remarks
#1	192	16.0, 13.9, 9.2, 6.5	16.0, 13.9, 9.2, 6.5	16.0, 13.9, 9.2, 6.5	Smectite, feldspars	Smectite
#2	244	15.7, 13.8, 9.1, 6.5	15.7, 13.8, 9.1, 6.5	15.7=0	Smectite, feldspars	Smectite
#3	362	10.1, 9.1, 9.0	10.1, 9.1, 9.0	10.1, 9.1, 9.0	Illite, zeolite	Illite,
#4	586	6,5	6,5	6.5=0	Feldspars	No clays
#5	690	6,5	6,5	6,5	Feldspars	No clays
#6	804	16.9, 15.1, 15.4, 6.5	16.9, 15.1, 15.4, 6.5	16.9=0, 15.4=0	Smectite	Smectite
#7	950	17.3, 15.5, 6.5	15.5=0, 6.5=0	Destroyed	Smectite	Smectite
#8	1068	6,5	6,5	6,5	Feldspars	No clays
#9	1186	8.6, 6.5, 6.4	8.6, 6.5, 6.4	8.6, 6.5, 6.4	Amphiboles , Feldspars	No clays
#10	1288	8,6	8,6	8,6	Amphiboles	No clays
#11	1426	8,6	8,6	8,6	Amphiboles	No clays
#12	1584	10.1, 8.6	10.1, 8.6	10.1, 8.6	Illite, amphiboles,	Minor illite , amphiboles
#13	1762	10,1	10,1	10,1	Illite	Minor illite
#14	1788	10.3, 8.6, 6.4	10.3, 8.6, 6.4	Destroyed	Illite, amphiboles, feldspars	Insignificant illite, amphiboles
#15	1886	10.3, 8.6, 6.4	10.3, 8.6, 6.4	8.6=0, 6.4=0	Illite, amphiboles, feldspars	Illite
#16	1956	10.3, 8.6, 6.4	10.3, 8.6, 6.4	6.4=0, 8.6=0	Illite, amphiboles, feldspars	Illite
#17	2032	8,6	8,6	8,6	Amphiboles	No clays
#18	2094	-	-	-	No clays	No clays

Adularia forms minute anhedral to euhedral crystals that are pseudo-orthorhombic and are usually diamond shaped. It occurs as replacement of sanidine and is occasionally deposited in veins as well as forming incrustations in fissured rocks. Where it occurs as a replacement of sanidine or K-feldspars, there is nearly an iso-chemical transformation to an optically and structurally different phase-adularia. In pseudomorphs after sanidine phenocryst, it produces a streaky extinction suggesting that the pseudomorphs are made up of numerous overlapping crystals of rhombic section. Adularia occurs in wells MW-04 at 1100 m to the bottom of the well. In well MW-02 and MW-07, adularia was not found.

Albite is a secondary mineral which by the breakdown of feldspars. The term albitization here is referred to replacement of primary K-feldspar and plagioclase phenocryst by hydrothermal albite. Albitized K-feldspar has a low refractive index and shows no zoning but typical chessboard like twinning is common. Albite alteration occurs from about 500 m to deeper zones in the Menengai.

Wollastonite is a calcium silicate mineral, which was noted at depth of the researched wells and was associated with the diminishing calcite. It is common in skarns or contact metamorphic rocks formed by the calcite-quartz reaction:

$$CaCO_3 + SiO_2 => CaSiO_3 + CO_2$$

Wollastonite is a metastable mineral at temperatures above $\geq 270^0$C. It is an alteration mineral which is usually associated with contact metamorphism and therefore its occurrence is probably related to the numerous intrusions in the caldera summit area. In the cuttings it appears as a white, colourless or grey and fibrous, aggregate of elongated fine radiating crystals. It rarely occurs as a single crystal and has an acicular habit. It is colourless in thin section with low interference colour of first order grey. The intense

CO_2 reported from the Menengai wells can be explained as a result of magma degassing and disintegration of calcite and the formation of wollastonite. It occurs mainly from 1450 m depth, in well MW-04 and from 1780 m in well MW-06, and prevails down to the bottom of the wells. Wollastonite was not found in well MW-02 and well MW-07.

TABLE 6: Results of XRD analysis of clay minerals from well MW-06

Sample no.	Depth (m)	d(001) UNT	d(001) GLY	d(001) HIT	Mineral	Type
#1	216	8,6	8,6	8,6	Feldspar, amphiboles,	No clays
#2	244	8.5, 6.5	8.5, 6.5	15.7=0	Amphiboles (weak) feldspars	No clays
#3	334	13.9, 10.1, 9.1, 6.5	13.9, 10.1, 9.1, 6.5	13.9, 10.1, 9.1, 6.5	Smectite, illite, feldspars	Insignificant smectite, illite
#4	414	8.6, 6.5	8.6, 6.5	8.6, 6.5	Amphiboles, feldspars	No clays
#5	552	-	-	-	No clays	No clays
#6	684	13,7	13,7	13,7	Minor smectite	No or minor smectite
#7	784	13.2, 10.1	13.2, 10.1	13.2, 10.1	Minor smectite,	No or minor smectite
#8	834	13.2, 12.9, 10.1	13.2, 12.9, 10.1	13.2=0, 12.9=0	Smectite, illite	Minor smectite
#9	910	13.1, 10.1	13.1, 10.1	13.1=0	Smectite, illite	Illite-smectite
#10	994	13.7, 8.6, 6.5, 6.4	13.7, 8.6, 6.5, 6.4	-	Smectite,amphiboles, feldspars	Smectite
#11	1110	13.3, 10.1, 8.6, 6.4	13.3, 10.1, 8.6, 6.4	13.3, 10.1, 8.6, 6.4	Smectite, illite Amphiboles, feldspars	Smectite, illite
#12	1238	8.6, 8.1, 6.5	8.6, 8.1, 6.5	8.6, 8.1, 6.5	Amphiboles, feldspars	No clays
#13	1498	-	-	-	No clays	No clays
#14	1564	10.1, 8.6, 6.4	10.1, 8.6, 6.4	10.1, 8.6, 6.4	Illite, amphiboles, feldspars	Minor illite, actinolite
#15	1628	11.8, 10.4, 6.5	11.8, 10.4, 6.5	-	Illite, amphiboles, feldspars	Illite, amphiboles
#16	1668	10.2, 8.6	10.2, 8.6	-	Illite, amphiboles	Minor amphiboles, illite
#17	1684	10.2, 8.6	10.2, 8.6	-	Illite, amphiboles	Minor amphiboles, illite
#18	1800	10.3, 8.6	10.3, 8.6	-	Illite, amphiboles	Minor illite, amphiboles

Actinolite is a member of amphibole group, which is a high temperature mineral, mostly found in altered and metamorphic iron rich basic rocks. It is an intermediate solid solution member between ferro-actinolite and tremolite. Usually, it appears as green to grey-green groundmass mineral, although the colour varies depending on the amount of iron. It usually occurs as radiating, acicular crystals or a massive to granular aggregates in the groundmass. In thin section, it is pale green to dark green with strong pleochroism and moderate relief. The interference colours of actinolite depend on the iron and magnesium content and are usually green or brown. It is formed by the replacement of ferromagnesian minerals in association with epidote and chlorite. Actinolite appeared from 2020 m in well MW-06 and at 1964 m in well MW-07. Actinolite was not found in well MW-02 and MW-04. Actinolite is a high temperature mineral which indicates temperature of above 280^0C and occurs as a replacement product of chlorite or pyroxene.

4.4.3 Vein and vesicle fillings

Veins form where the fluids flow through open space fractures and precipitate mineralization along the walls of the fracture, eventually filling it completely. The form of mineralization and alteration associated with faults is highly variable, and may include massive to fine-grained, networks of veinlet's, and occasionally vuggy textures. Deposition of alteration minerals in veins, vesicles and vugs depend on various factors such as porosity, fluid composition, temperature, permeability and duration of the interaction of fluid and the host rock. In geothermal veins, the initial minerals to are usually fine grained clays and low temperature silica (chalcedony). As the temperature increases and hydrothermal alteration progresses, this low temperature metastable minerals assemblage transforms towards equilibrium at high-temperature yielding minerals such as wollastonite, quartz, chlorite, actinolite epidote etc. Pyrite infill vesicles at a wide range of temperatures imply the steady flux of sulphide in the permeable rocks.

TABLE 7: Results of XRD analysis of clay minerals from well MW-07

Sample no	Depth (m)	d(001) UNT	d(001) GLY	d(001) HIT	Mineral	Remarks
#1	68	8.7, 6.5	8.7, 6.5	8.7, 6.5	Amphiboles , Feldspars	No clays
#2	182	8.5, 6.5	8.7, 6.5	8.7, 6.5	Amphiboles , Feldspars	No clays
#3	388	10.1, 6.5, 6.4	10.1, 6.5, 6.4	10.1, 6.5, 6.4	Amphiboles , Feldspars	No clays
#4	472	-	-	-	-	No clays
#5	530	10,3	10,3	10,3	Amphiboles , illite Feldspars	Illite
#6	614	7,2	7,2	7.2=0	-	No clays
#7	716	14.6, 10.3, 7.2	14.6, 10.3, 7.2	14.5=0, 7.2=0	Chlorite, smecite	Trace smectite, chlorite
#8	822	10,3	10,3	10,3	Illite	Illite
#9	916	7,18	7,18	7.18=0	Kaolinite	Disordered Kaolinite
#10	962	-	-	-	No clays	No clays
#11	1018	10,2	10,2	10,2	Illite	Trace illite
#12	1068	10.2, 7.1, 6.5, 6.4	10.2, 7.1, 6.5, 6.4	7.4=0	Illite, kaolinite, feldspars	Trace illite
#13	1100	10.2, 7.1	10.2=0, 7.1=0	10.2=0, 7.1=0	Chlorite, illite	chlorite, minor illite
#14	1150	7,2	7,2	7.2=0	Kaolinite	Trace of diordered kaolinite
#15	1246	-	-	-	-	No clays
#16	1368	-	-	-	-	No clays
#17	1482	-	-	-	-	No clays
#18	1558	13.3, 6.5	13.3, 6.5	13.3=0	Chlorite, Feldspars	Smectite
#19	1634	6,5	6,5	6,5	Feldspars	No clays
#20	1740	-	-	-	-	No clays
#21	1872	10.3, 8.5, 6.4	10.3, 8.5, 6.4	10.3, 8.5, 6.4	Illite, Amphiboles, feldspars	Illite, amphiboles
#22	1960	10.3, 8.6, 6.4	10.3, 8.6, 6.4	10.3, 8.6, 6.4	Illite, Amphiboles, feldspars	Illite, amphiboles

Vein minerals in Menengai field include calcite, quartz, prehnite and epidote. Due to use of rotary drilling in the study wells, most of the macroscopic vein fillings and amygdales textures were lost.

4.4.4 Hydrothermal mineral zonation

Some secondary minerals are good geothermometers and are stable at specific temperatures, crystallizing at distinct temperature range (Reyes, 2000). With few exceptions, minerals that provide information on their formation temperatures are those that contain in their structures either (OH) or nH_2O (Reyes, 2000). They include clays, prehnite, zeolites, garnet and amphiboles. The distribution of alteration minerals gives information about formation temperature at the time of deposition. Reaction of host rock with hydrothermal fluids has formed a prograde hydrothermal alteration sequence with depth. Alteration zones in the Menengai geothermal system have been defined by the presence of one or more index minerals. The distribution of key indicator minerals overlaps to some extent, so the top of the zone is normally defined at the depth when reasonable index mineral appears. Therefore, depth boundaries vary from well to well. Four hydrothermal alteration zones were identified within Menengai geothermal field.

Unaltered zone (0-380 m)
This zone represents the shallow depth of the study wells. It extends from 0-444 m, 0-430 m and from 0-386 m depth in wells, MW-04, MW-06 and MW-07 respectively. This zone represents the fresh young post-caldera lava. This zone is characterized by fractured fresh and mildly oxidized lava with some minor tuff intercalations as illustrated in Figures 11-14.

Smectite-zeolite zone (380-750 m)
This zone forms the lowest grade alteration zone and is mainly represented by cowlescite and mesolite as the index minerals. In all wells this zone is characterized with abundant calcite and appearance of some pyrite. Zeolite decline in abundance with depth in this zone and illite and quartz appears as illustrated in Figures 11-14. In well MW-02, smectite appears from 300 m to 800 m and well MW-07; smectite persisted to 1200 m depth. However it disappears at about 650 m and 700 m in well MW-04 and MW-06 respectively.

Quartz-illite zone (750-1150 m)
This zone corresponds with the upper zone of the geothermal reservoir in Menengai system. The zone is characterized by the occurrence of secondary quartz which occurs as a replacement of chalcedony and illite clays. Quartz indicates temperature over 180°C (Reyes, 2000). The depth and thickness of this zone is variable from well to well. Illite started appearing from 500 and 620 m, respectively, in wells MW-04 and MW-06. Its presence indicates formation temperature of over 220^{O}C. However these minerals started appearing at slightly deeper zones in wells MW-02 and MW-07 as they occur from 1200 and 800 m depth in wells MW-02 and MW-07, respectively.

Illite-epidote zone (1150-1750 m)
This zone forms the deepest reservoir zone in well MW-02 and MW-07. The appearance of epidote indicates formation temperature of above 230^{o}C. Epidote was first recognized in well MW-02 and well MW-07 from 1400 and 1100 m, respectively.

Wollastonite-actinolite zone (1750-2190 m)
Wollastonite and actinolite were only found in well MW-04 and MW-06. Actinolite and wollastonite were not found in wells MW-02 and MW-07. Wollastonite and actinolite indicate formation temperature of over 270°C and over 280°C respectively (Franzson, 1998). Wollastonite was first identified at about 1800 and 1600 m depth in wells MW-06 and MW-04, respectively. This is the final and the deepest alteration zone. Actinolite was first recognized in wells MW-04 and MW-06 at 1840 and 2064 m, respectively.

4.4.5 Alteration minerals geothermometry

Hydrothermal index minerals such as epidote, quartz, wollastonite and illite were used in this study to compare the alteration minerals and measured temperature. The formation of alteration minerals evolves progressively from low-temperature to high-temperature minerals with the last mineral to precipitate appearing on top or at the centre of the sequence. The sequence of deposition can therefore be used to determine the thermal history and relative time scale of alteration minerals within geothermal system (e.g. Franzson, 2010). Wells MW-04 and MW-06 indicate higher formation temperatures than the alteration temperature (Figure 15).

The inferred reservoir temperature is between 200 and more than 270°C based on the occurrence of quartz, illite, epidote, wollastonite and actinolite as shown in Figure 15. However, the measured temperatures from wells MW-04 and well MW-06 below 1900 m depth in the wells recorded temperature of over 350°C suggesting the system is heating up. Fluid inclusion studies on quartz and calcite (Mibei, 2012) indicate that the system is heating up within the caldera summit area where the study wells are located.

4.5 Aquifers

Structural features like fractures, faults, joints, lithological contacts, clasts, fragmented matrixes and palaeosoils are positive indicators of geothermal feed-zones (e.g. Reyes, 2000; Franzson, 1998). These zones are associated with abundance of calcite and pyrite. The rocks are generally highly altered implying high interaction of fluids with the host rock as a result of good permeability. In contrast, low permeable zones are associated with less altered rocks implying less or insignificant water-rock interaction. The movement of subsurface fluid is controlled by the type of the rock formations,

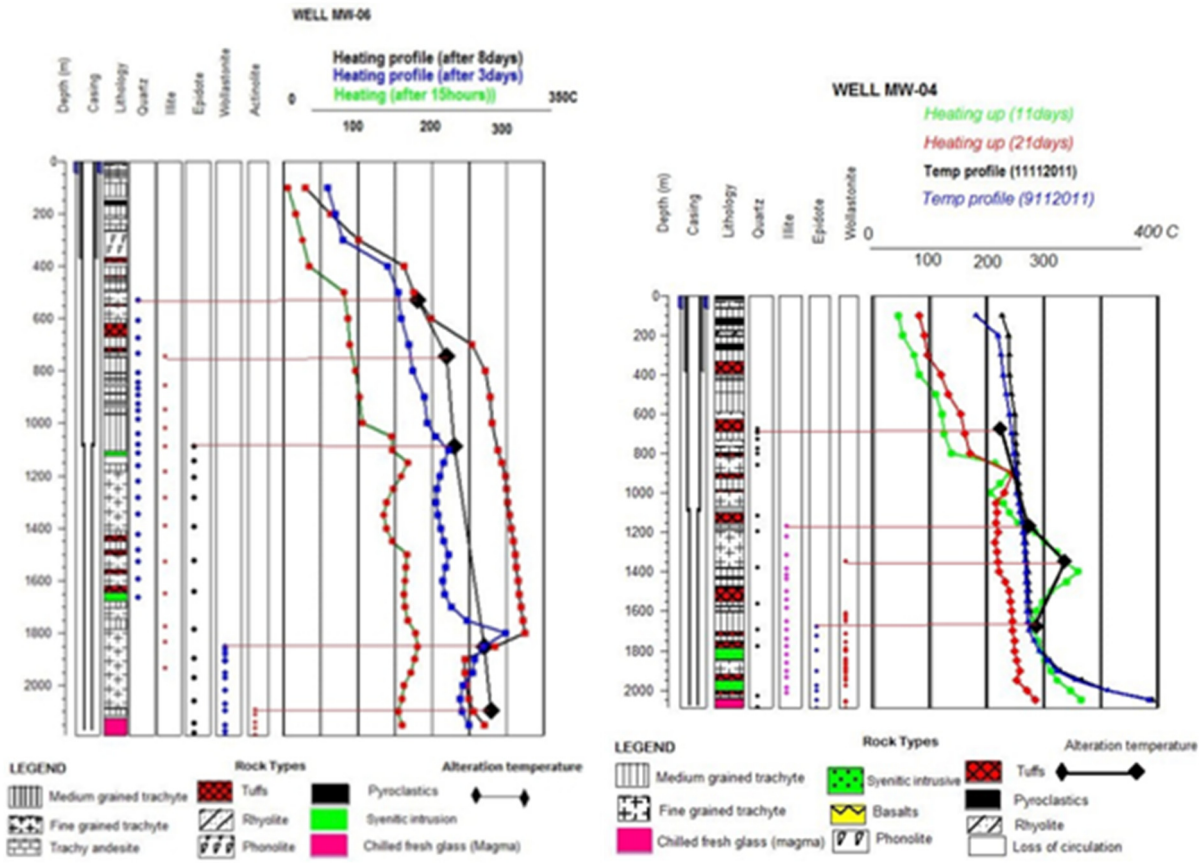

FIGURE 15: Lithostratigraphy, selected alteration minerals, temperature logs in correlation with the status of geothermal system in wells MW-04 and MW-06.

characteristics of its permeability, porosity, hydraulic gradient, temperature, pressure and the nature of natural recharge (Reyes, 2000).

In the Menengai geothermal field, most of the aquifers are related to lithological boundaries and margins of intrusions which are associated with fracture permeability in the reservoir. Aquifers can either be cold or hot. The accurate locations of aquifers were established using down-hole temperature pro-files, circulation loss zones, penetration rates as well as hydrothermal alteration. In the studied wells, aquifers were found to occur at 3-4 different depths intervals.

In well MW-04, aquifers occur at 250-300, 850-900, 1500-1550 and 1900-2000 m depth (Figure 16). However from temperature logs, from 1850-1900 m depth to the bottom of the well, there seem to be low permeability, but the well is very hot reaching bottom hole temperatures of 398°C. For geothermal exploitation of deep aquifers, the two cold aquifers in the upper part of the well were cased off to avoid quenching of the deeper hot aquifers. Production casing in this well was positioned at 1092 m depth. Aquifers at the bottom of this well, which were associated with circulation losses recorded temperature as high as 398°C indicating that, any possible mobile fluid at this feed-zone is superheated.

Aquifers in well MW-06 were identified in five distinct areas; at 350-400, 1000-1100, 1450-1500, 1800-1900 and 2050-2090 m depths. With the production casing set at 1088 m depth, the upper shallow cold aquifer was cased off (Figure 17). The feed-zone at 1800 m depth reached temperatures of almost 350°C (slightly below the critical temperature of water, 374°C), implying that the steam at this zone may be super-heated as was later suggested to be as a result of shallow heat source evidenced by the presence of fresh chilled and quenched glass cuttings at 2174 m depth. It is interesting how hot the well is only after 8 days of heating up (Figure 17). Normally the well requires significantly longer heating up time to reach anything close to the formation temperature.

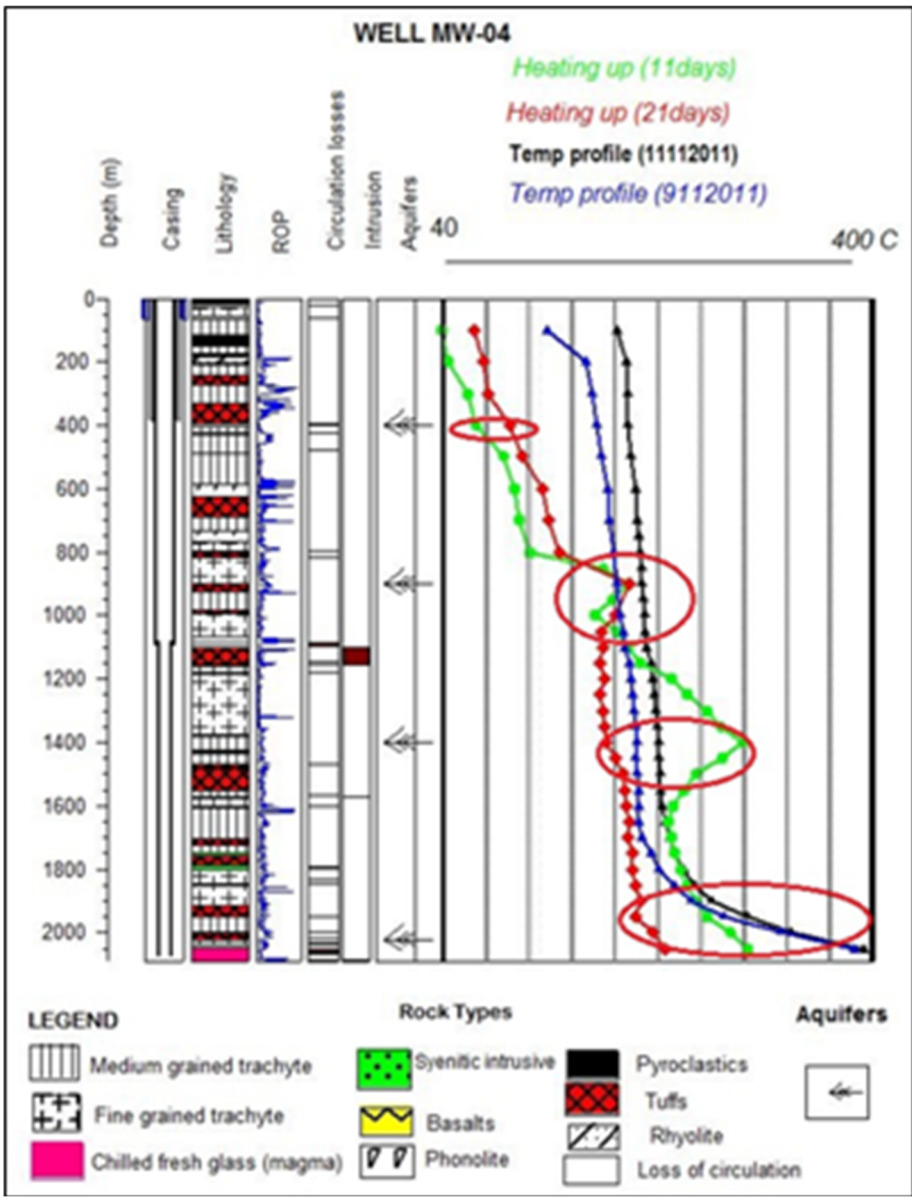

FIGURE 16: Lithostratigraphy, penetration rate and aquifers in well MW-04; aquifers are inferred from loss of circulation, penetration rate and temperature logs

Four aquifers were identified in well MW-02 (Figure 18). These aquifers were at 250-300, 1000-1100, 2200-2250 and 3100-3150 m depth. The aquifers were inferred from circulation losses, high penetration rates, loss of circulation and from temperature profiles. Most of the aquifers in well MW-02 are occurs between contact boundaries. Well MW-02, which was drilled to 3189 m never discharged upon opening and the temperature logs indicate maximum temperature of less than 200°C, one year after drilling.

The temperature logs (Figure 18) show cold down-flow between 1100-200 m. This can be attributed by several factors. From rock chemistry of the cuttings samples, well MW-02 plots with the rift-rock samples (see Figure 20) outside the caldera as opposed to other samples which plot in the more evolved trachytic section. The well was sunk in pre-caldera volcanics (Section 4.6) and therefore it may be located by the Menengai caldera fault zone where vertical permeability may allow cold inflow to penetrate into the well, as the production casing was set at 791 m depth, and cool down deeper and hot aquifers.

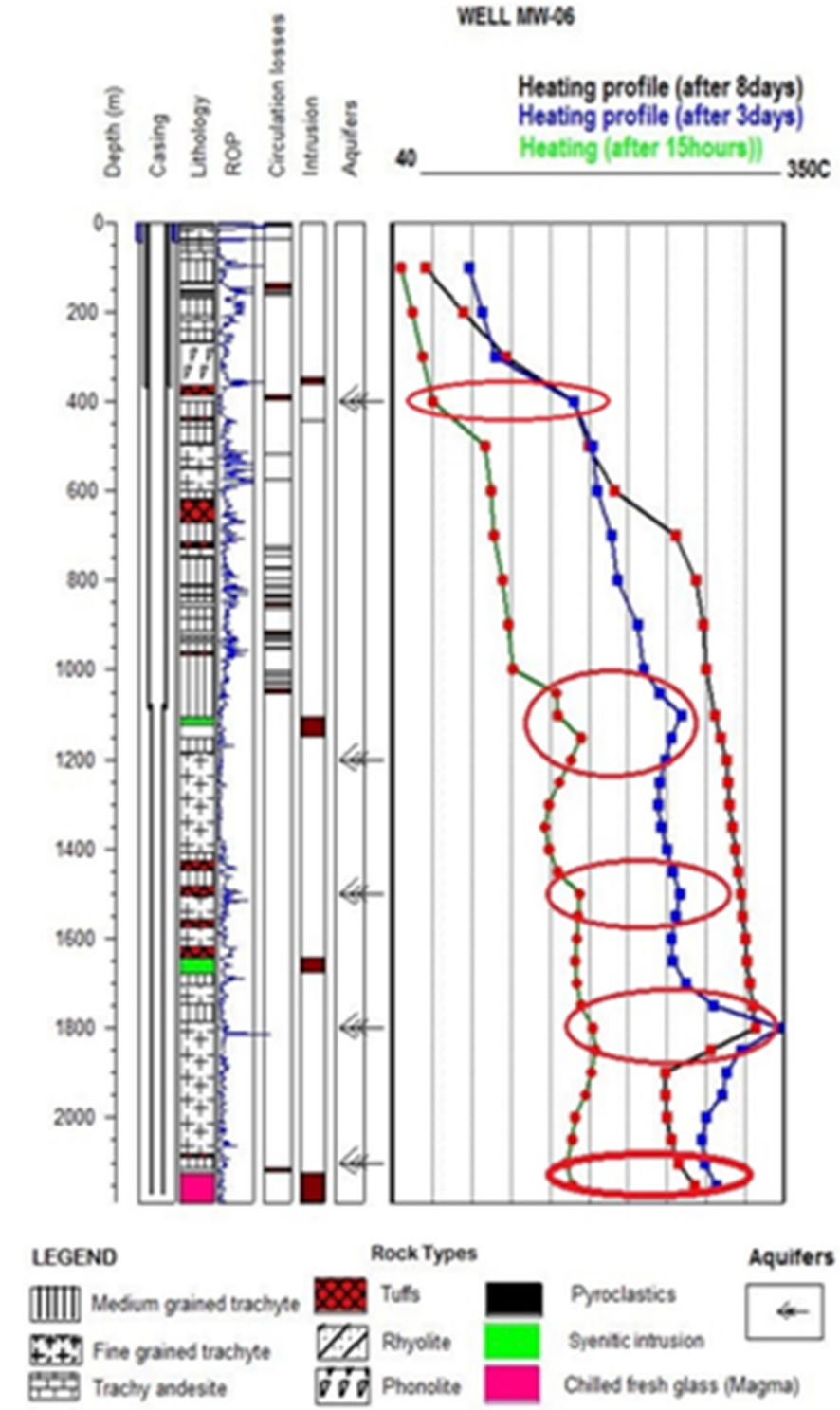

FIGURE 17: Lithostratigraphy, penetration rate and aquifers in well MW-06; aquifers are inferred from loss of circulation, penetration rate and temperature logs

Aquifers in well MW-07 were found in three distinct depths (Figure 19). These aquifers were at 400-450, 1500-1500 and 1900-2000 m depth. However, the upper aquifer was cased off, since the production casing was set at 1168 m depth (Figure 19). Due to unavailability of penetration rate data and temperature profiles, aquifers were identified by circulation losses coupled with intensity of alteration at lithological boundaries. Logging of equilibrated temperature was not conducted below 900 m due to obstructions in the well, so the temperature below 900 m is not known. The well never discharges upon opening and therefore very scarce information about it is available.

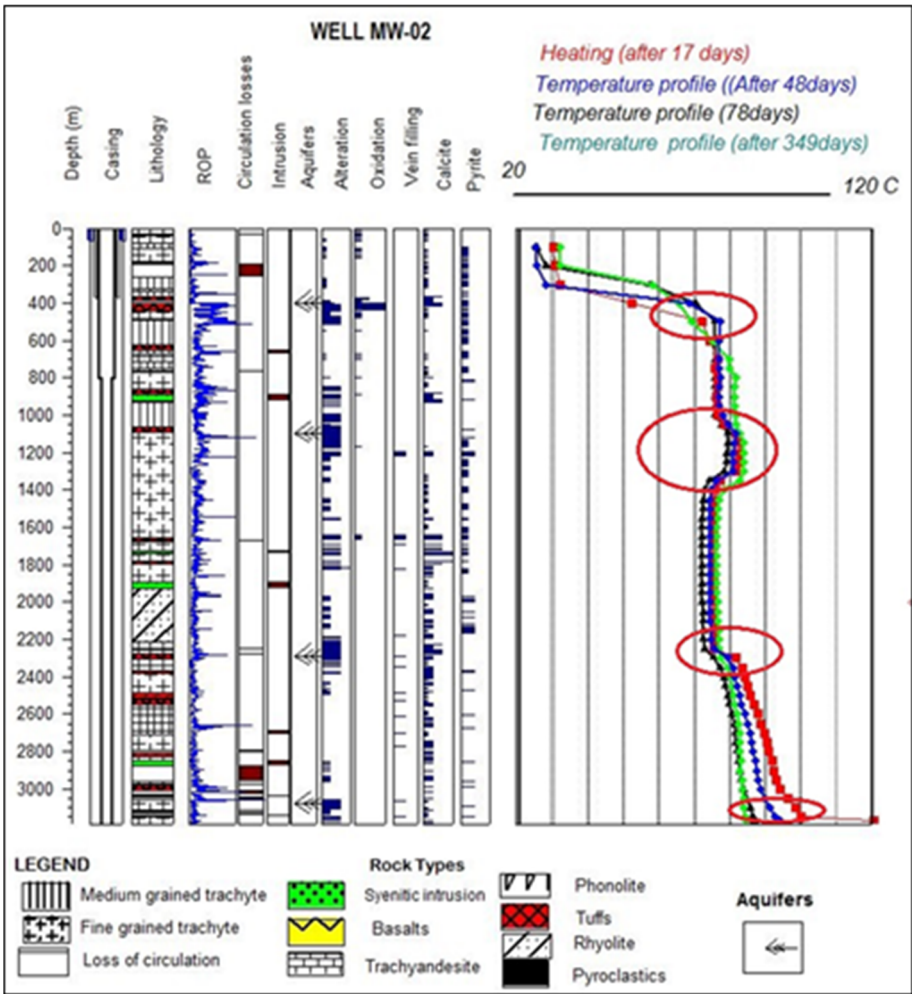

FIGURE 18: Lithostratigraphy, penetration rate and aquifers in well MW-02; aquifers are inferred from loss of circulation, penetration rate and temperature logs

4.6 Whole-rock chemistry

4.6.1 Classification of rock types

Petrologists have developed several ways of classifying different rock types. As techniques for chemical analyses of silicate rocks were developed, it was soon recognized that these compositional data are valuable in the development of petrological concepts. Since then, various methods of manipulating chemical data, and chemical classifications, have been published. However, no single method is conclusive in classifying all igneous rocks. Traditionally, the so called TAS diagram based on total alkalies (Na2O+ K2O) and silica concentrations, has been used to separate alkalic and sub-alkalic rocks. The diagram was first proposed by Iddings (1892) and has been further developed, by several authors, for example, and Harker (1909), Le Bas et al. (1986), Macdonald and Katsura (1964) and Mitchell (1986). Results of 101 samples, on major and trace elements of the study wells is shown in Tables 8-12, below.

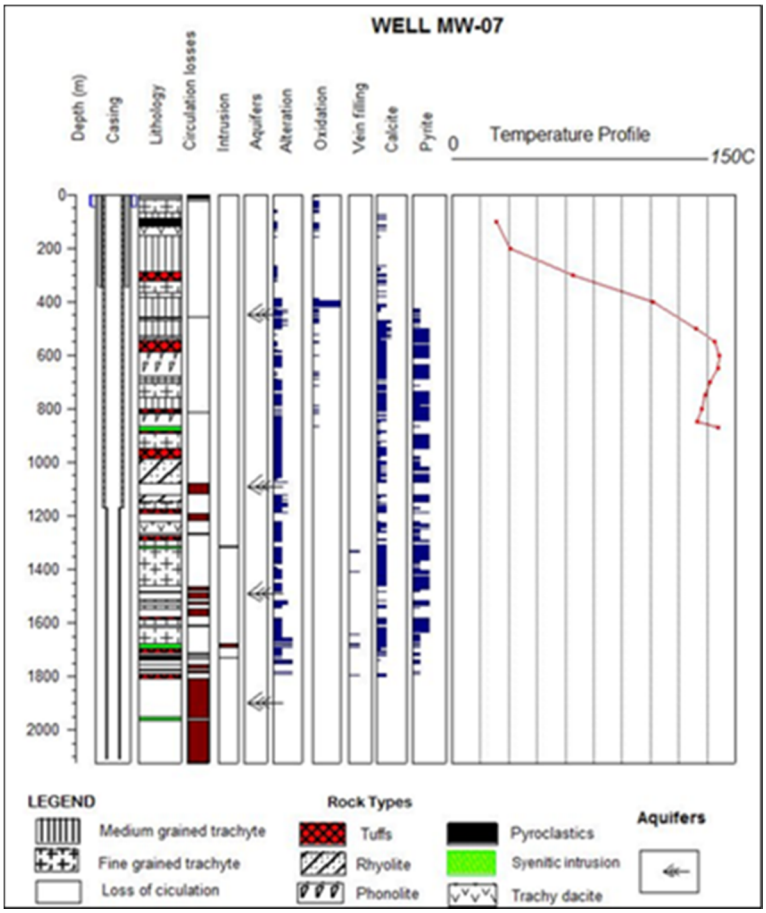

FIGURE 19: Lithostratigraphy, loss of circulation and aquifers in well MW-07, aquifers are inferred from loss of circulation, and temperature logs

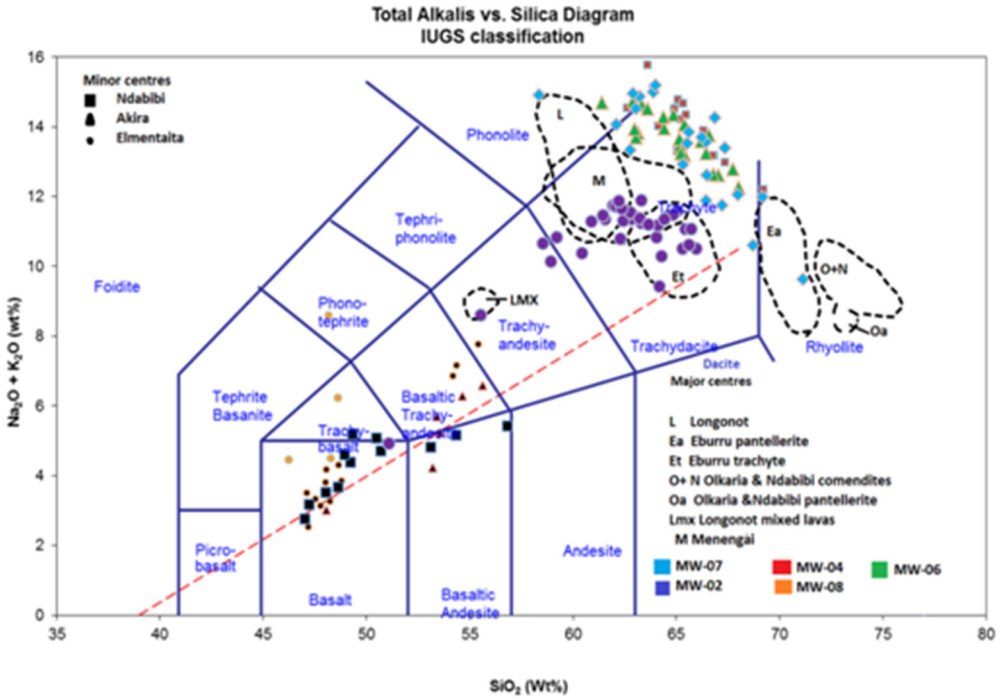

FIGURE 20: Alkali-silica plot showing the compositional range of Menengai subsurface rocks from wells MW-02, MW-04, MW-06, MW-07 and MW-08 and the neighbouring volcanic centres (modified from Clarke et al., 1990; Macdonald, 2006; Mitchell, 1986)

TABLE 8: Major and trace elements of Well MW-02 based on ICP-ES analyses

Major elements in wt. %.																		
Depth (m)	**154**	**270**	**344**	**472**	**546**	**628**	**712**	**806**	**948**	**1060**	**1110**	**1232**	**1338**	**1430**	**1520**	**1646**	**1728**	**1816**
SiO_2	65.44	64.63	65.05	64.04	65.71	64.11	63.07	64.17	62.30	65.29	64.29	61.95	62.81	62.42	63.29	62.76	63.23	62.30
Al_2O_3	12.21	13.65	13.40	12.90	12.75	13.68	14.20	13.27	12.85	12.75	14.22	15.67	14.68	15.24	15.61	15.20	14.38	15.65
FeO	8.68	7.29	7.07	8.94	7.96	8.18	8.15	8.91	8.43	8.62	7.80	8.12	7.66	7.77	7.15	7.21	8.19	7.47
MnO	0.34	0.33	0.31	0.34	0.28	0.30	0.32	0.46	0.33	0.36	0.30	0.36	0.32	0.30	0.32	0.33	0.34	0.34
MgO	0.18	0.30	0.32	0.40	0.16	0.20	0.29	0.23	0.44	0.24	0.35	0.29	0.34	0.31	0.35	0.37	0.35	0.37
CaO	1.08	1.37	1.35	1.39	1.21	1.44	1.69	2.71	3.78	1.25	1.80	1.04	1.87	1.72	1.12	1.64	1.26	1.24
Na_2O	6.46	6.50	6.67	6.15	5.51	5.35	6.28	3.97	6.18	5.70	4.91	6.64	5.95	5.92	6.06	6.24	6.47	6.18
K_2O	4.62	4.95	4.91	4.67	5.56	5.84	5.14	5.45	4.61	4.80	5.38	5.11	5.40	5.40	5.19	5.31	4.89	5.52
TiO_2	0.68	0.69	0.68	0.79	0.60	0.57	0.60	0.54	0.77	0.70	0.64	0.52	0.66	0.61	0.63	0.65	0.61	0.63
P_2O_5	0.07	0.11	0.10	0.16	0.11	0.16	0.08	0.12	0.13	0.09	0.14	0.07	0.14	0.14	0.11	0.11	0.08	0.11
Trace elements (ppm)																		
Ba	17.92	101.74	105.78	347.65	114.29	127.89	306.16	237.79	252.85	158.63	161.99	59.51	384.54	328.77	90.92	86.02	97.72	88.62
Co	4.62	4.67	4.83	6.65	4.11	4.03	4.51	4.75	7.03	5.08	4.91	4.20	5.42	6.21	4.28	5.66	5.32	4.08
Cr	4.95	8.22	7.53	5.72	2.62	9.72	9.98	4.73	11.99	7.55	16.08	16.82	23.79	20.27	8.07	31.24	26.08	13.60
Cu	18.38	17.50	17.41	22.29	23.54	24.20	22.46	23.42	24.08	20.32	24.49	22.31	28.33	24.08	18.70	26.00	25.49	22.85
La	316.98	205.66	164.18	256.73	164.73	196.22	182.22	184.08	208.73	219.42	181.41	265.09	155.41	176.96	191.32	221.35	183.43	217.13
Ni	3.03	3.95	3.28	5.68	2.30	3.09	6.39	4.05	9.05	5.56	6.97	6.40	6.08	10.10	2.93	4.33	8.53	8.37
Rb	65.27	82.35	97.53	69.19	99.51	92.33	67.07	57.36	71.29	114.26	83.94	94.34	120.66	86.55	91.78	99.52	57.76	105.37
Sc	3.04	4.87	5.55	4.49	2.40	2.24	3.36	2.11	4.10	3.78	3.76	2.66	3.74	3.35	4.04	4.57	3.66	4.13
Sr	9.86	13.52	11.35	49.78	18.39	21.88	31.22	24.17	51.26	13.58	19.23	16.61	35.88	32.21	20.18	23.49	17.99	24.64
V	10.41	7.25	9.83	22.22	7.73	8.97	15.39	16.45	15.96	20.68	26.28	31.39	15.08	14.00	6.60	11.40	18.31	12.59
Y	240.47	154.16	128.07	185.26	137.92	174.88	155.01	205.49	165.70	181.66	157.77	208.43	148.43	149.41	153.75	153.80	165.38	162.14
Zn	237.36	173.85	160.25	215.41	167.05	174.05	176.25	164.88	193.59	202.39	180.59	207.28	161.08	166.95	162.69	201.17	175.46	166.51
Zr	1414.90	921.52	769.44	1111.09	720.30	937.58	847.75	763.67	901.62	958.18	776.73	1295.25	700.81	763.72	852.26	768.18	1035.92	947.58

TABLE 9: Major and trace elements of Well MW-04 based on ICP-ES analyses

Sample	**186**	**490**	**624**	**734**	**846**	**988**	**1074**	**1180**	**1274**	**1340**	**1462**	**1544**	**1608**	**1704**	**1824**	**1970**
Major elements in weight %																
SiO_2	69.23	65.08	63.89	62.63	66.82	65.33	63.61	64.16	64.91	65.23	67.37	65.49	66.33	65.34	66.75	65.05
Al_2O_3	8.93	11.77	11.82	12.47	10.63	12.33	11.72	11.52	12.02	11.77	10.36	11.48	10.51	11.06	10.48	9.91
FeO	7.53	5.88	6.12	5.77	6.79	4.18	5.98	7.00	5.69	5.71	7.26	6.44	7.02	7.33	7.27	8.41
MnO	0.29	0.23	0.24	0.21	0.26	0.16	0.23	0.25	0.23	0.23	0.30	0.26	0.29	0.30	0.31	0.32
MgO	0.10	0.24	0.38	0.76	0.24	0.39	0.33	0.40	0.36	0.34	0.07	0.14	0.16	0.34	0.21	0.17
CaO	0.93	1.32	1.44	2.23	1.14	1.83	1.42	1.62	1.37	1.54	0.86	1.00	1.02	1.26	1.02	1.99
Na_2O	6.49	7.78	7.82	7.48	6.28	5.55	7.29	6.59	6.76	6.66	6.37	7.60	7.14	7.22	6.72	7.34
K_2O	5.70	6.98	7.30	7.05	6.89	9.10	8.48	7.42	7.75	7.54	6.61	6.73	6.73	6.31	6.45	5.97
TiO_2	0.58	0.54	0.71	0.97	0.63	0.63	0.71	0.81	0.68	0.68	0.53	0.51	0.57	0.62	0.58	0.62
P_2O_5	0.05	0.04	0.10	0.17	0.09	0.27	0.14	0.12	0.13	0.17	0.02	0.12	0.05	0.06	0.06	0.04
Trace elements (ppm)																
Ba	10.97	85.03	350.07	1516.92	375.47	1693.55	164.07	151.62	231.36	156.32	25.16	15.89	26.78	23.41	22.84	19.66
Co	3.58	4.56	6.43	10.29	4.43	5.11	5.24	10.54	9.90	5.57	3.87	3.65	4.36	7.12	10.87	4.51
Cr	0.00	0.00	0.00	0.00	0.00	0.00	0.00	20.85	11.13	3.48	0.00	0.00	0.00	0.59	5.40	0.00
Cu	65.19	12.41	21.58	8.23	19.87	11.49	14.94	15.56	23.07	12.56	16.81	15.41	13.96	17.55	12.91	44.37
La	208.57	155.28	156.17	81.97	231.14	45.18	88.28	91.58	84.79	94.07	325.01	222.52	206.30	195.63	204.56	232.29
Ni	11.59	0.00	3.02	0.13	0.00	0.00	3.55	0.62	1.43	1.22	0.00	0.00	0.12	0.00	3.00	2.87
Rb	298.86	133.79	180.85	177.14	275.74	252.52	207.04	202.13	127.51	219.44	278.73	301.21	368.46	229.33	234.01	177.65
Sc	3.06	4.59	5.47	7.57	3.68	6.43	7.25	7.56	6.68	7.45	1.96	2.69	3.44	4.79	3.86	2.51
Sr	7.88	11.63	26.41	160.39	31.94	60.06	10.64	12.69	15.01	11.67	13.38	8.57	9.31	12.44	9.36	21.76
V	0.51	0.00	0.00	13.77	1.58	9.76	0.00	0.00	0.00	0.00	0.00	4.27	0.00	16.66	1.70	0.00
Y	184.90	127.24	125.44	61.10	209.83	39.87	68.94	72.53	60.95	71.14	257.61	193.81	167.13	166.52	166.54	218.10
Zn	238.83	146.20	156.89	112.00	206.08	72.72	132.08	127.83	109.36	112.79	246.77	166.67	174.05	176.43	176.58	260.69
Zr	757.52	623.89	558.67	254.99	981.53	107.40	264.38	287.65	252.44	532.00	1264.78	1324.81	739.50	742.76	753.47	866.66

TABLE 10: Major and trace elements of well MW-06 based on ICP-ES analyses

Depth (m)	**100**	**188**	**288**	**406**	**480**	**564**	**638**	**744**	**828**	**926**	**1038**	**1152**	**1226**	**1362**	**1408**	**1536**	**1650**	**1788**	**1820**	**1966**	**2080**	**2190**
Major elements in wt. %.																						
SiO_2	65.42	65.19	61.42	66.20	66.44	64.42	66.60	64.40	63.15	63.04	63.34	64.88	62.97	65.42	63.60	67.74	67.06	68.02	65.16	66.81	65.24	62.92
Al_2O_3	10.01	10.26	12.17	10.29	9.77	13.63	11.87	12.55	13.07	12.31	12.38	11.66	13.07	12.15	12.94	9.93	10.55	10.42	10.90	10.14	10.89	9.70
FeO	8.69	8.56	9.02	7.45	7.85	4.25	4.46	4.87	5.14	6.24	4.84	6.59	6.17	5.65	6.16	7.30	7.58	7.12	7.26	7.45	7.96	9.11
MnO	0.32	0.32	0.37	0.28	0.29	0.15	0.17	0.18	0.21	0.23	0.19	0.26	0.22	0.20	0.24	0.29	0.30	0.28	0.26	0.30	0.30	0.37
MgO	0.13	0.10	0.16	0.24	0.36	0.69	0.50	0.54	0.75	0.92	0.93	0.22	0.67	0.32	0.30	0.16	0.06	0.12	0.44	0.43	0.26	0.53
CaO	1.34	1.22	1.17	1.11	1.24	2.06	1.71	1.95	2.52	2.33	2.58	1.18	1.97	1.39	1.35	0.97	1.05	0.97	1.49	1.40	1.25	1.52
Na_2O	6.98	7.16	7.91	7.10	7.17	6.09	5.81	6.22	6.16	6.51	6.97	7.53	6.33	6.45	6.51	6.35	6.42	5.61	7.59	6.69	6.15	8.57
K_2O	6.22	6.30	6.78	6.49	6.06	7.86	7.95	8.06	7.66	7.17	7.64	6.82	7.61	7.60	7.99	6.44	6.19	6.66	6.06	5.94	7.08	6.16
TiO_2	0.67	0.65	0.75	0.61	0.57	0.58	0.68	0.79	0.80	0.87	0.73	0.63	0.76	0.61	0.69	0.57	0.50	0.57	0.58	0.60	0.62	0.79
P_2O_5	0.05	0.05	0.04	0.04	0.03	0.09	0.13	0.25	0.31	0.19	0.21	0.09	0.14	0.12	0.11	0.05	0.08	0.05	0.06	0.05	0.06	0.08
Trace elements (ppm)																						
Ba	11.07	0.00	14.40	32.01	17.04	749.31	491.26	1228.2	1143.5	963.00	1189.34	62.05	413.38	224.72	137.97	83.78	26.05	26.70	24.93	19.95	25.05	292.55
Co	5.48	5.17	5.37	5.64	6.18	8.20	6.14	6.94	8.02	8.86	8.42	5.19	8.27	4.77	6.56	4.58	3.33	4.61	7.01	6.02	6.04	8.80
Cr	0.00	0.00	0.00	11.73	2.80	21.16	12.65	0.00	0.00	16.97	3.30	0.00	11.45	1.21	3.10	0.00	0.00	0.00	0.00	1.01	2.58	0.17
Cu	11.66	14.39	13.45	13.16	13.37	13.66	15.98	7.95	12.94	11.52	14.07	10.13	19.64	10.16	12.65	10.08	7.03	7.49	19.90	16.24	13.49	19.13
La	204.09	246.57	283.27	218.99	292.04	118.60	65.63	60.19	61.06	60.57	57.35	163.43	67.43	80.83	101.64	235.94	223.96	190.76	205.38	259.37	227.4	329.14
Ni	1.64	2.98	0.00	0.00	0.00	6.41	0.24	0.00	0.00	3.23	0.00	0.00	0.00	0.00	0.00	0.00	0.00	0.00	1.47	0.00	0.00	3.04
Rb	240.23	166.35	0.60	260.89	307.16	137.61	203.97	239.17	85.86	314.60	156.65	200.01	34.29	197.67	195.88	380.49	438.38	345.03	427.75	317.44	227.4	266.14
Sc	3.98	3.29	3.37	3.40	3.72	5.65	7.28	8.61	10.18	11.01	9.96	4.95	9.44	6.64	6.66	3.22	2.32	3.69	4.97	4.80	4.27	5.17
Sr	13.83	9.53	14.01	15.42	13.56	53.49	25.15	47.89	113.28	90.85	115.80	15.43	37.60	17.89	13.12	12.43	8.95	8.28	15.93	14.85	12.73	30.47
V	6.33	0.00	30.50	11.14	14.14	61.99	18.76	0.00	31.92	31.85	36.59	0.00	8.33	0.00	6.32	0.00	0.00	0.00	30.45	35.72	16.49	36.47
Y	189.45	223.60	246.78	193.91	238.85	86.09	46.62	42.01	44.89	55.34	45.44	143.08	51.43	61.14	80.05	200.34	206.56	167.78	187.55	209.52	202.9	282.77
Zn	215.30	241.46	276.04	195.36	225.99	107.00	85.65	87.59	99.90	98.24	85.89	155.07	106.27	106.18	128.57	194.48	193.52	176.06	167.97	191.16	199.1	276.86
Zr	754.84	916.24	1121.66	956.79	1185.49	383.34	179.49	171.08	664.03	239.34	187.20	605.76	210.16	250.14	335.50	899.76	1058.69	721.00	823.05	931.12	851.9	1095.9

TABLE 11: Major and trace elements of well MW-07 based on ICP-ES analyses

Depth (m)	182	266	388	472	530	614	822	916	1018	1068	1100	1154	1246	1368	1482	1588	1634	1740	1872	1960	1962	1968
Major elements in wt. %.																						
SiO2	63.05	65.34	65.53	66.46	62.79	63.22	58.38	66.47	69.18	67.35	71.14	67.24	68.74	62.93	63.89	64.02	66.86	62.11	66.48	67.99	66.25	65.61
Al2O3	12.23	10.29	11.10	10.76	13.36	12.77	13.35	12.10	11.23	12.58	11.38	11.86	9.79	12.97	12.38	12.06	11.15	13.15	10.60	10.08	12.73	10.31
FeO	7.70	8.32	6.11	7.10	8.30	6.52	8.16	6.75	5.62	3.28	4.82	6.82	8.48	6.13	6.10	5.69	5.52	5.99	7.70	7.69	5.53	7.73
MnO	0.33	0.31	0.28	0.21	0.26	0.31	0.32	0.31	0.22	0.28	0.26	0.29	0.34	0.27	0.25	0.20	0.21	0.19	0.28	0.28	0.38	0.32
MgO	0.18	0.51	0.55	0.11	0.20	0.21	0.64	0.15	0.08	0.15	0.19	0.17	0.10	0.31	0.26	0.42	0.19	1.03	0.32	0.12	0.11	0.20
CaO	1.16	1.37	1.91	1.01	0.97	1.52	2.31	1.57	1.15	2.24	1.90	1.09	1.15	1.52	1.30	1.41	1.00	2.46	1.22	1.00	0.80	1.05
Na2O	7.38	6.76	6.89	6.17	5.93	4.66	6.00	4.64	5.27	5.31	4.68	5.24	2.80	6.86	7.04	7.44	6.84	6.51	7.37	5.43	6.34	7.31
K2O	7.13	6.14	6.62	7.39	7.39	10.20	8.90	7.23	6.71	8.08	4.95	6.51	7.79	8.07	7.94	7.74	7.42	7.55	5.25	6.61	7.35	6.53
TiO2	0.63	0.60	0.66	0.57	0.60	0.40	1.32	0.45	0.35	0.43	0.44	0.53	0.48	0.70	0.61	0.76	0.58	0.74	0.56	0.55	0.34	0.66
P_2O_5	0.05	0.08	0.12	0.06	0.07	0.04	0.44	0.16	0.04	0.09	0.06	0.09	0.06	0.14	0.13	0.17	0.11	0.14	0.05	0.04	0.03	0.06
Trace elements (ppm)																						
Ba	32.42	19.40	945.10	92.90	105.42	133.23	696.68	72.64	85.72	1.355.9	1.006.1	215.76	46.10	113.51	183.55	135.90	132.98	727.79	20.09	14.56	137.86	19.19
Co	3.72	6.62	6.66	4.08	5.31	3.10	19.83	2.56	1.38	3.02	2.95	3.82	4.59	5.26	4.66	6.19	3.48	9.98	4.60	4.66	1.99	4.95
Cr	0.00	10.85	0.00	0.00	10.38	0.00	17.97	0.00	0.00	0.00	0.00	0.00	29.82	10.41	32.97	0.42	2.07	30.67	0.00	0.00	0.00	0.00
Cu	10.52	12.39	9.25	14.00	18.92	12.92	20.74	15.52	10.05	9.01	16.71	13.39	19.05	10.99	16.32	6.30	9.94	29.74	14.57	19.62	12.05	10.28
La	237.78	324.90	161.92	183.32	142.06	165.64	108.29	163.64	171.24	80.00	78.73	150.92	358.54	103.33	87.34	84.21	129.16	46.26	227.06	270.03	121.22	257.00
Ni	0.00	4.15	0.00	1.95	0.00	1.64	2.19	4.39	0.00	0.00	0.00	1.06	1.57	0.00	2.08	0.00	0.00	8.07	0.84	1.91	0.00	0.00
Rb	38.22	294.44	308.60	175.08	48.58	164.32	53.32	80.00	201.49	303.84	258.82	289.56	308.56	34.38	45.19	249.14	258.90	64.00	212.34	251.82	234.91	320.42
Sc	3.88	3.87	6.03	2.58	2.74	1.95	12.03	1.92	1.32	2.37	2.49	2.59	1.79	6.61	6.47	7.91	5.09	9.42	4.40	2.85	1.59	3.57
Sr	15.14	15.43	90.72	15.41	26.01	23.50	108.94	28.77	21.49	66.05	70.86	33.82	20.23	18.17	14.07	15.86	11.87	53.36	12.69	11.15	19.33	10.06
V	0.00	16.72	0.00	0.00	9.58	0.00	62.05	3.40	0.00	5.43	0.00	1.82	11.93	0.00	6.44	0.00	-10.19	52.98	36.50	30.00	0.00	3.30
Y	209.01	290.81	134.54	191.39	126.70	151.06	109.58	183.73	139.33	62.13	77.36	143.56	348.00	85.83	80.36	53.87	96.07	36.16	200.21	233.98	126.74	216.49
Zn	245.35	305.25	161.26	174.14	197.30	160.42	172.05	178.18	164.37	92.59	135.79	190.79	259.37	138.41	112.23	107.97	155.93	93.43	193.94	213.92	144.76	221.74
Zr	902.69	1.461	535.59	730.36	612.24	605.35	412.08	1.020	582.94	249.28	315.26	602.35	1.362.0	341.81	305.53	238.61	409.58	132.78	886.60	1.063.12	574.22	942.46

TABLE 12: Major and trace elements of well MW-08 based on ICP-ES analyses

Major elements in wt. %.													
Depth (m)	**SiO2**	**Al_2O_3**	**FeO**	**MnO**	**MgO**	**CaO**	**Na_2O**	**K_2O**	**TiO_2**	**P_2O_5**			
1640	48.17	14.89	11.68	0.25	3.56	7.59	4.90	3.68	2.87	2.15			
1700	48.63	15.16	11.18	0.18	5.13	9.64	4.85	1.38	2.48	1.14			
1782	46.25	14.18	14.46	0.22	5.38	9.64	3.40	1.04	3.47	1.68			
1784	48.30	14.55	11.37	0.20	6.84	10.58	3.26	1.24	2.39	0.97			
Trace elements (ppm)													
Depth (m)	**Ba**	**Co**	**Cr**	**Cu**	**La**	**Ni**	**Rb**	**Sc**	**Sr**	**V**	**Y**	**Zn**	**Zr**
1640	1174.0	50.40	12.14	29.21	65.92	15.16	0.00	21.89	556.49	195.01	56.22	109.48	225.33
1700	728.89	59.43	97.64	59.81	31.38	70.73	0.00	33.36	682.51	292.39	31.41	95.48	107.16
1782	1136.9	75.24	98.44	61.15	40.29	46.15	0.00	33.29	612.09	424.85	40.04	115.62	126.44
1784	1222.5	57.73	170.90	74.87	36.75	83.18	0.00	34.82	680.61	299.86	38.35	100.47	141.10

In Figure 20, the Menengai samples are plotted on the TAS diagram. The rocks show a chemical variation ranging from basalt through to trachyte and rhyolite in composition. It is instantly noticeable that the MW-02 samples do not plot with samples from the other analysed wells; in fact there is barely an overlap. The samples however, plot with published analyses of surface rocks which may indicate they were formed from a similar magma source as the regional rocks. These samples from well MW-02 plot in lesser evolved trachyte and therefore means, volcanics might have a similar source with the regional rift rocks (Figure 20). The variation and composition of both major and trace elements (see Figures, 27-31 later) shows that well MW-02 has different trends and concentrations compared with the other wells, suggesting that the lava was derived from a different magma source.

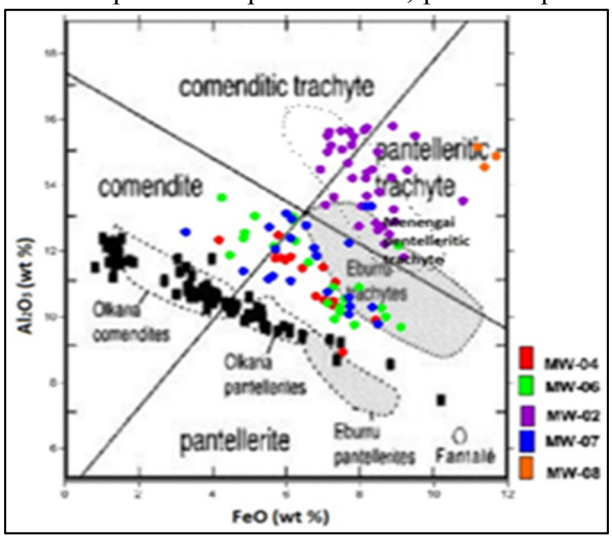

FIGURE 21: Al_2O_3 versus FeO classification of the Menengai rocks and the neighbouring volcanic centres (modified from Macdonald, 1974)

In Al_2O_3 versus FeO diagram, the studied subsurface samples display two unique distinct trends, with well MW-02 showing similar chemical clustering with surrounding surface samples from Menengai while the other wells, MW-04, MW-06 and MW-07 cluster between pantellerites and comendite (Figure 21). Selected samples from well MW-08 plots in the

pantelleritic trachyte field. The two plots clearly show the importance of fractional crystallization even though other processes like magma mixing, assimilation and hydrothermal activities may possibly be involved. This is addressed in subsequent sections. Geochemical trends for volcanic rocks represent a 'liquid line of descent'. This is the path taken by residual liquids as they evolve through the differential withdrawal of minerals from the magma (e.g. Cox et al., 1979).

4.6.2 Geochemical evolution of the Menengai caldera

The discussion on the geochemistry of the Menengai is based on 101 new whole-rock chemical analyses of drill cuttings from wells MW-02, MW-04, MW-06, MW-07 and MW-08. The results are compared and supplemented by the available surface geochemical data (Clarke et al., 1990; Leat 1983; Macdonald et al., 2006, 1994). Several elements were plotted in order to discriminate, what magmatic processes control the geochemical variation observed in the subsurface samples from the Menengai wells. All major elements were plotted against SiO_2 (Harker diagrams) for better interpretation (Figure 22). This study reveals that, TiO_2, FeO, MgO and CaO all show rather similar behavior and decrease as SiO_2 increases. These coherent groups, correlate strongly with each other as they are removed from the melt during fractional crystallization of ferromagnesian minerals and feldspar, whereas FeO content increase in more fractionated melts (Figure 22). Na_2O and K_2O are mobile and are rather easily leached from rocks during fluid-rock interaction and many rocks are in fact more scattered in those elements (Figure 22)

However, in spite of a few low-Na samples, most samples in this study surprisingly show little scatter as observed in relatively fresh surface rocks. Incompatible elements such as Zr, Rb and La found in the study wells are generally believed to be enriched in evolved magma (Figure 23). This is mainly interpreted to be as a result of crystal fractionation.

Ba and Zr show significant variation ranges and were used extensively in this study to depict the evolution episodes in different stratus. Zr was used in this study as an index of fractionation because of its incompatible character for early rock forming minerals and accordingly its large variation (0-1500 ppm, Figure 23). Zr also has high solubility in peralkaline melts (Leat, 1993) and has been used as abscissa in geochemical plots from many volcanoes of the Kenya rift valley. In the post-caldera volcanics, high Zr was recorded with very low Ba values. The same trend is repeated in the lower pre-caldera volcanics. This trend suggests the two volcanic units being more evolved compared to the syn-caldera and upper pre-caldera volcanics (Figure 24). Basaltic intrusive samples clearly show very low Zr with high iron suggesting a different source for the basalts as compared to the more evolved rocks.
A total of 13 trace elements were plotted in different variation and spider-diagrams. The distribution of trace elements suggests different evolutionary history for different volcanics as was depicted from different incompatible elements such as Ba and Zr (Figures 24, 25).

Averages of trace elements from each volcanic unit, from each well were plotted together for interpretation (Figure 25). The results show comparable trends in wells MW-04, MW-06 and MW-07. The post-caldera volcanics in all wells, plotted with the highest Zr values with upper pre-caldera volcanics plotting as the least evolved volcanics (Figure 25). Compatible trace elements concentrations change dramatically in an igneous liquid during fractional crystallization as they become depleted as the rocks evolves. For instance, the depletion trend of strontium (Figures, 24, 25 and 26) is probably as a result of fractional crystallization of plagioclase. Element distribution may, however, be slightly modified by geothermal alteration. Some of the scattering in variation diagrams was interpreted to be as a result of background "noise" introduced by using analyses of porphyritic samples (e.g. Wilson, 1989). Zr variation with depth of the study wells was tabulated along with lithostratigraphy of wells MW-02,

MW-04, MW-06 and MW-07 for comparison purposes (Figure 26). Comparable trends were depicted from wells MW-04, MW-06 and MW-07 and this enable a clear distinction of these volcanic units. However, well MW-02 shows completely different trend compared with the other studied wells. This trend therefore confirmed the earlier suggestions that well MW-02 volcanics are from completely different magma source.

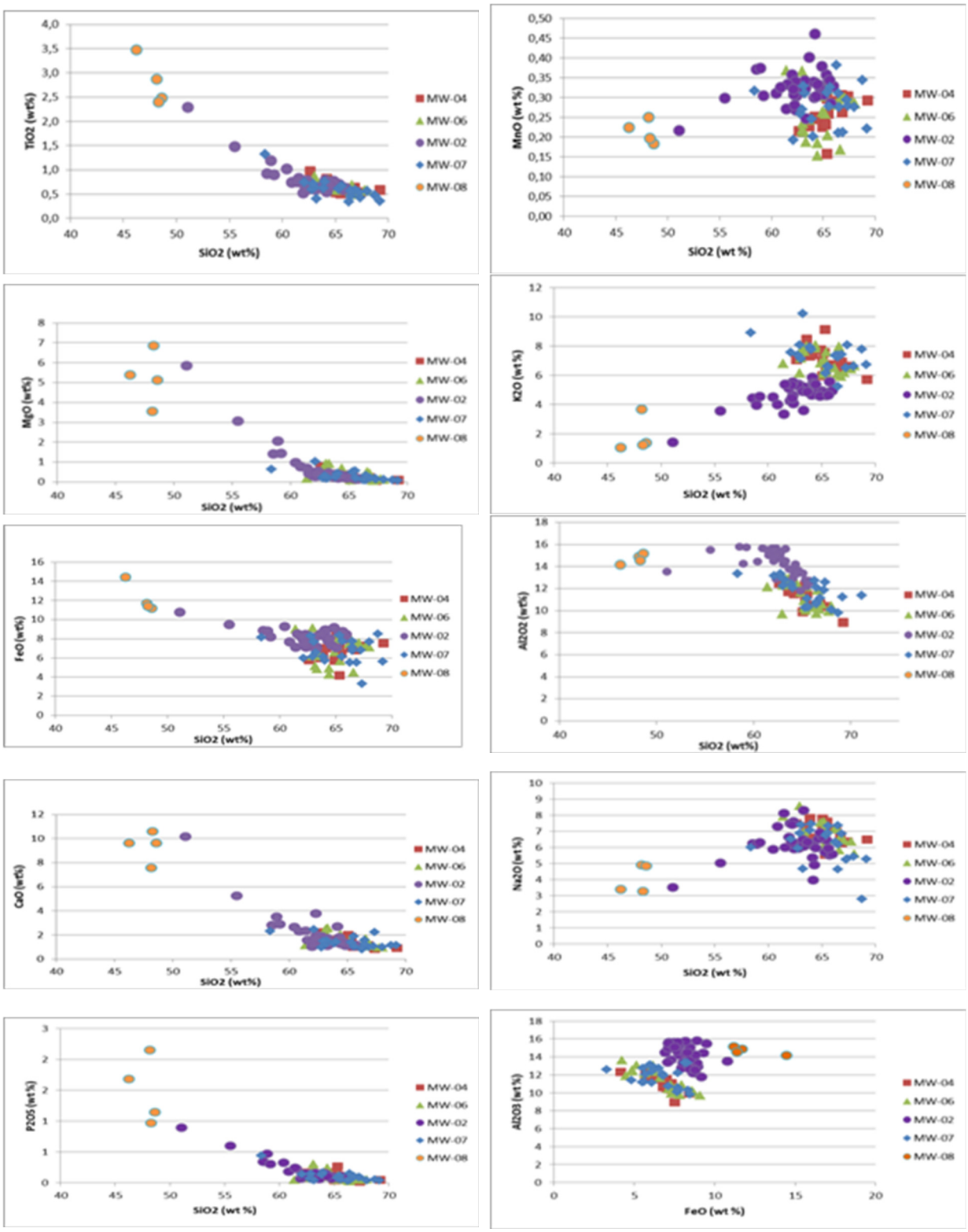

FIGURE 22: Major elements plotted against SiO_2 and FeO versus Al_2O_3 of wells MW-02, MW-04, MW-07 and MW-08

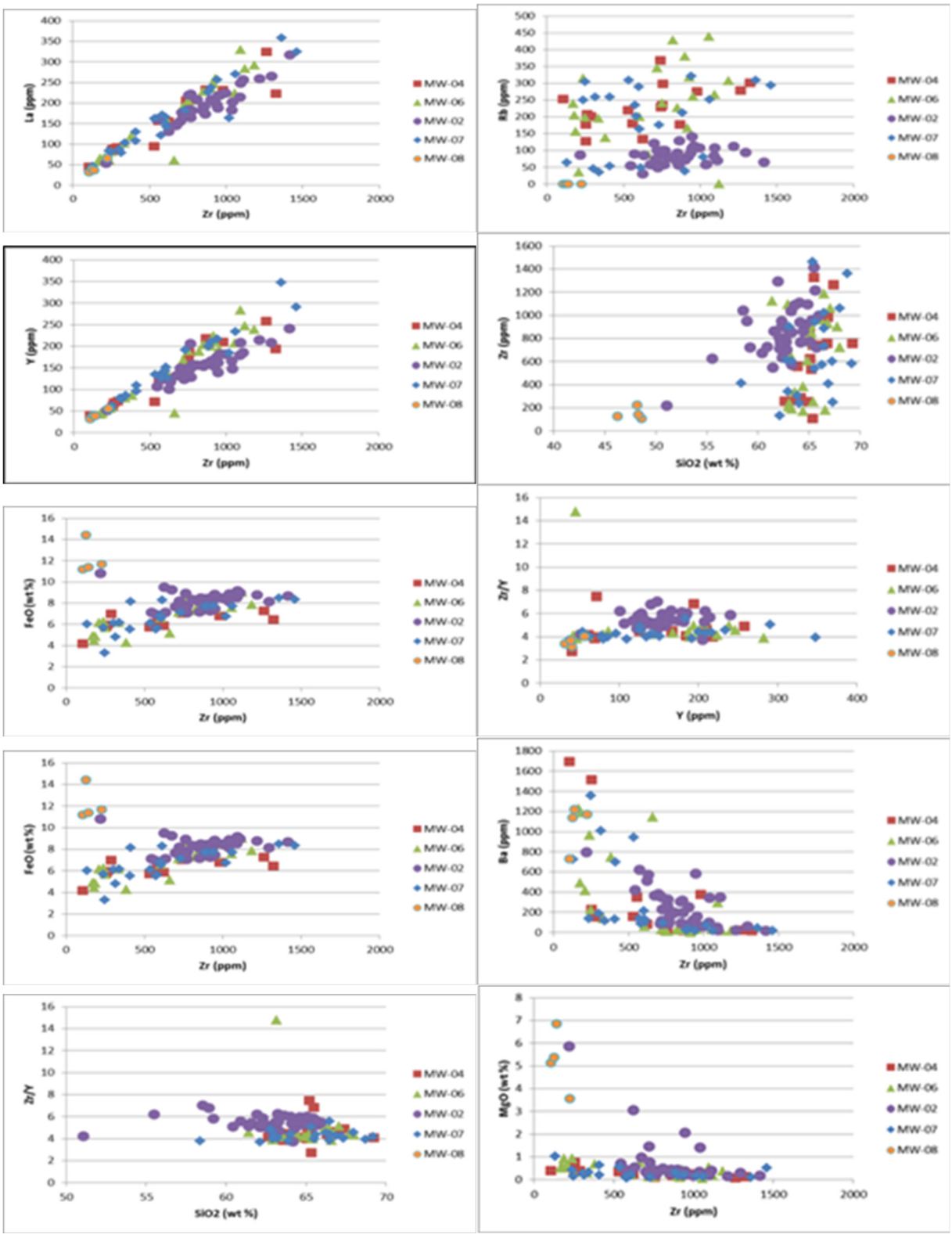

FIGURE 23: Zirconium variation with other selected elements from wells MW-02, MW-04, MW-06, MW-07 and MW-08

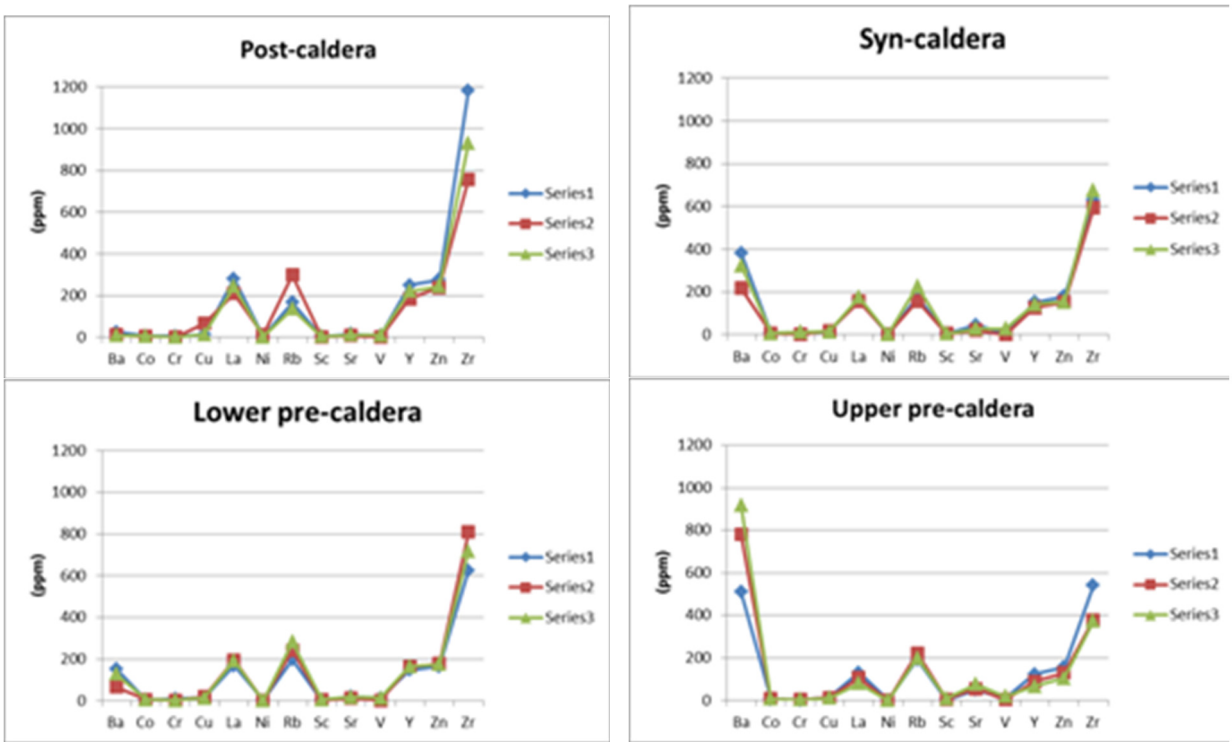

FIGURE 24: Trace element variation within volcanic units in Menengai wells. Series 1 from well MW-07, series 2, well MW-04 and series 3 from well MW-06

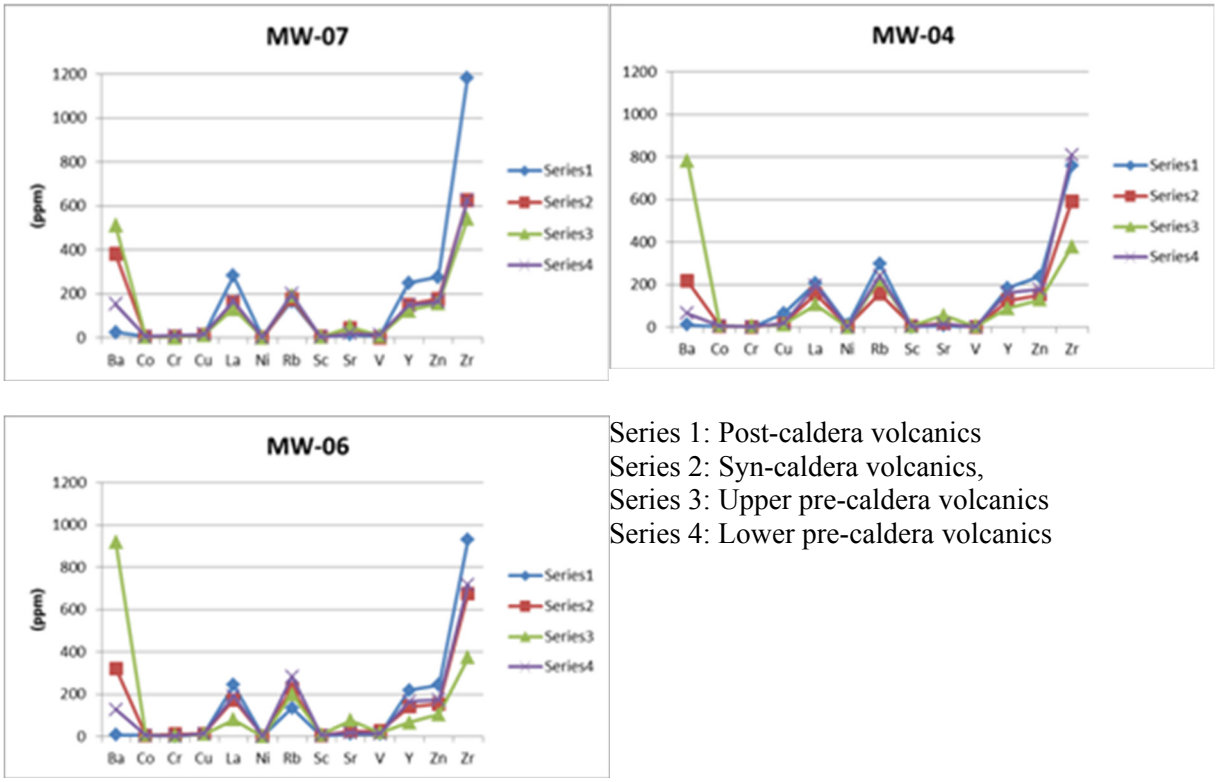

Series 1: Post-caldera volcanics
Series 2: Syn-caldera volcanics,
Series 3: Upper pre-caldera volcanics
Series 4: Lower pre-caldera volcanics

FIGURE 25: Trace element variation within volcanic units in wells MW-07, MW-04 and MW-06

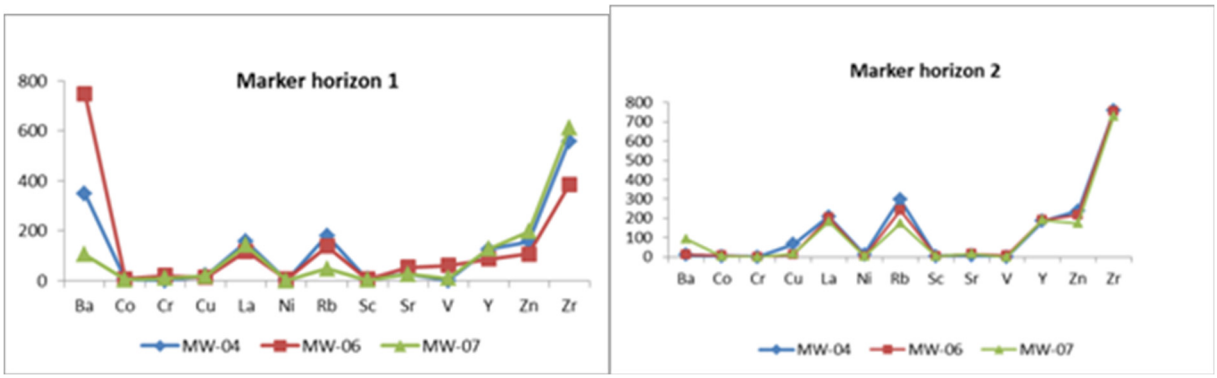

FIGURE 26: Tuff marker horizon 1 and 2 of Menengai wells

It is highly unlikely that each batch of parental magma will be identical in composition and consequently, the differentiation process may not be exactly the same in each case. This accounts for scatter in addition to other processes like magma mixing, assimilation and hydrothermal alteration. All the samples which lie on a linear trend of incompatible elements may indicate a common source (single magma chamber).

Trace elements in marker tuff horizons (1 and 2) were plotted and depicted similar trends as the volcanic units (Figure 26). Tuff marker horizon 1 shows high Ba concentration in all wells and low Zr values whereas tuff marker horizon 2 show high Zr values and low Ba values. This suggest that tuff marker horizon 2 is more evolved compared with marker horizon 1 as they have higher abundances of Zr which behaved as incompatible elements in this field.

Comparison of Zr variation in wells MW-02, MW-04, MW-06 and MW-07 with depth was plotted (Figure 27). High Zr values were noted in post-caldera volcanics compared to syn-caldera volcanics. Similar trend was also noted in pre-caldera volcanics, with lower pre-caldera volcanics having higher Zr values than upper pre-caldera volcanics. However, Zr variation trend with depth in well MW-02 show different trends compared with the other study well (Figure 27).

In the studied wells, Zn ranges from 50-300 ppm in all analysed samples (Figure 28). Zn variation with depth of the study wells depicts a similar trend as Zr variation. Wells MW-04, MW-06 and MW-07 show distinct spatial trends which defined different volcanic units (Figure 28).

Low Ba values were noted in post-caldera and lower pre-caldera volcanics compared with syn- and upper pre-caldera volcanics (Figure 29). Ba depletion in these units was interpreted to be mainly, as a result of fractional crystallization and removal of large quantities of plagioclase and alkali feldspar from the melt. Ba spatial trends therefore support the previous trace elements spider diagrams trends, of volcanic units in the Menengai wells.

The variation trends indicate processes which are of fundamental importance in producing the diversity of igneous rocks found in the researched wells. Rb and La variation trends were plotted in the study wells as shown in Figures 30 and 31 respectively. Low values were noted in well MW-02 samples from top to the bottom of the well. However similar trends were depicted in wells MW-04, MW-06 and MW-07. These trends further confirmed the volcanics from well MW-02 are of different source origin than the other study wells.

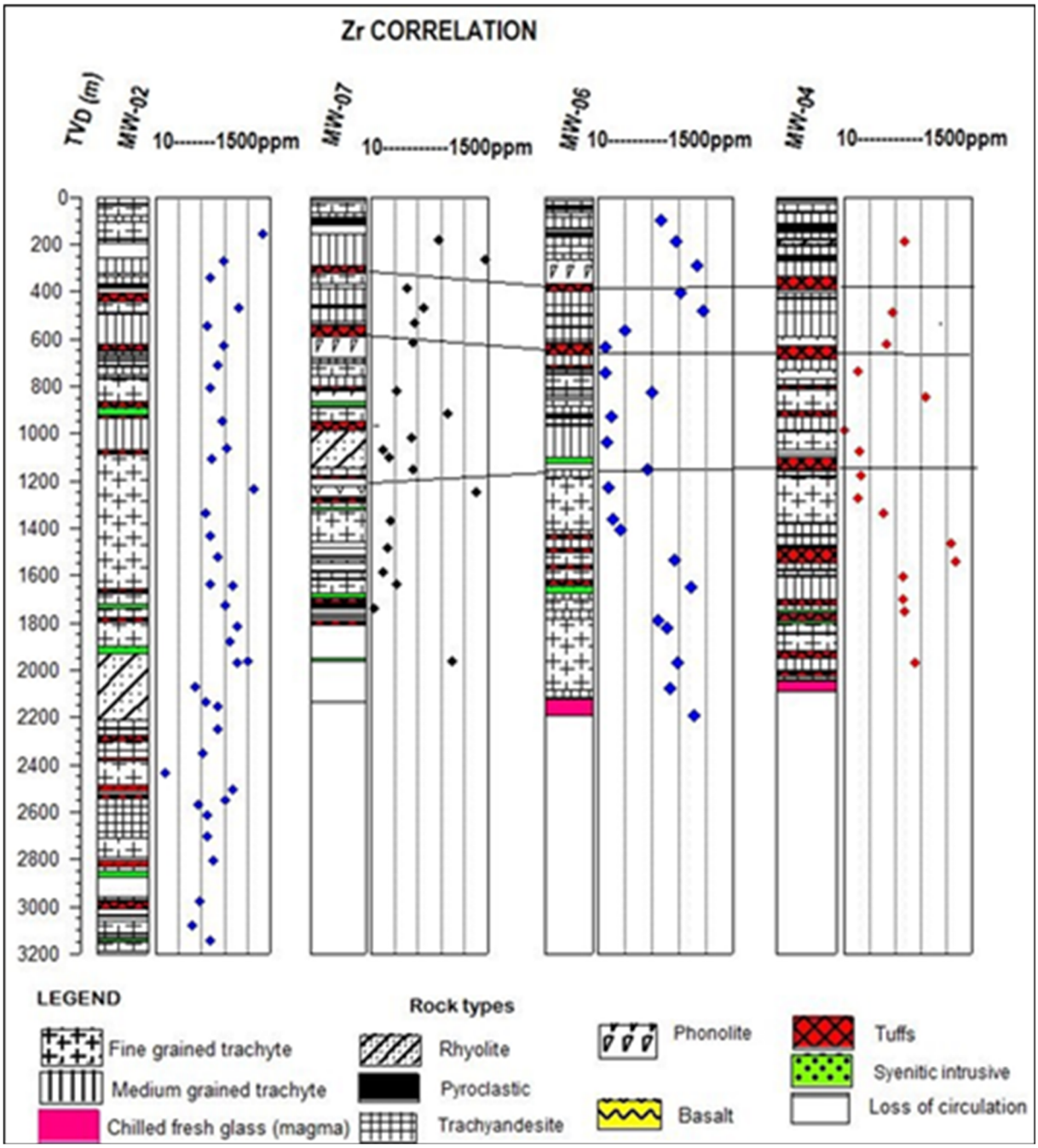

FIGURE 27: Lithostratigraphy and spatial variation of zirconium in wells MW-02, MW-04, MW-06 and MW-07

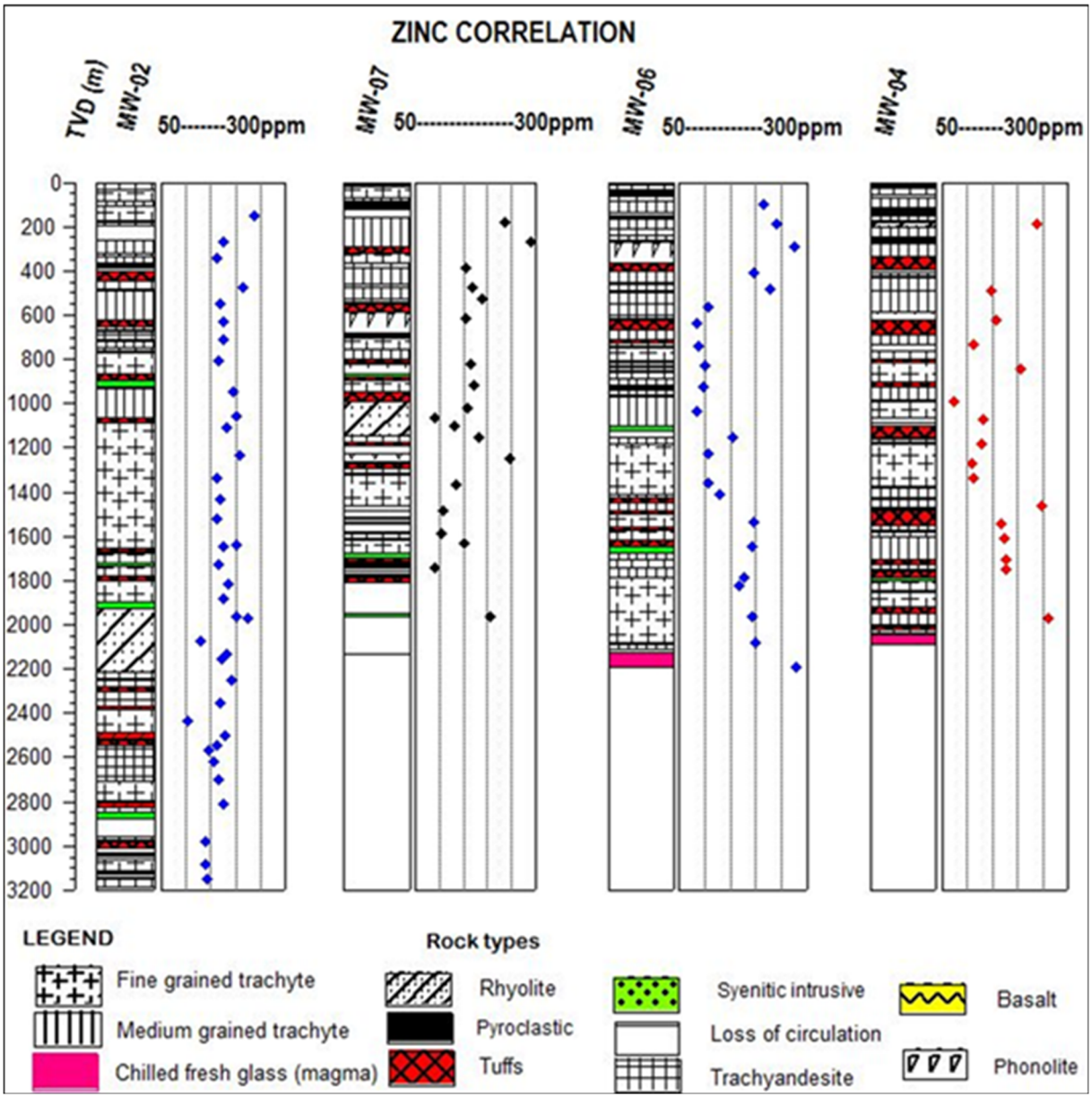

FIGURE 28: Lithostratigraphy and spatial variation of zinc in wells MW-02, MW-04, MW-06 and MW-07

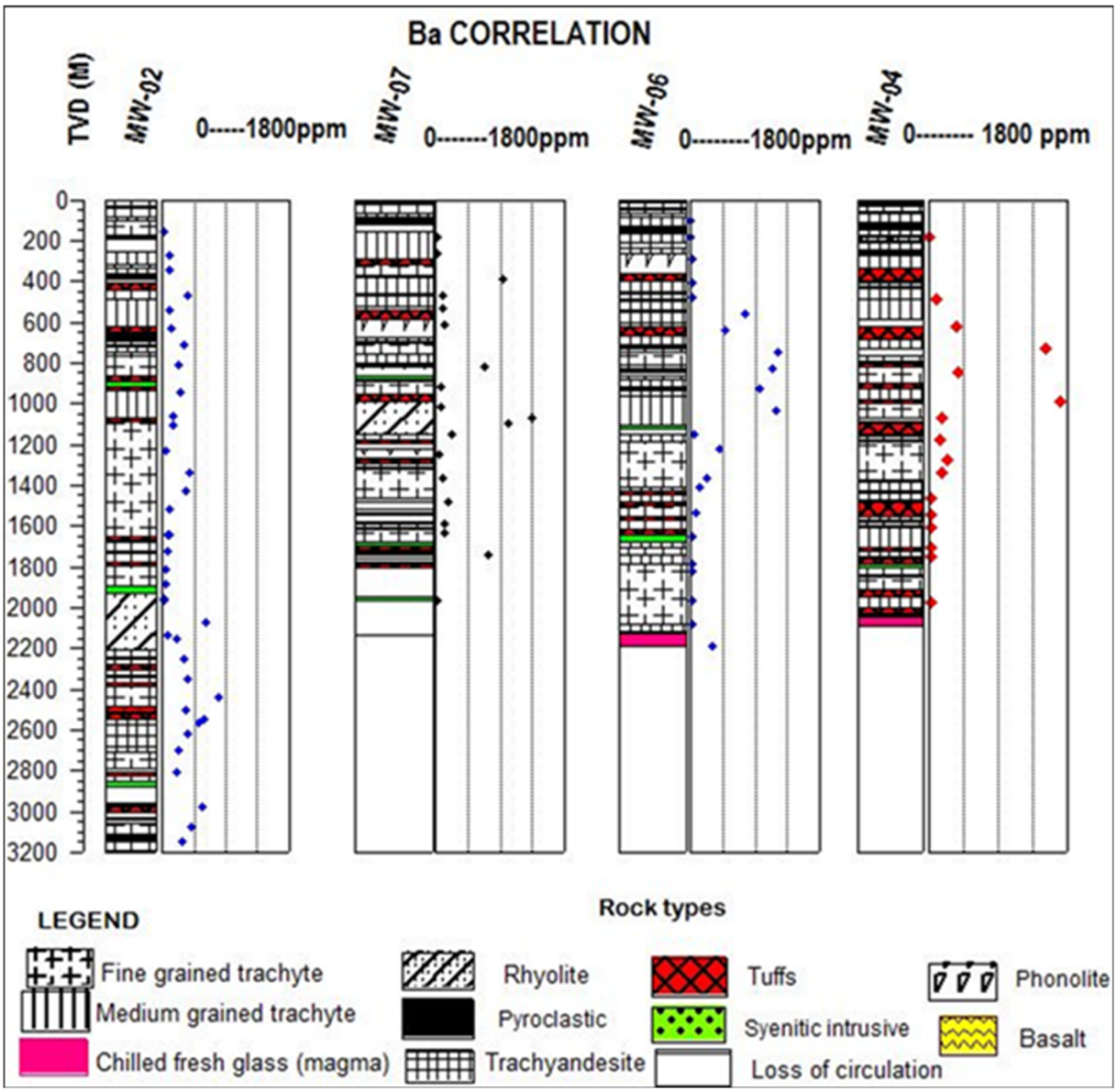

FIGURE 29: Lithostratigraphy and spatial variation of barium in wells MW-02, MW-04, MW-06 and MW-07

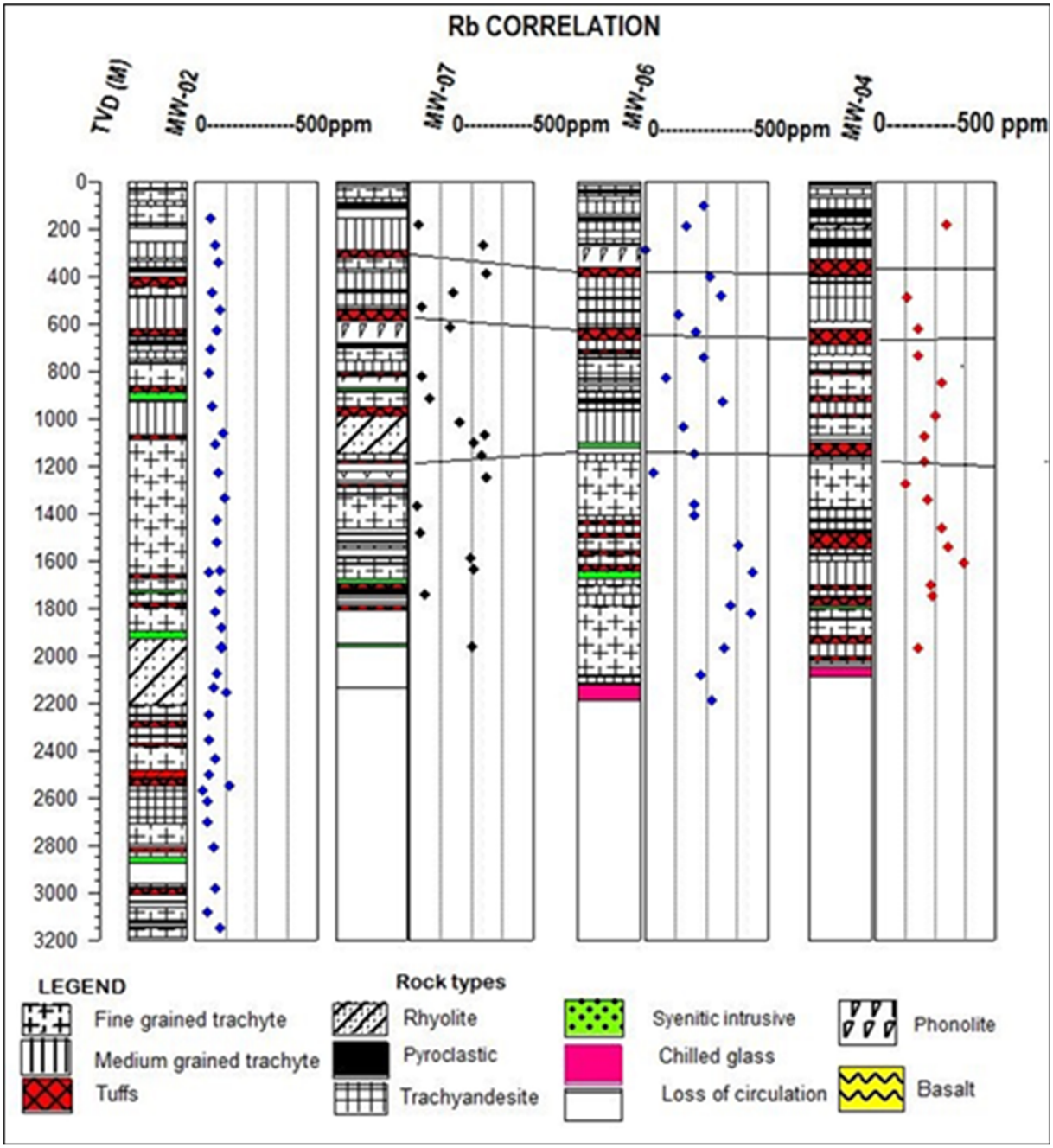

FIGURE 30: Lithostratigraphy and spatial variation of rubidium in wells MW-02, MW-04, MW-06 and MW-07

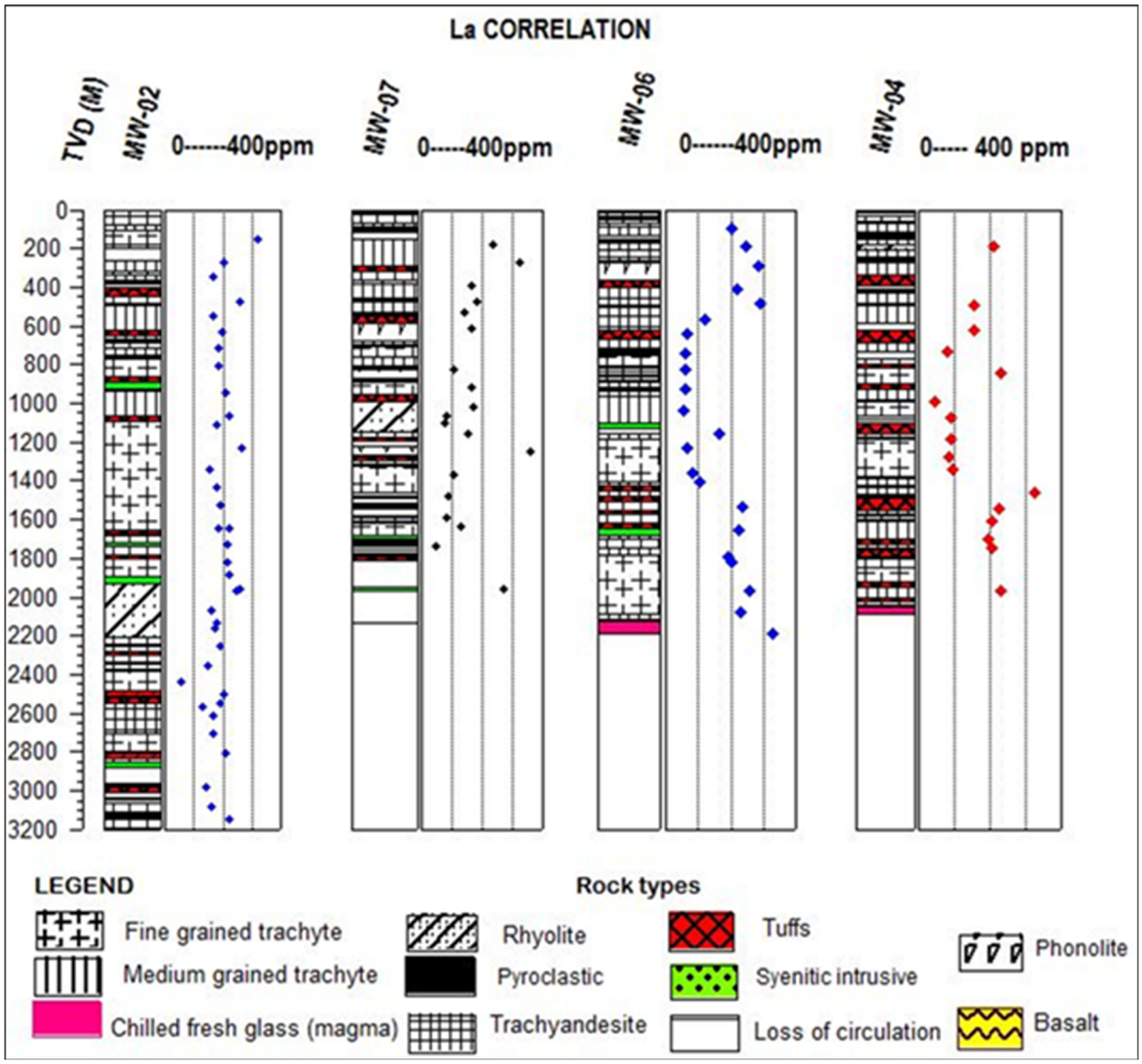

FIGURE 31: Lithostratigraphy and spatial variation of lanthanum in wells MW-02, MW-04, MW-06 and MW-07

5. CONCEPTUAL GEOLOGICAL MODEL

GDC (2010) developed the initial Menengai geothermal conceptual model using data from geological, geochemical, geophysical and heat loss surface exploration surveys and has updated the model as more exploration and well data has become available (Figure 32). The Geothermal Advisory Board (GAB, 2013) came up with the initial geothermal system conceptual cross-section model based on the subsurface data. Leat (1983) hypothesized an inner caldera within the one presently visible to account for the lower ash tuff outcropping in the caldera wall.

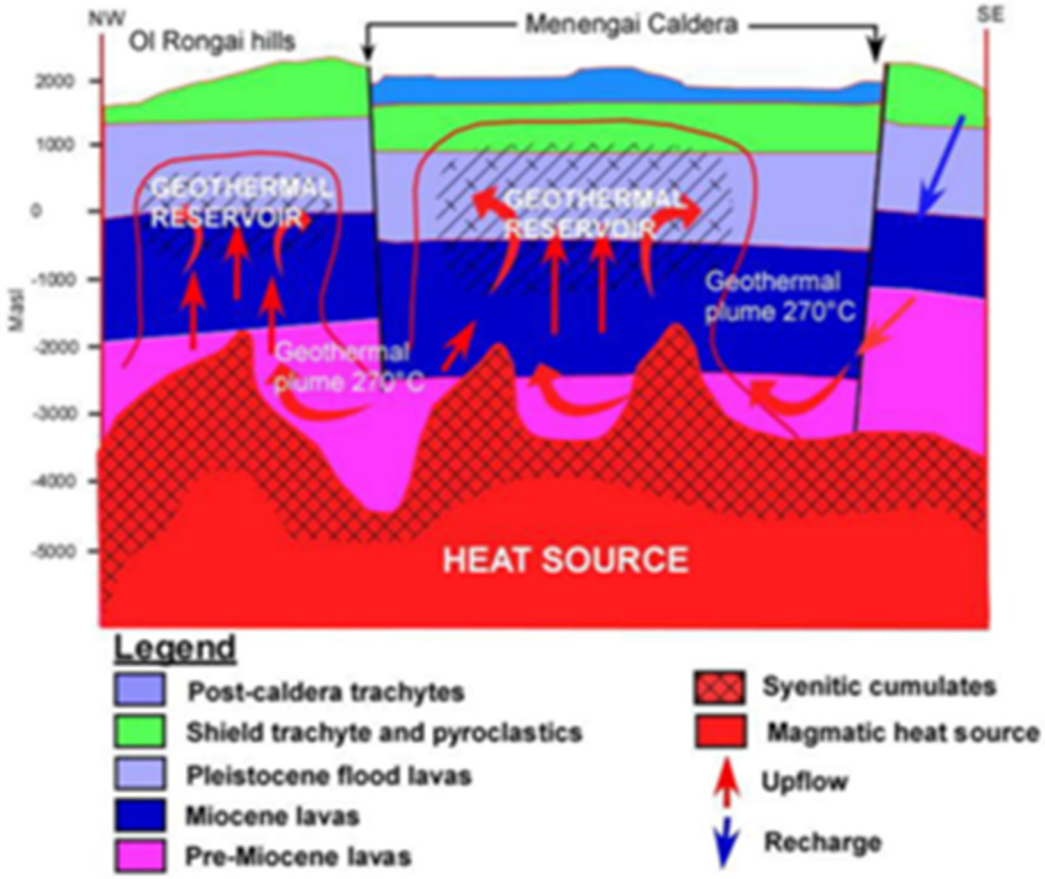

FIGURE 32: Geological conceptual model of the Menengi based on surface exploration data. (GDC, 2010)

With the current subsurface data from geothermal wells, this research has re-defined and incorporated new data and visualized a more refined model (Figure 33). The deep flow of groundwater from highland to lowland areas is through permeable structures driven by the hydraulic gradient. At just over 2 km depth, some drill holes entered a soft layer, which corresponds to fresh, glassy and quenched cuttings. This zone coincides with extremely high temperatures, exceeding 350°C to about 400°C as was recorded in wells MW-04, MW-06 and MW-01 and MW-03 (Mbia et al., 2010), and this is inferred to be a magma body or intrusive complex underneath the central part of the caldera at 2 km depth (GAB, 2013). The intrusive activity provides an additional heat source as superheated fluids. From this, it is assumed that the thickness of the geothermal reservoir where the magma is located may not be more than 1.5 km, from hydrostatic level at ~400 m to 2,000 m (e.g. GAB, 2013). It is speculated that water entering the ground water body below the Menengai caldera floor may be rain falling on the caldera floor, but also distantly derived groundwater that flows from the east (mainly from Bahati escarpment) and west (mainly Mau escarpment), particularly along fractures, but also from any other direction as determined by the hydraulic head and permeability (Figure 33). From this study, well MW-02 volcanics seems to be related with the rift volcanics and this was defined by chemical variation from the other study wells. MW-07, may be located slightly away from the heat source, though inside the caldera as the well never discharge upon opening.

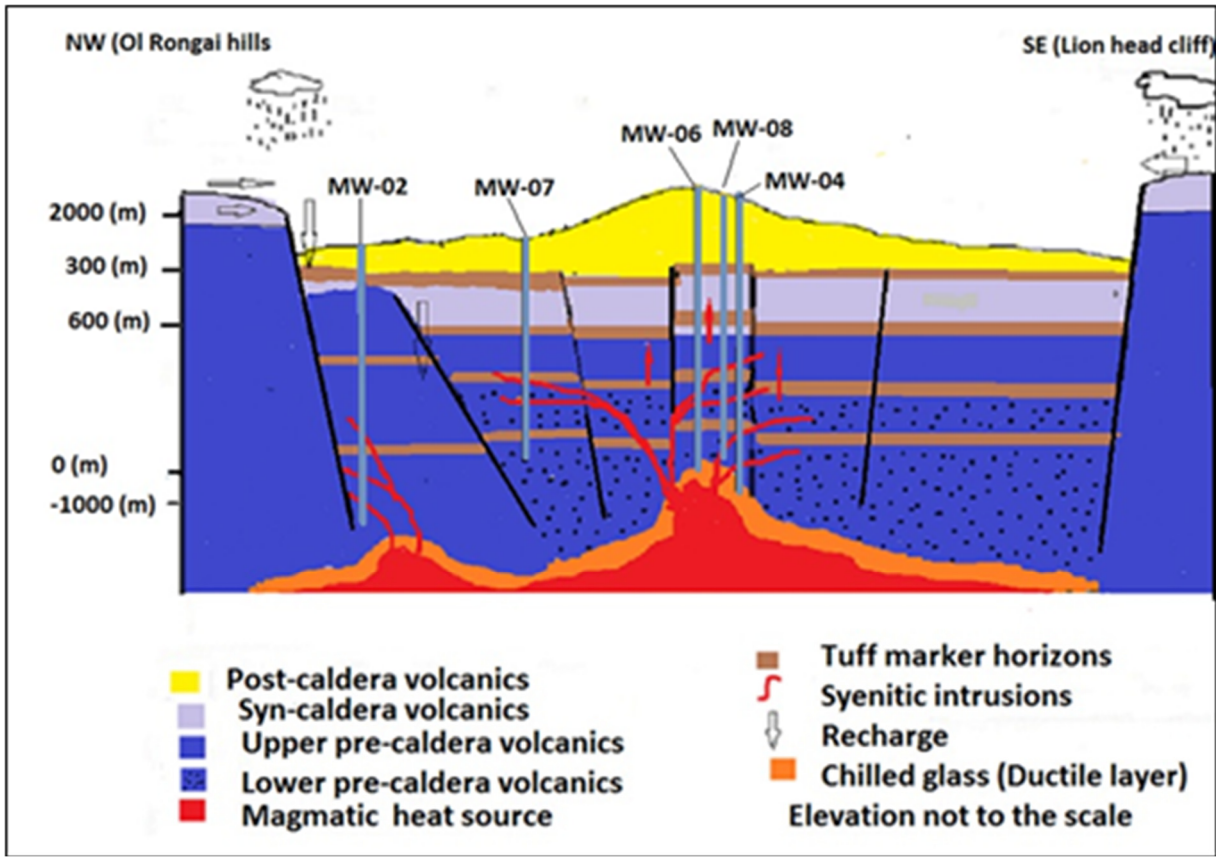

FIGURE 33: Geological conceptual model of the central Menengai caldera. Vertical scale and relative volumes are approximate (modified from GDC, 2010)

6. DISCUSSION

The rocks analysed in the study wells are mainly volcanics and intrusives. These include trachyte, pyroclastics, trachy-basalt, phonotephrite, trachy andesite, tuff, phonolite, rhyolite, and basalt and syenite intrusive. Trachyte constitutes over 90% of the total rocks.

Major and trace elements studies of the study wells show that, fractional crystallization is the dominant process involved in the diversification of the primary magma spectrum, generating the wide variety of igneous rock compositions found in the Menengai field. However, chemical trend such as Y versus Zr from well MW-02 suggests partial melting and contamination while fractional crystallization was well displayed by depletion and linear trends displayed by residual and incompatible elements such as Zr, La and Y from the other wells. The samples from well MW-02 suggest less evolved rocks and are comparable with the rift samples of the Menengai and surrounding area. This may suggests that this well is drilled in a pre-caldera shield and is associated with the caldera escarpment which is cold and associated with open fractures.

This study shows that the Menengai caldera has a complex compositional variation with time as summarized in, for example, Zr, La and Ba variation and spider diagrams. This was also evidenced in TAS, FeO-Zr plot and Al_2O_3-FeO plots which show the evolution of trachytic magma. Leat (1983) suggested that prior to major ash flow eruptions, the Menengai magma reservoir would grow by the addition and mixing of two or more trachytic melts, only slightly different in composition. Therefore, the geochemical variation within the volcanic units may have been caused by episodic hybridization of the magma residing in the magma with batches of incoming trachytic magma. In addition, they have interacted with hydrothermal fluids during or after their solidification.

Zoning patterns presented in volcanic units in the study wells, with an in situ differentiation signature, probably suggest progressive chemical stratification of an initially homogeneous magma body as crustal melting and contamination would lead to much more marked enrichment of most incompatible elements than would fractional crystallization, as the wall rocks of the magma reservoir may indeed include evolved rocks (e.g. Bechmann et al., 2008; Cox, 1978; Eichelberger, et al., 1977; Mahood, 1986; Marsh, 1982; McBirney, 1980). These processes are of fundamental importance in producing the diverse chemistry of igneous rocks presently found in the Menengai caldera. The chemical stratification depicted in the study wells suggests that the magma chamber changes as it evolves. This may account for the contrast in the geometries of zoning patterns typical for tuffs and volcanic units as well as the generally weaker zoning within distinct volcanic units. This may be what happened in the Menengai during several piecemeal eruption episodes.

Mobile elements such as Na, Mn, K, Rb, Sr and Ba were partly leached or deposited away from original rocks by hydrothermal processes as was interpreted by scattering of these elements. However, this scattering is surprisingly small when compared to relatively fresh rocks.

Hydrothermal minerals found in the Menengai are mainly present in veins and vesicles. These minerals form when circulating fluids and reservoir rocks react resulting in a compositional change of both the solid and the fluid (e.g. Ármannsson, 2012; Larsson et al., 2001; Browne, 1984). The reaction normally involves dissolution of major rock-forming minerals and precipitation of hydrated secondary silicates, carbonates, sulphates and sulphides. Their distribution is pro-grade as is commonly the case with geothermal fields. Hydrothermal index minerals of interest found in the study wells include chalcedony, pyrite, illite, albite, actinolite, calcite, quartz, albite, wollastonite and epidote. Epidote is rare in the Menengai as expected due to low iron content of the rocks and reducing condition that may arise from volcanic emanations (hydrogen, hydrogen sulphide) that favours the formation of Fe (2^+) minerals such as pyrite. Since epidote is essentially the host mineral for Fe (3^+), it requires an oxidized environment to form in any abundance. In systems with low total iron the Fe (3^+) also resides in magnetite and hematite, making epidote a less probable secondary mineral. Rare epidote was also interpreted to be as a result of a relative young age of the Menengai caldera. High CO_2 content is an inhibitor to the formation of calcium bearing minerals like actinolite, wollastonite, and epidote due to their affinity to calcium. Formation of wollastonite in wells MW-06 and MW-04 at depth was interpreted to be partially

as a result of breakdown of calcite and release of CO_2. This was arrived after the appearance of wollastonite in these wells below 1700 m which coincided with decreasing calcite.

The volcanic centres, which erupted the post-caldera lavas within the summit at the caldera centre, could suggest the on-going magmatic activity at depth. It is therefore reasonable to assume that magma is at a shallow depth around the caldera summit. Microseismic studies (Simiyu, 2009) indicate a near-surface magma body that indicates depths of around 4-3.5 km. Further, Gichira (2012) interpreted a low-resistivity anomaly seen at 4000 m below the surface of the Menengai caldera as a deep conductor which was suggested to be a shallow heat source beneath the caldera. However, chilled cuttings from well MW-04 and MW-06 were noted at much shallower depth from 2082-2106 m and 2174-2190 m respectively. These zones were also characterized by extremely high temperatures of over 350^0C.

In the Menengai caldera, two main structures are of particular importance. The Molo TVA which trends NNW-SSE and the Solai TVA, which trends NNE-SSW direction (Figure 7). Solai TVA cuts the Menengai caldera at the northern end and has a southern extension under the Menengai volcanic pile and therefore, is an important hydrogeological domain that possibly favours permeability in the area. These two structures seem to converge beneath the caldera and this has enhanced permeability of the geothermal system within the caldera.

Aquifers in the Menengai are mainly related to lithological boundaries and margins of intrusions, which are associated with fracture permeability in the reservoir. These zones are associated with abundance of calcite and pyrite. The rocks are generally highly altered implying high interaction of fluids with the host rocks as a result of permeability. Temperature surveys, loss of circulation and penetration rate suggest two main feed zones in the research wells. A shallow feed zone system occurs at around 900-1300 m depth, which corresponds to a shallow aquifer system and is mainly liquid dominated, while the deeper feeder zone system, occurring below 1400 m depth corresponds to the lower aquifers system. Hydrothermal alteration minerals assemblage indicates an area that has had temperatures of above 270°C as shown by the occurrence of wollastonite and actinolite. However measured temperatures in well MW-06 recorded temperatures over 350°C , with well MW-04 recording temperature of 398°C at the bottom of the well. Similar temperatures, close to 400°C, was recorded in wells MW-01 and MW-03, in the Menengai caldera (Mbia et al., 2010). This suggests a strong conductive heat flow from wells bottom, probably magmatic, and point to a shallow heat source (Figures, 16, 17). Correlation of hydrothermal alteration and temperature profiles of wells MW-04 and MW-06, indicating the system is heating up from the bottom. Earlier studies on fluid inclusions (Kipchumba, 2013; Mibei, 2012), done in the area, indicates that the geothermal system around the caldera summit is generally heating up. This could be attributed to the recent magmatic intrusions in the area.

The chemical composition and mineralogy of the source region exerts a fundamental control over the chemistry of magmatic rocks (e.g. Rollinson, 1993). The major and trace element composition of a melt is determined by the melting process and the degree of partial melting, although the composition of the melt can be substantially modified en route to the surface (e.g. Rollinson, 1993). The composition of the source itself is a function of mixing processes in the source region. Fresh batches of relatively primitive magma, as evidenced by basaltic lava, must have been periodically injected into the base of the chamber from the underlying mantle source and this may have triggered contemporaneous volcanic eruptions, which resulted in numerous thin lava layers encountered in the subsurface section of the analysed wells.

Wilson (1987) suggested that the extent of mixing between such fluxes and the resident magma chamber depends on both the input rate and on the relative densities and viscosities of the two magmas. O'Hara and Mathews (1981) suggested that magma chambers in general must be regarded as open systems which are periodically tapped and continuously fractionated. At any stage during their ascent from source to the surface, magma may become variably contaminated by assimilation of their wall rocks. The petrography of the basalt and trachytic end members analysed in this project reveal distinct mineral parageneses that may be ascribe to two or more distinct magma types from which the different mineral assemblages crystallized. Magma chamber processes frequently modify the chemical composition of the primary magma, produced by partial melting of the source, through fractional crystallization, magma mixing, contamination or a dynamic mixture of several of these processes. The presence of minor

volume of basaltic lava found in wells MW-02 and MW-08, may suggest basaltic magma intrusions in a trachytic magma chamber in the Menengai caldera. The principal inference is that basaltic magmas intruded the trachytic magma chamber below the caldera and were erupted in recent times within the caldera.

The occurrence of basalt-trachyte mixing events cannot be considered definitive evidence of a parent-daughter relationship between basaltic and trachytic magmas in the Menengai (e.g. as explained in crystal fractionation models) because of the lack of intermediate rocks. It simply suggests that mafic melts intruded the cooling felsic magma chamber. The supply of basaltic magma from the upper mantle and melting of gabbro-cumulates at the base of the crust are separate phenomena which may occur simultaneously and drive magma evolution (e.g. Turner and Campbell, 1986).

Romengo et al. (2012) suggested that mixing between basaltic melts and trachyte derived by partial melting could affect the evolution of the magma, possibly determining minor differences in the degree of peralkalinity and in the trace element chemistry of the felsic magmas. Following emplacement or eruption, igneous rocks maybe chemically modified, either by outgassing or by interaction with fluid (Romengo et al., 2012). The volcanic cycles depicted in this study shows that the Menengai rocks are extremely evolved and indicate end of volcanic cycles.

7. CONCLUSIONS AND RECOMMENDATIONS

7.1 Conclusions

Fractional crystallization, possibly in combination with magma mixing and crustal contamination is the most important processes that control the geochemical evolution of the Menengai rocks. The scattering of the residual trace elements variation shows that the rocks may have been generated by processes more complex than simple fractional crystallization. However, some of the scattering in variation diagrams may be as a result of background "noise" introduced by using analyses of porphyritic samples and hydrothermal alteration. These variations may also imply that primitive material with complete hybridization occurred prior to eruption.

The rocks analysed in this study are mainly volcanics and intrusives. These include trachyte, pyroclastics, trachy-basalt, phonotephrite, trachy andesite, tuff, phonolite, rhyolite, and basalt and syenite intrusive. Trachyte constitutes over 90% of the total rocks.

At the Menengai, two main structures are of particular importance. The Molo TVA which trends NNW-SSE and the Solai TVA, which trends NNE-SSW direction (Figure 7). Solai TVA cuts the Menengai caldera at the northern end and this would indicate that these faults are younger than the caldera. However these faults are poorly exposed within the caldera floor though it has a southern extension under the Menengai volcanic pile and therefore is an important hydrogeological domain that possibly favours permeability in the area. These two structures seem to converge beneath the caldera and this has enhanced permeability of the geothermal system within the Menengai caldera.

Hydrothermal alteration minerals assemblage indicates an area that has had temperatures of above 270°C as shown by the occurrence of wollastonite and actinolite. However measured temperatures in some wells, such as MW-01 and MW-06 recorded temperatures over 350°C, while well MW-04 recording temperature of 398°C at the bottom of the well (Figures 15 and 16) Therefore correlation of hydrothermal alteration mineralogy and temperature logs of well MW-04 and well MW-06 indicating that the system may be heating up. Earlier studies on fluid inclusions done in the area, indicates that the geothermal system around the caldera summit is generally heating up. This could be attributed to the recent magmatic intrusions in the area

Four hydrothermal zones are recognized in the Menengai geothermal system; the zeolite-smectite zone, quartz-illite zone, illite-epidote zone and wollastonite-actinolite zone.

Aquifers are related to lithological boundaries, margins of intrusions and palaeo-tectonic (intra-caldera) structures which are associated with the Molo TVA. Porosity and permeability levels are not related to the rock chemistry but are related to intrusions and palaeo-tectonics and lithological boundaries.

The degree of alteration and secondary mineralization is directly related to the permeability. Permeability in the area was inferred from fractured cuttings (high alteration intensity) high oxidation marking lithological contacts, the occurrence of abundant pyrite, calcite and loss of circulation. Low permeability was inferred from low alteration in cuttings and low penetration rates during drilling.

Small batches of basaltic rocks found in well MW-02 and MW-08 may suggest that, basaltic melts were able to intrude the shallow, low density, felsic magma body and mix with the resident magma.

7.2 Recommendations

Radiogenic and stable isotope geochemistry studies would confirm different origin of MW-02 volcanics, since distinctive trace elements and Sr-Nd-Pb isotopic signatures are associated with different magma generation environments. This could be important because it would indicate that there may be a fracture zone between MW-02 and the reminder of the caldera. If that could be the case, the well can be important for reinjection.

Isotopes survive the chemical fractionation which accompanies the formation and evolution of magmas. This therefore implies that, isotopes can be used as geochemical tracers of magma origins even where trace elements concentrations and ratios have been extensively modified by hydrothermal effects as in the Menengai geothermal field. This will help, in ruling out the source of basalt from the more evolved alkaline rocks found in the Menengai field. It will also help in justifying the evidence of crustal contamination which might have happened in the Menengai while the magma was ascending and interacting with the crustal rocks as was interpreted in this study.

For geothermal development, production wells should be drilled at reasonable distance away from the caldera wall, and more so towards the caldera summit area. However re-injection wells should be drilled near the caldera wall due to the expected high vertical permeability related to the caldera wall.

REFERENCES

Ármannsson, H., 2012: Geochemical aspects of geothermal utilization. In: Saying A., (ed.) *Comprehensive Renewable Energy, 7*, 95-168.

Baker, B.H., and Wohlenberg, J., 1971: Structure and evolution of the Kenya Rift Valley. *Nature, 229*, 538-542.

Baker, B.H., Mitchel, J.G., and Williams, L.A.J., 1988: Stratigraphy, geochronology and volcano-tectonic evolution of the Kedong-Naivasha Kinangop region, Gregory Rift Valley, Kenya. *Geological Society of London, 145,* 107-116.

Baker, B.H., Mohr, P.A., and Williams, L.A.J., 1972: *Geology of the Eastern Rift System of Africa*. *Geol. Soc. of America, Special Paper, 136*, 67 pp.

Bechmann, O., and Bergantz, G.W., 2008: Deciphering magma chamber dynamics from styles of compositional zoning in large silicic ash flow sheet. *Review in Mineralogy and Geochemistry, 69,* 651-674.

Browne, P.R.L., 1984: *Lectures on geothermal geology and petrology*. UNU-GTP, Iceland, report 2, 92 pp.

Browne, P.R.L., and Ellis, A.J., 1970: The Ohaaki-Broadlands hydrothermal area, New Zealand; Mineralization in active geothermal systems. *Economic Geology, 79*, 671-695.

Chorowicz, J., 2005: The East African rift system. *J. Afr. E. Sci,. 43*, 379-410.

Clarke, M.C.G., Woodhall, D.G., Allen, D., Darling, G., 1990: *Geological, volcanological and hydrogeological controls of the occurrence of geothermal activity in the area surrounding Lake Naivasha.* Min. of Energy, Nairobi, report 150, 138 pp.

Corti, G., 2011: Evolution and characteristics of continental rifting: Analog modelling-inspired view and comparison with examples from the East African Rift System, *Tectonophysics, 522–523 (2012),* 1–33.

Cox, KG., Bell, J.D. and Pankhurst, R.J., 1979: *The interpretation of igneous rocks*. Springer Science+Business Media B.V., Netherlands, 464 pp.

Dunkley P.N., Smith, M., Allen, D. J. and Darling, W. G., 1993: *The geothermal activity and geology of Northern sector of the Kenya Rift Valley.* British geological survey research report, 93, 1.

Eichelberger, J.C. and Gooley, R., 1977: Evolution of silicic magma chambers and their relationship to basaltic volcanism. *A.G.U. Geophys. Monogr., Washington, 20,* 57-77.

Ellis, A.J., 1963: The solubility of calcite in sodium chloride solutions at high temperatures: *American J. of Science, 261*, 259-267.

Fairhead, J.D., 1976: The structure of the lithosphere beneath the Eastern rift, East Africa, deduced from gravity studies. *Tectonophysics, 30*, 269-298.

Fernandes, R.M., Ambrosius, B.A.C., Noomen, R., Bastos, L., Combrinck., Miranda, J.M. and Spakman, W., 2004: Angular velocities of Nubia and Somalia from continuous GPS data: Implications on present-day relative kinematics. *Earth Planet. Sci. Lett., 222,* 197-208.

Franzson, H., 2010: Borehole geology. UNU-GTP, Iceland, unpublished lecture notes.

Franzson, H., 1998: Reservoir geology of the Nesjavellir high-temperature field in SW-Iceland. *Proceedings of the 19th Annual PNOC-EDC Geothermal Conference Manila, Philippines,* 13-19.

Fridleifsson, G.Ó., 1983: *The geology and the alteration history of the Geitafell central volcano, southeast Iceland*. University of Edinburgh, Grant institute of Geology, unpubl. PhD thesis.

Fridleifsson, G.Ó., 1991: *Hydrothermal systems and associated alteration in Iceland*. Geological Survey of Japan, Report 277, pp. 83-90.

GAB., 2013: *Geothermal Advisory Board (GAB) report*. Geothermal Development Company (GDC), internal report.

Garrels, R.M., and Christ, C.L., 1965: *Solutions, minerals, and equilibria.* Freeman, Cooper and Company, San Francisco, 450 pp.

GDC., 2010: *Menengai geothermal prospect; an investigation for its geothermal potential*. Geothermal Development Company (GDC), Geothermal resource assessment project, unpubl. report.

GDC., 2013: *Menengai geothermal project; Data integration report*. Geothermal Development Company (GDC), Geothermal resource assessment project, unpubl. report.

Geotermica Italiana Srl., 1987: *Geothermal reconnaissance survey in the Menengai- Bogoria area of the Kenya Rift Valley.* UN (DTCD)/GOK.

Gichira, J.M., 2012: Joint 1 D inversion of MT and TEM data from Menengai field, Kenya. Report 11 in: *Geothermal training in Iceland 2012*. UNU-GTP, Iceland, 137-168.

Giggenbach, W.F., 1980: Geothermal gas equilibria. *Geochim. Cosmochim. Acta, 44*, 2021-2032.

Giggenbach, W.F., 1984: Mass transfer in hydrothermal alteration systems- A conceptual approach. Geochim. Cosmochim. Acta, 48, 2693–2711.

Hardarson, B.S., 1993: *Alkalic rocks in Iceland with special reference to the Snaefellsjökull volcanic system*. Univ. of Edinburgh, unpubl. PhD thesis.

Harker, A., 1909: *The natural history of igneous rocks*. MacMillan, New York.

Hersir, G.P., and Bjornsson, A., 1991: *Geophysical exploration for geothermal resources. Principles and applications.* UNU-GTP, Iceland, report 15, 94 pp.

Iddings J.P., 1892: Origin of igneous rocks. *Bull. Phil. Soc. Washington, 12, 89-213.*

Jones, W.B., 1981: Chemical effects of deuteric alteration in some Kenyan trachyte lavas, *Mineral. Mag, 44,* 279-285.

Jones, W.B., 1985: Discussion on geological evolution of trachytic caldera volcano, Menengai, Kenya Rift Valley. *J. Geol. Soc. Lond, 142*, 711-712.

Jones, W.B., and Lippard, S.J., 1979: New age determinations and the geology of the Kenya Rift-Kavirondo Rift junction, West Kenya. *J. Geol. Soc. Lond., 136*, 693-704.

Keller, G.V., and Frischknecht, F.C., 1966: *Electrical methods in geophysical prospecting*. Pergamon Press Ltd., Oxford, 527 pp.

Kipchumba, L.J., 2013: Borehole geology and hydrothermal alteration of wells MW-08 and MW-11, Menengai geothermal field, Kenya. Report 10 in: *Geothermal training in Iceland 2013*. UNU-GTP, Iceland, 143-176.

Kipng'ok, J.K., 2011: Fluid chemistry, feed zones and boiling in the first geothermal exploration well at Menengai, Kenya. Report 15 in: *Geothermal training in Iceland 2011.* UNU-GTP, Iceland, 281-302.

KRISP Working Group., 1987: Structure of the Kenya rift from seismic refraction. *Nature, 325,* 239-242.

Kristmannsdottir, H., 1979: Alteration of basaltic rocks by hydrothermal activity at 100-300o C. In: Mortland, M., Farmer, V. (Eds.), Developments in sedimentology, Elsevier, Amsterdam, pp. 359-367.

Lagat, J.K., 1995: Borehole geology and hydrothermal alteration of well OW-30, Olkaria geothermal field Kenya. Report 6 in: *Geothermal training in Iceland.* UNU-GTP, Iceland, 135-154.

Larsson, D., Gronvold, K., Óskarsson, N., and Gunnlaugsson, E., 2001: Hydrothermal alteration of plagioclase and growth of secondary feldspar in the Hengill volcanic centre, SW Iceland. *J. Vol. & Geothermal Res., 114*, 275-290.

Leat, P.T., 1983: *The structural and geochemical evolution of Menengai caldera volcano, Kenya Rift Valley.* Univ. of Lancaster, Lancaster, UK, PhD thesis.

Leat, P.T., 1984: Geological evolution of the trachytic volcano Menengai, Kenya Rift Valley. *J. Geol Soc London, 141, 1057-1069*.

Leat, P.T., 1991: Volcanological development of the Nakuru area of the Kenya rift valley. *J of African Earth sciences, 13, 3/4,* 483-498.

Leat, P.T. and Macdonald, R., 1984: Geochemical evolution of the Menengai caldera volcano, Kenya. *J. Geo. Soc. Lond., 89*, 8571-8592.

Le Bas, M.J., Le Maitre, R.W., Streckeisen, A., and Zanettin, B., 1986: A chemical classification of volcanic rocks based on the total alkali-silica diagram. *J. Petrology, 27*, 745-750.

Lopeyok, T.P., 2013: Borehole geology and hydrothermal alteration of wells MW-09 and MW-12, Menengai geothermal field, Kenya. Report 15 in: *Geothermal training in Iceland 2013*. UNU-GTP, Iceland, 289-324.

Low, J.W., 1977: Examination of well cuttings and the lithological logs. In: Leroy, L.W., Leroy, D.O., and Raese, J.W. (eds.), S*ubsurface geology* (4th ed.). Colorado School of Mines, Golden, Col., 286-303.

Macdonald, R., 1974: Nomenclature and petrochemistry of the peralkaline oversaturated extrusive rocks. *Bulletin Volc., 38*, 498-516.

Macdonald, R., 2002: Magmatism of the Kenya Rift Valley: a review. *Trans. Royal Society of Edinburgh: Earth sciences, 93,* 239-253.

Macdonald, R., and Baginski, B., 2009: The central Kenya peralkaline province: a unique assemblage of magmatic systems. *Mineralogical Magazine, 73*, 1-16.

Macdonald, R., Baginski, B., Leat, P.T., White, J.C and Dzierzanowski., 2011: Mineral stability in peralkaline silicic rocks: Information from trachytes of the Menengai volcano, Kenya. *Lithos, 125*, 553-568

Macdonald, R., Navarro, J.M., Upton, B.G.J., and Davies, G.R., 1994: Strong compositional zonation in peralkaline magma: Menengai, Kenya Rift Valley. *J. Volc Geotherm Res, 60, 301-325.*

Macdonald, R., and Katsura T., 1964: Chemical composition of Hawaiian lavas. *J. Petrol., 5*, 82-133.

Macdonald, R., and Scaillet, B., 2006: The central Kenya peralkaline province: insights into the evolution of peralkaline salic magmas. *Lithos, 91*, 59-73.

Mahood, G.A., 1986: Waxing and waning magma chambers: A comparison of Zoning in ignimbrites and plutons: *14th General Meeting, International Mineralogical Association*, 163.

Marks, N., Schiffman, P., Zierenberg, R., Franzson, H., and Fridleifsson, G., 2010: Hydrothermal alteration in the Reykjanes geothermal system: Insights from Iceland deep drilling program well RN-17. *J. Vol. and Geothermal Res., 189*, 172-190.

Marsh, B.D., 1982: On the mechanics of igneous diapirism, stopping and zone melting. *Am. J. Sci., 282,* 808-855.

Mbia, P.K., 2010: Borehole geology and hydrothermal alterations of well HE-39, Hellisheidi geothermal field, SW-Iceland. Report 19 in: *Geothermal Training in Iceland 2010*. UNU-GTP, Iceland, 437-465.

Mbia, P.K., Kipngok, J., and Miyora, T.O., 2012: Preliminary report of exploration well MW-01 in the Menengai geothermal field. Geothermal Development Company (GDC), unpubl. internal report.

McBirney, A.R. and Noyes, R.M., 1980: Crystallization and layering of the Skaergaard intrusion. *J. Petrol., 20,* 487-554.

McCall, G.J.H., 1957a: The Menengai caldera, Kenya Colony. *20th Int. Geol. Congress, section 1,* 55-69.

McCall, G.J.H., 1957b: *Geology and groundwater conditions in the Nakuru Area.* M.o.W., Hydraulic Branch, Nairobi, tech. report 3.

McCall, G.J.H., 1964: Froth flows in Kenya. *Geol. Runsch., 54*, 1148-1195.

McCall, G.J.H., 1967: *Geology of the Nakuru - Thomson's Fall - Lake Hannington area*. Geolog. Surv. Kenya, Rep., 78.

Mibei, G.K., 2012: Geology and hydrothermal alteration of Menengai geothermal field-Case study of Wells MW-04 and MW-05. Report 21 in: *Geothermal training in Iceland 2012*. UNU-GTP, Iceland, 437-466.

Mitchell, R.H., 1986: *Kimberlites: mineralogy, geochemistry and petrology*. Plenum Press, NY.

Mohr, P., 1982: Musings on continental rifts. In Pálmason, G., (ed.), *Continental and oceanic rifts*. Am. Geophys. Union, Washington DC, 293-309.

Mungania, J., 2004: *Geological studies of Menengai geothermal prospects*. KenGen Ltd., internal report, 18pp.

Nick, R., Macdonald, R., Fitton, G.J., Rhiannon, G., Smith, M and Barreiro, B., 2000: Two mantle plumes beneath the East African rift system: Sr, Nd and Pb isotope evidence from Kenya Rift basalts.

O'Hara, M.J. and Mathews, R.E., 1981: Geochemical evolution in an advancing, periodically replenished, periodically tapped, continuously fractionated magma chamber. *J. Geol. Soc. Lond., 138,* 237-77.

Omenda, P.A., 1993: *Geological investigation of Suswa geothermal prospect, Kenya*. KPC, internal report, 35 pp.

Omenda, P.A., 1997: *The geochemistry evolution of quaternary volcanism in the south-central portion of the Kenya rift.* University of Texas, El Paso, Ph.D. thesis, 218 pp.

Omenda, P.A., 2012: Geology and geothermal activity of the East African Rift. *Proceedings of Short Course VII on Exploration for Geothermal Resource*s, UNU-GTP, KenGen and GDC, Naivasha, Kenya.

Omenda, P.A., Onacha, S.A. and Ambusso, W.J., 1993: Geological setting and characteristics of the high temperature geothermal systems in Kenya. *Proceedings of the New Zealand Geothermal Workshop 15,* 161-167.

Omondi, C., 2011: Borehole geology and hydrothermal of wells MW-01 and MW-02, Menengai geothermal field, Central Kenya Rift valley. Report 30 in: *Geothermal training in Iceland 2011*. UNU-GTP, Iceland, 737-774.

Putnis, A., 1992: *Introduction to mineral sciences*. Cambridge University Press, 457 pp

Reyes, A.G., 1990: Petrology of Philippine geothermal systems and the application of alteration mineralogy to their assessment. *J. Volc.& Geothermal Res., 43,* 279-309.

Reyes, A.G., 2000: *Petrology and mineral alteration in hydrothermal systems. From diagenesis to volcanic catastrophes.* UNU-GTP, Iceland, report 18-1998, 77pp.

Riaroh, D. and Okoth, W., 1994: The geothermal fields of the Kenya rift. *Tectophysics 236*, 117-130.

RockWare Inc., 2007: *Log Plot program.* RockWare Inc., USA.

Rogers, N., Macdonald, R., Fitton, J. G., George, R., Smith, M., Barreiro, B., 2000: Two mantle plumes beneath the East African rift system: Sr, Nd and Pb isotope evidence from Kenya Rift basalts. *Earth and Planetary Science Letters, 176*, 387-400.

Rollinson, H.R., 1993: *Using geochemical data: evaluation, presentation, interpretation*. Longman, Edinburgh Gate, 352 pp.

Romengo, N., Landi, P., and Rotolo. S.G., 2012: Evidence of basaltic magma intrusions in a trachytic magma chamber at Pantelleria (Italy). *J. Min., Crystallography, Geochemistry, Ore Deposits, Petrology, Volcanology and Applied Topics on Environment, Archeometry and Cultural Heritage.*

Simiyu, S.M., 2009: Application of micro-seismic methods to geothermal exploration: Examples from Kenyan rift. *Proceedings of Short Course IV on Exploration for Geothermal Resource*s, UNU-GTP, KenGen and GDC, Naivasha, Kenya, 27 pp.

Simiyu, S.M., and Keller, G.R., 2001: An integrated analysis of the lithospheric structure across the East African plateau based on gravity analysis and recent seismic studies. *Tectonophysics, 278*, 327-352.

Simiyu, S.M and Keller, G.R., 1997: An integrated analysis of lithospheric structure across the East African plateau based on gravimetry anomalies and recent seismic studies. *Tectonophysics 278*, 291–313.

Simmons, S.F., and Christenson, W. B., 1994: Origin of calcite in boiling geothermal system. *Am. J. Sci., 294,* March, 361-400.

Smith, R.L., and Bailey, R. A., 1968: Resurgent cauldrons. *Men. Geol. Soc. Am., 116*, 613-662.

Smith, M., and Mosley, P., 1993: Crustal heterogeneity and basement influence on the development of the Kenya Rift, East Africa. *Tectonics 12-2,* 591-606.

Thompson, A.O., and Dodson, R.G., 1963: *Geology of the Naivasha area*. Gov. of Kenya, Geol. Surv., report. 55, 80 pp.

Turner, J.S., and Campbell, I.H., 1986: Convection and mixing in magma chambers. *Earth Sci. Rev. 23,* 255-352.

Wilson, M., 1989: *Igneous petrogenesis. A Global tectonic approach*. Unwin Hyman, London, Boston, Sydney, Wellington, 466 pp.

APPENDIX A: Procedure for ICP-ES analysis

Sample preparation

Rock cuttings were ground into about 100 Mesh powder in agate mortar.

About 100 mg ±2 mg of sample and 200 mg± 2 mg of powdered lithium metaborate ($LiBO_2$) flux were weighted into an epicure graphite crucible fused in electric furnace at 1000°C for 30 minutes.

Reference samples for instrument calibration were in house standards A-THO, B-ALK and B-HTO (BIR-. The fused bead was then transferred to a beaker containing 30 ml of complexion acid mixture (5% conc HNO_3. 1.33% HCl and 1.33% semi-saturated oxalic acid) solution and stirred to complete dissolution. The sample was then ready for ICP analysis for major and trace elements.

Analytical session (Spectra CIROS ICP-spectrometer) was started with running the three calibration standards. The Spectra Vision software was then used to calculate a two or three point calibration line for each element of the analytical routine.

Instrumental reference sample (REF) for monitoring eventual fluctuations during analysis was made of equal parts of the three reference samples. This sample was analyzed at the beginning of the session and with ten samples interval through the session. One of the reference samples (B-THO) was analyzed within each batch of 10 samples in order to demonstrate instrument reproducibility in multiple analyses.

The raw data where analytical sums may vary from 98-102 weight percent were pasted into a correction spreadsheet. All analyses of the batch are normalized to 100% sum. The spreadsheet then calculate time dependent variation down each column (element) of the analysis by finding the difference between the first and the last readings of the reference sample. The total variation was then divided into 10 equal parts. Each line was then corrected by adding the variation-increment which was added to all subsequent lines of the batch. Then all sums were normalized to 100%.

After the insignificant time dependent variation –correction has been applied to the batch, the absolute values of the reference samples at the beginning and at the end of a sample batch are equal.

The normalized values listed in the text are used for plotting and calculations.

APPENDIX B: Procedure for X-ray Diffractometer analysis

Selected samples were grounded into about 100 mesh powder in agate mortal.

The samples were then placed into a clean test-tube and filled with distilled water to about two-third full.

The samples were then placed in a mechanical shaker/vibrator for about 4 hours.

Few millilitres/drops of the solution were then pipetted from each tube, approximately 5drops on a labelled glass plate, and were allowed to dry at room temperature overnight.

The samples were run in range 2-14° for a time of about 15 minutes on the XRD machine.

After running the air dried samples, they were then placed in a desiccator containing glycol solution and stored at room temperature for 24hours.

The glycolated samples were then run in the XRD machine.

The glycolated samples were then put into an oven and heated to about 550^0C for one hour and allowed to cool. The samples were then analysed with the XRD machine and the results were tabulated in Tables 4, 5, 6 and 7 in the text.

APPENDIX C: Lithological description and hydrothermal alteration minerals of well MW-02

0-6 m Pyroclastics: Soils, obsidian glass, lithic clasts and other rock fragments. These fragments are oxidized into reddish oxides (mainly hematite and magnetite) as a result of surface water, oxygen and rock interaction. Alteration minerals: Oxides.

6-30 m Fine-grained trachyte: Dark grey fine-grained, fresh slightly oxidized porphyritic rock. The phenocrysts consist mainly of sanidine, aegirine and pyroxene. Flow texture was evidenced by tiny sanidine crystals. The matrix is glassy and is characterized by flow aligned minute microlites. Alteration minerals: Oxides.

30-36 m Loss of circulation (No cuttings)

36-82 m Fine-grained trachyte: Brownish grey fine-grained feldspar porphyritic rock. The rock is oxidized into reddish brown oxides. The rock consists of microphenocrysts of euhedral sanidine set in a fine-grained groundmass. Alteration minerals: Oxides.

82-106 m Medium-grained trachyte: Light grey to brownish grey, medium-grained sanidine and pyroxene porphyritic rock. The rock exhibits flow trachoid texture. The rock is relatively fresh with minor oxidized surfaces. Alteration minerals: Oxides.

106-176 m Fine-grained trachyte: Light grey to brownish grey, fine-grained feldspar and pyroxene porphyritic lava. The rock is moderately fresh with minor oxidized surfaces. Alteration minerals: Oxides.

176-182 m Tuff: Light grey poorly crystalline rock with few phenocrysts of feldspars and mafic. The rock is highly altered and has glassy texture. Alteration minerals: Oxides.

182-194 m Fine-grained trachyte: Light grey fined-grained sanidine and pyroxene porphyritic trachyte. The groundmass is fine-grained and contains mainly sanidine. Some minerals have a slight greenish coloration due to alteration into oxides. Alteration minerals: Oxides.

194-258 m No cuttings (Lost circulation)

258-322 m Medium-grained trachyte: Dark grey medium-grained sanidine and pyroxene porphyritic lava. The groundmass is fine-grained and contains mainly sanidine. The rock is massive fractured and slightly altered. Alteration minerals: oxide, Pyrite, smectite, zeolite and calcite.

322-338 m Fine-grained trachyte: Light grey fine-grained sanidine and pyroxene porphyritic lava. The groundmass is fine-grained and contains mainly sanidine. Some minerals have a slight greenish coloration maybe nepheline. Alteration minerals: Oxides, smectite, zeolite, pyrite and calcite.

338-364 m Medium-grained trachyte: Dark grey medium-grained sanidine and pyroxene porphyritic rock. The groundmass is fine-grained and contains mainly sanidine. The rock is massive and slightly altered. Alteration minerals: smectite, zeolite, pyrite, oxide and calcite minerals.

364-386 m Tuff: Light grey, poorly crystalline rock with few phenocrysts of feldspars and mafic. The rock is highly altered and has glassy texture. Alteration minerals: Oxides, smectite, zeolite, pyrite and calcite.

386-404 m. Medium-grained trachyte: Dark grey medium-grained sanidine and pyroxene porphyritic trachyte. The groundmass is fine-grained and contains mainly sanidine. The rock is massive and slightly altered. Pyrite, smectite and oxides are the main secondary minerals.

404-446 m Tuff: Light grey phyric poorly crystalline rock with phenocrysts of feldspars and mafic. The rock is highly altered and has glassy texture. Alteration minerals: Oxides, smectite, pyrite and calcite.

446-486 m Fine-grained trachyte: Light grey fine-grained sanidine and pyroxene porphyritic rock. The groundmass is fine-grained and containing sanidine crystallites with riebeckite and arfvedsonite. Some minerals have a slight greenish coloration due to alteration into clays. Alteration minerals: Oxides, pyrite and calcite.

486-492 m Tuff: Light grey phyric poorly crystalline vitric rock with phenocrysts of feldspars and mafic. The formation is highly altered and has glassy texture. Alteration minerals: Oxides, pyrite, chalcedony smectite and minor calcite.

492-622 m Fine-grained trachyte: Light grey fine-grained sanidine and pyroxene porphyritic trachyte. The groundmass is fine-grained and containing mainly sanidine crystallites with riebeckite and pyroxene. Minor veins filled up with chalcedony and calcite was noted. Greenish tinge was noted in some cuttings, may be due to the presence of nepheline minerals. Alteration minerals: Oxides, pyrite chalcedony, smectite and minor calcite.

622-650 m Tuff: Light grey phyric poorly crystalline rock with phenocrysts of feldspars and mafic. The rock is vesicular and has glassy texture. Alteration minerals: Oxides, chalcedony, pyrite and calcite (minor).

650-654 m No cuttings (Loss of circulation)

654-670 m Syenitic intrusion: Light grey, coarse-grained, sanidine and pyroxene porphyritic rock. The rock is fresh with slightly altered on some faces. It has massive feldspar laths aligned in preferred trachoid flow texture. The rock is mixed with altered lava indicating an intrusive rock. Alteration minerals: Oxides, pyrite and calcite (minor).

670-674 m No cuttings (Loss of circulation)

674-686 m Fine-grained trachyte: Brownish grey, fine-grained feldspar porphyritic lava. The rock is moderately altered and veined with the veins filled up with calcite and clays. Alteration minerals: Oxides, calcite (minor), chalcedony and pyrite.

686-690 m No cuttings (Loss of circulation)

690-714 m Fine-grained trachyte: Light grey fine-grained sanidine and pyroxene porphyritic trachyte. The groundmass is fine-grained and contains mainly sanidine. Some minerals have a slight greenish coloration due to alteration to clays. Alteration minerals: Pyrite smectite, and calcite.

714-718 m No cuttings (Loss of circulation)

718-750 m Medium-grained trachyte: Brownish grey, medium-grained feldspar porphyritic lava. The rock is moderately altered and veined with the veins filled up with calcite and clays. Alteration minerals: Oxides, smectite, pyrite and calcite (minor).

750-764 m Fine-grained trachyte: Light grey fine-grained sanidine and pyroxene porphyritic trachyte. The groundmass is fine-grained and contains mainly sanidine. Some minerals have a slight greenish coloration due to alteration to clays. Alteration minerals: Pyrite, calcite (minor).

764-770 m No cuttings (Loss of circulation)

770-862 m Fine-grained trachyte: Light grey fine-grained sanidine and pyroxene porphyritic trachyte. The groundmass is fine-grained and contains mainly sanidine. Some minerals have a slight greenish coloration due to alteration to clays. Alteration minerals: Pyrite and minor calcite.

864-892 m Tuff: Light grey phyric poorly crystalline and vesicular rock with phenocrysts of feldspars and mafic. The rock is highly altered with calcite and clays infill in vesicles and voids. Alteration minerals: Pyrite and calcite.

892-922 m Syenitic intrusion: Light grey, coarse-grained, fresh, sanidine and pyroxene porphyritic rock. The rock is fresh with slightly altered on some faces. The groundmass is fine-grained and is mainly feldspathic. Alteration minerals: Pyrite, quartz and calcite.

922-932 m Tuff: Light grey, vesicular, poorly crystalline rock with phenocrysts of feldspars and mafic. The rock is fractured and highly altered. Alteration minerals present include pyrite, calcite, clays and quartz.

932-1066 m Medium-grained trachyte: Brownish grey medium-grained sanidine and pyroxene porphyritic trachyte. The groundmass is fine-grained and contains large phenocrysts mainly of sanidine. Some minerals have a slight greenish coloration due to alteration to clays. Alteration minerals present include calcite, clays (illite) and quartz.

1066-1090 m Tuff: Greyish, phyric, poorly crystalline rock highly glassy and vesicular rock. Alteration minerals present include calcite, pyrite, illite and quartz.

1090-1656 m Fine-grained trachyte: Greenish grey to brownish grey fine-grained sanidine and feldspar porphyritic lava. The rock is moderately to highly altered into clays. Quartz occurs in veins and vesicles .The rock is bleached to whitish clays. Alteration minerals present include calcite, pyrite, illite and quartz.

1656-1672 m Tuff: Brownish grey phyric, poorly crystalline rock with phenocrysts of feldspars and mafic. The rock shows a high intensity of alteration with abundant pyrite, calcite, illite epidote and quartz.

1672-1678 m No cuttings (Loss of circulation)

1678-1722 m Fine-grained trachyte: Light grey fine-grained sanidine and pyroxene porphyritic rock. The groundmass is fine-grained and contains mainly sanidine. Some minerals have a slight greenish coloration due to alteration to clays. Alteration minerals: pyrite, calcite, and illite.

1722-1736 m Syenitic intrusion: Light grey, coarse-grained Sanidine and pyroxene porphyritic rock. The rock is fresh with slightly altered on some faces. Its massive feldspar laths aligned in preferred trachoid flow texture. Alteration minerals present include calcite, pyrite, illite and quartz.

1736-1778 m: Fine-grained trachyte: Light grey fine-grained sanidine and pyroxene porphyritic lava. The rock is moderately altered into greenish clays. The groundmass is fine-grained and contains mainly sanidine. Alteration minerals: pyrite, epidote, calcite and illite.

1778-1798 m Tuff: Light grey, poorly crystalline and vesicular rock. The rock is highly altered and has fine-grained glassy matrix. Alteration minerals: Calcite, quartz, pyrite and clays.

1798-1896 m Fine-grained trachyte: Light grey fine-grained sanidine and pyroxene porphyritic trachyte. The groundmass is fine-grained and contains mainly sanidine. Some minerals have a slight greenish coloration due to alteration to clays. Alteration minerals: Calcite, quartz, pyrite illite epidote and chlorite.

1896-1930 m Syenitic intrusion: Light grey, coarse-grained sanidine and pyroxene porphyritic rock. The rock is fresh with slightly altered on some faces. Its massive feldspar laths aligned in preferred trachoid flow texture. The groundmass is fine-grained and is mainly feldspathic. Alteration minerals: Calcite, quartz, pyrite illite, chlorite and epidote.

1930-2210 m Rhyolite: Light grey fine-grained feldspar and quartz phyric lava. The rock is moderately to highly altered and has quartz and sanidine feldspar phenocrysts in fine-grained groundmass displaying trachytic flow texture. Alteration minerals: Calcite, quartz, pyrite illite, chlorite and epidote.

2210-2246 m Fine-grained trachyte: Light grey fine-grained sanidine and pyroxene porphyritic trachyte. The groundmass is fine-grained and contains mainly sanidine. Some minerals have a slight greenish coloration due to alteration to clays. Alteration minerals: Calcite, quartz, pyrite and illite and chlorite.

2246-2252 m: No cuttings (Loss of circulation).

2252-2278 m Fine-grained trachyte: Light grey fine-grained sanidine and pyroxene porphyritic trachyte. The groundmass is fine-grained and contains mainly sanidine crystallites with riebeckite and pyroxene. Some minerals have a slight greenish coloration due to alteration to clays. Alteration minerals: Calcite, quartz, pyrite and illite.

2278-2302 m Tuff: Light grey, poorly crystalline and vesicular rock with phenocrysts of feldspars and mafic. The rock is highly altered and bleached into whitish clays. Alteration minerals: Calcite, quartz, chlorite, pyrite and illite.

2302-2336 m Fine-grained trachyte: Light grey fine-grained sanidine and pyroxene porphyritic trachyte. The groundmass is fine-grained and contains mainly sanidine. Some minerals have a slight greenish coloration due to alteration to clays. Alteration minerals: Calcite, quartz, pyrite and illite.

2336-2342 m No cuttings (Loss of circulation)

2342-2370 m Fine-grained trachyte: Light grey fine-grained sanidine and pyroxene porphyritic trachyte. The groundmass is fine-grained and contains mainly sanidine. Some minerals have a slight greenish coloration due to alteration to clays. Alteration minerals: Calcite, quartz, pyrite and illite.

2370-2384 m Basalt: Dark grey, fine-grained rock consisting plagioclase and minor clinopyroxenes phenocrysts in a glassy groundmass. The rock is slightly altered into clays and calcite. Alteration minerals: Calcite, quartz, pyrite, epidote and illite.

2384-2484 m Fine-grained trachyte: Light grey fined-grained sanidine and pyroxene porphyritic lava. The groundmass is fine-grained and contains mainly sanidine. Some minerals have a slight greenish coloration due to alteration. Alteration minerals: Calcite, quartz, pyrite and illite.

2484-2514 m Basalt: Dark grey, fine-grained rock consisting plagioclase and minor clinopyroxenes phenocrysts in a glassy groundmass. The rock shows slight to moderately to clays and replacement by calcite. Calcite also occurs as vein fillings in association with quartz and epidote.

2522-2546 m Tuff: Light grey phyric poorly crystalline rock with phenocrysts of feldspars and mafic. It is highly altered into greenish and reddish brown clays. Calcite, chlorite, illite and quartz are the main secondary mineral.

2546-2584 m Trachy andesite: Light grey fine-grained feldspar and quartz phyric lava. The rock is moderately to highly altered and has quartz and sanidine phenocrysts in fine gained groundmass displaying trachytic flow texture. Alteration minerals: Epidote, calcite, pyrite and illite

2586-2684 m Trachyandesite: Light grey fine-grained sanidine and pyroxene porphyritic rock. The groundmass is fine-grained and contains mainly sanidine. The rock is highly altered and has a slight greenish coloration due to alteration to clays. Alteration minerals: pyrite, calcite, illite, quartz and chlorite.

2684-2708 m Syenitic intrusion: Light grey, coarse-grained sanidine and pyroxene porphyritic rock. The rock is fresh with slightly altered on some faces. Its massive feldspar laths aligned in preferred trachoid flow texture. The groundmass is fine grained and is mainly feldspathic. Alteration minerals: calcite, pyrite, and illite.

2708-2792 m Fine-grained trachyte: Light grey fine-grained sanidine and pyroxene porphyritic trachyte. The groundmass is fine-grained and contains mainly sanidine. Some minerals have a slight greenish coloration due to alteration to clays. Alteration minerals: pyrite, calcite, chlorite, epidote and illite.

2792-2806 m No cuttings (Loss of circulation)

2806-2828 m Trachy-andesite: Dark grey, fine-grained plagioclase feldspar phyric lava. The rock has glassy groundmass and is slight to moderately altered. Calcite illite and pyrite are the main secondary minerals.

2828-2850 m Fine-grained trachyte: Light grey to brownish grey, fine-grained sanidine and pyroxene porphyritic trachyte. The groundmass is fine-grained and contains mainly sanidine. Some minerals have a slight greenish coloration due to alteration to clays. Alteration minerals: calcite, pyrite epidote, chlorite and illite.

2850-2876 m Syenitic intrusion: Light grey, coarse-grained sanidine and pyroxene porphyritic rock. The rock is fresh with slightly altered on some faces. It is massive and has feldspar laths aligned in preferred trachoid flow texture. The groundmass is fine grained and is mainly feldspathic. Alteration minerals: calcite, pyrite chlorite and illite.

2876-2960 m No cuttings (Loss of circulation)

2960-2972 m Fine-grained trachyte: Light grey to brownish grey, fine-grained sanidine and pyroxene porphyritic trachyte. The groundmass is fine-grained and contains mainly sanidine. Some minerals have a slight greenish coloration due to alteration to chlorite. Alteration minerals: Calcite, quartz, pyrite, chlorite and illite.

2972-2980 m No cuttings (Loss of circulation)

2980-3006 m Tuff: Light grey poorly crystalline and vesicular rock with minor phenocrysts of feldspars and mafic. The rock is highly altered and has vesicle infill with calcite and clays. Alteration minerals: Calcite, quartz, pyrite and illite.

3006-3032 m No cuttings (Loss of circulation)

3034-3042 m Syenitic intrusion: Light grey, coarse-grained sanidine and pyroxene porphyritic rock. The rock is generally fresh with slightly altered chilled surfaces. The groundmass is fine grained and is mainly feldspathic. Alteration minerals: Calcite, chlorite, quartz, pyrite and illite.

3044-3060 m No cuttings (Loss of circulation)

3060-3112 m Fine-grained trachyte: Light grey fine-grained sanidine and pyroxene porphyritic trachyte. The groundmass is fine-grained and contains mainly sanidine. Some minerals have a slight greenish coloration due to alteration to clays. Alteration minerals: Calcite, quartz, pyrite and illite.

3112-3120 m No cuttings (Loss of circulation)

3120-3128 m Fine-grained trachyte: Light grey fine-grained sanidine and pyroxene porphyritic trachyte. The groundmass is fine-grained and contains mainly sanidine. Some minerals have a slight greenish coloration due to alteration to clays. Alteration minerals: Calcite, quartz, pyrite, chlorite and illite.

3128-3140 m No cuttings (Loss of circulation)

3140-3148 m Syenitic intrusion: Light grey, coarse-grained sanidine and pyroxene porphyritic rock. The rock is generally fresh with slightly altered chilled margins. The groundmass is fine-grained and is mainly feldspathic. Alteration minerals: Calcite, quartz, pyrite and illite clays.

3148-3188 m Fine-grained trachyte: Light grey fine-grained sanidine and pyroxene porphyritic trachyte. The groundmass is fine-grained and contains sanidine crystallites with riebeckite. The rock is moderate to highly altered into greenish clays. Alteration minerals: Calcite, epidote, quartz, pyrite and illite.

APPENDIX D: Lithological description and hydrothermal alteration minerals of well MW-04

*0-6 m No cuttings (*Loss of circulation)

6-22 m Pyroclastics: Rock fragments consisting of mixed soils, obsidian glass and lithic clasts. These fragments are oxidized into reddish oxides as a result of surface water and rock interaction. Alteration minerals: Oxides

20-28: No cuttings (Loss of circulation).

28-54 m Fined-grained trachyte: Brownish grey fine-grained sanidine and pyroxene porphyritic rock. The groundmass is fine-grained and contains mainly sanidine. The rock is massive and generally fresh with minor oxidized surface due to surface water-rock interaction. Alteration minerals: Oxides.

54-58 m Medium-grained trachyte: Grey medium-grained sanidine and pyroxene porphyritic lava. The rock is generally unaltered though has minor fractured surface. It has fine-grained groundmass consisting mainly sanidine. The rock is massive and slightly oxidized. Alteration minerals: oxides.

58-68 m No cuttings (Loss of circulation)

68-74 m Medium-grained trachyte: Light grey medium-grained sanidine and pyroxene porphyritic trachyte. The groundmass is fine-grained and contains mainly sanidine. The rock is massive and generally fresh with minor fractured surfaces. Alteration minerals: Oxides.

74-78 m No cuttings (Loss of circulation)

78-84 m Medium-grained trachyte: Light grey medium-grained sanidine and pyroxene porphyritic lava. The groundmass is fine-grained and contains mainly sanidine. The rock is massive and slightly altered with minor fractured surfaces. Alteration minerals: oxides.

84-86 m No cuttings (Loss of circulation)

86-114 m Medium-grained trachyte: Light grey to dark grey fine to medium-grained sanidine and pyroxene porphyritic trachyte. The groundmass is fine-grained and contains mainly sanidine. The rock is massive and slightly altered. Alteration minerals: Oxides.

114-152 m Tuff: Light grey to brownish grey, poorly crystalline, vesicular and fragmental rock. The fragments are small while the vesicles are irregularly spaced. The rock is oxidized and has glassy matrix. Alteration minerals: Oxides.

152-178 m Medium-grained trachyte: Light grey sanidine and pyroxene porphyritic trachyte. The groundmass is fine-grained and contains mainly sanidine. The rock is massive and slightly altered exhibiting flow trachoid texture. Alteration minerals: Oxides.

178-180 m No cuttings (Loss of circulation)

180-182 m Tuff/Pyroclastics: Grey fined-grained porphyritic and poorly crystalized trachyte with scare Sanidine. The rock is vesicular and altered. The vesicles are irregularly spaced. Alteration minerals: Pyrite and oxides.

182-188 m Rhyolite: Light grey, fine-grained porphyritic rock. The phenocrysts contain mainly feldspar and euhedral quartz and minor pyroxene. The groundmass is glassy with chalcedony being deposited into vesicles. The rock is massive and slightly altered. It is fractured with mild oxidized surfaces. Alteration minerals: pyrite and oxides.

188-192 m No cuttings (Loss of circulation)

192-204 m Rhyolite: Light grey, fine-grained quartz and feldspar porphyritic rock. The phenocrysts contain mainly sanidine and euhedral quartz and minor pyroxene. The groundmass is glassy with chalcedony being deposited into vesicles. The rock is generally fresh with minor fractured and altered surfaces. Alteration minerals: smectite, zeolite, chalcedony, pyrite and clays.

204-206 m: No cuttings (Loss of circulation).

206-244 m Medium-grained trachyte: Dark grey medium-grained sanidine and pyroxene porphyritic trachyte. The groundmass is fine-grained and contains mainly sanidine. The rock is massive and slightly

altered. Minor fractured surfaces were noted. Pyrite cubes disseminated in fine-grained groundmass. Alteration minerals: Oxides, pyrite, smectite and zeolites.

244-272 m Pyroclastic/tuff: Brownish grey to reddish grey poorly crystalline ashy, vesicular and mixed cuttings. The rock has minor phenocrysts of mafic minerals (pyroxenes) and feldspars. Feldspar phenocrysts are altered and bleached into clays. Alteration minerals: oxides, pyrite, smectite and zeolite.

272-304 m: Fine-grained trachyte: Grey medium-grained sanidine and pyroxene porphyritic rock. Pyrite cubes are disseminated in fine-grained matrix. The rock is highly altered and fractured especially between 282-288 m. Alteration minerals: oxides, smectite and pyrite.

304-322 m medium-grained trachyte: Grey medium-grained sanidine and pyroxene porphyritic lava. The groundmass is fine-grained and contains mainly sanidine and pyroxenes. The rock is massive and slightly fractured and altered. Alteration minerals: oxides, pyrite and calcite.

322-354 m Tuff/Pyroclastics: Greenish grey poorly crystalline fragmental rock. The rock is vesicular and oxidized. The greenish colour is ascribed to clay alteration. Alteration minerals: smectite, zeolite, pyrite, calcite and smectite.

354-394 m Medium-grained trachyte: Grey medium-grained sanidine and pyroxene porphyritic lava. The rock is fractured and moderately altered. Alteration minerals: calcite, pyrite, and smectite.

394-406 m: No cuttings (Loss of circulation).

406-422 m Medium-grained trachyte: Grey medium-grained sanidine and pyroxene porphyritic lava. The rock is slightly fractured and moderately altered. Alteration minerals: calcite, pyrite, smectite and zeolite.

422-430m: No cuttings (Loss of circulation).

430-478 m Tuff: Grey Greenish grey mixed fragmental rocks. The rock is vesicular and moderately altered and oxidized. The vesicles are irregularly spaced. Alteration minerals: oxides, pyrite and calcite.

478-482 m: No cuttings (Loss of circulation).

482-488 m Medium-grained trachyte: Grey medium-grained sanidine and pyroxene porphyritic trachyte. The groundmass is fine-grained and contains mainly sanidine. The rock is massive and slightly altered. Alteration minerals: oxides, pyrite calcite and smectite.

488-490 m: No cuttings (Loss of circulation).

490-492 m Medium-grained trachyte: Brownish grey to reddish grey medium-grained, sanidine and pyroxene porphyritic lava. The groundmass is fine-grained and contains mainly sanidine. The rock is massive and slightly altered. Alteration minerals: Oxides, calcite pyrite and smectite.

492-496m No cuttings (Loss of circulation)

496-512 m Medium-grained trachyte: Brownish grey to reddish grey medium-grained sanidine and pyroxene porphyritic lava. The groundmass is fine-grained and contains mainly sanidine. The rock is moderately altered. Alteration minerals: oxides, smectite, pyrite and calcite.

512-514 m No cuttings (Loss of circulation)

514-562 m Medium-grained trachyte: Brownish grey to reddish-grey medium-grained sanidine and pyroxene porphyritic trachyte. The groundmass is fine-grained and contains mainly sanidine. The rock is massive and slightly altered. Alteration minerals: Chalcedony, calcite and pyrite.

562-564 m No cuttings (Loss of circulation)

564-588 m Pyroclastics: Light grey to brownish grey ashy and reworked rock fragments. Some fragments have greenish coloration due to alteration to clays. Alteration minerals: oxides, calcite, pyrite and chalcedony.

588-626 m Phonolite: Light grey medium-grained brownish grey to reddish sanidine and pyroxene porphyritic trachyte. The groundmass is fine-grained and contains mainly sanidine. The rock is massive and slightly altered. Minor pyrite is disseminated in fine-grained matrix. Alteration minerals: smectite, pyrite, calcite and oxides.

626-648 m Tuff: Light grey, fine-grained poorly crystalline glassy fragmental rock debris. The rock is bleached and highly altered into whitish clays. Alteration minerals: smectite, pyrite, calcite and oxides.

648-686 m: Medium-grained trachyte: Grey to reddish grey, medium-grained sanidine and pyroxene porphyritic lava. The groundmass is fine-grained and contains mainly sanidine. The rock is massive and slightly altered. Some cuttings have greenish coloration due to alteration to clays. Alteration minerals: pyrite, calcite, chalcedony and oxides.

686-706 m Fine-grained trachyte: Light grey to greenish grey, fine-grained sanidine and pyroxene porphyritic lava. The groundmass is fine-grained and contains mainly sanidine and mafic (mainly pyroxene). Alteration minerals: pyrite, calcite, chalcedony, quartz and illite.

706-732 m Fine-grained trachyte: Light grey, fine-grained sanidine and pyroxene porphyritic lava. The groundmass is fine-grained and contains mainly sanidine. The rock is fractured and highly altered. Oxidation is also apparent due to presences of brown specs of grains. Alteration minerals: pyrite, calcite, quartz and illite.

732-766 m Phonolite: Light grey, fine-grained sanidine and pyroxene porphyritic lava. The rock is fractured and moderately to highly altered. The rock is bleached and altered into whitish clays. Alteration minerals: calcite, pyrite, quartz and illite.

766-796 m Fine-grained trachyte: Light grey fine-grained sanidine and pyroxene porphyritic trachyte. The groundmass is fine-grained and contains mainly sanidine and pyroxene. The rock is moderate to highly altered. Abundant calcite was noted with quartz veining at these depths. Alteration minerals: quartz, calcite, pyrite and illite.

796-798 m No cuttings (Loss of circulation)

798-800 m: Tuff: Light grey, fine-grained poorly crystalline glassy and fragmental rock. The rock is vesicular with medium sized irregular vesicle. It is fractured and highly altered into whitish clays. Alteration minerals: calcite, pyrite, quartz and clays.

800-804 m: No cuttings (Loss of circulation).

804-816 m Tuff: Light grey, poorly crystalline, vesicular and scoracious rock. The rock is fractured and highly altered. Alteration minerals: pyrite, calcite chalcedony and quartz.

816-818 m No cuttings (Loss of circulation)

818-848 m Tuff: Light grey poorly crystalline rock with scoracious textures it is vesicular with medium sized and irregular vesicle. The rock is highly altered with pyrite, calcite and some clays being deposited in vesicles. Alteration minerals: pyrite, calcite and clays.

848-870 m Fine-grained trachyte: Light grey, fine-grained sanidine and pyroxene porphyritic lava. The groundmass is fine-grained and contains mainly sanidine and mafic minerals. Some cuttings have a slight greenish coloration due to alteration to clays. Alteration minerals: pyrite, calcite and chlorite.

870-872 m No cuttings (Loss of circulation)

872-892 m: Fine-grained trachyte: Light grey to greenish grey, fine-grained sanidine and pyroxene porphyritic lava. The groundmass is fine-grained and contains mainly sanidine and mafic minerals (mainly pyroxene) showing flow texture typical of trachyte. Alteration minerals: calcite, pyrite, illite and chlorite.

892-896 m: No cuttings (Loss of circulation).

896-902 m: Fine-grained trachyte: Light grey fine-grained sanidine and pyroxene porphyritic trachyte. The groundmass is fine-grained and contains mainly sanidine. Some minerals have a slight greenish coloration due to alteration of nepheline into clays. Alteration minerals: calcite, pyrite and clays.

902-904 m: No cuttings (Loss of circulation).

904-916 m: Tuff: Light grey, fine-grained poorly crystalline glassy and fragmental rock. The rock is bleached and highly altered into whitish clays. Partial returns with total loss of circulation were experienced in this zone. Alteration minerals: Quartz, calcite, pyrite and chlorite clays.

916-918 m No cuttings (Loss of circulation)

918-922 m Tuff: Light grey, to greenish grey, glassy, vesicular and fragmental rock. The rock is fractured, bleached and highly altered into whitish clays. Partial returns with total loss of circulation were experienced in this zone. Alteration minerals: Quartz, calcite, pyrite and illite.

922-926 m No cuttings (Loss of circulation)

926-970 m Medium-grained trachyte: Light grey, medium-grained sanidine and pyroxene porphyritic lava. The rock is highly altered and fractured. Minor greenish tinges present were due to nepheline. Alteration minerals present include, calcite, quartz, pyrite and chlorite clays.

970-976 m No cuttings (Loss of circulation)

976-984 m Medium-grained trachyte: Light grey, medium-grained sanidine and pyroxene porphyritic lava. The rock is moderate to highly altered. The groundmass is mainly sanidine feldspar and some mafic minerals. Alteration minerals: Quartz, calcite, pyrite and illite.

984-986 m No cuttings (Loss of circulation)

986-994 m Tuff: Light grey, fine-grained poorly crystalline rock, with phenocrysts of feldspar and mafic minerals. From 988 m the rock appears fragmental with some grains exhibiting vesicular texture. Alteration minerals: Quartz, calcite, pyrite and illite.

994-996 m No cuttings (Loss of circulation)

996-998 m Fine-grained trachyte: Light grey, fine-grained sanidine and pyroxene porphyritic lava. The rock is moderately to highly altered into greenish clays. The rock is massive and has minor quartz veins. Alteration minerals present include calcite, pyrite, oxides, quartz and illite.

998-1000 m No cuttings (Loss of circulation)

1000-1006 m: Fine-grained trachyte: Light grey fine-grained sanidine and pyroxene porphyritic lava. The rock is moderately to highly alter into greenish clays. Alteration minerals present include calcite, pyrite, oxides quartz and illite.

1006-1016 m No cuttings (Loss of circulation)

1016-1018 m Fine-grained trachyte: Light grey fine-grained sanidine and pyroxene porphyritic lava. The rock is moderately to highly alter into greenish clays. Alteration minerals present include calcite, pyrite, oxides quartz and illite.

1018-1022 m No cuttings (Loss of circulation)

1022-1026 m: Fine-grained trachyte: Brownish grey to greenish grey, fine-grained sanidine and pyroxene porphyritic lava. The rock is moderately to highly alter into greenish clays. Alteration minerals present include calcite, pyrite, oxides quartz and illite.

1026-1030 m No cuttings (Loss of circulation)

1030-1034 m: Fine-grained trachyte: Light grey fine-grained sanidine and pyroxene porphyritic lava. The rock is moderately to highly alter into greenish clays. Alteration minerals present include calcite, pyrite, oxides quartz and illite.

1034-1040 m No cuttings (Loss of circulation)

1040-1044 m Fine-grained trachyte: Dark greenish grey fine-grained sanidine porphyritic lava. The ground mass is feldspar fine grained. The rock is massive with calcite and some chlorite clays as the secondary minerals.

1044-1048 m: No cuttings (Loss of circulation).

1048-1046 m Fine-grained trachyte: Brownish grey to greenish grey, fine-grained sanidine and pyroxene porphyritic lava. The rock is moderately to highly alter into greenish clays. Alteration minerals present include calcite, pyrite, oxides quartz and illite.

1046-1048 m No cuttings (Loss of circulation)

1048-1052 m: Fine-grained trachyte: Brownish grey to greenish grey, fine-grained sanidine and pyroxene porphyritic lava. The rock is moderately to highly alter into greenish clays. Alteration minerals present include calcite, pyrite, oxides quartz and illite.

*1052-1056 m: No cuttings (*Loss of circulation).

1056-1066 m: Fine-grained trachyte: Dark greenish grey fine-grained sanidine and pyroxene porphyritic lava. The rock is highly altered and has minor quartz veins. Alteration minerals present include, pyrite, calcite quartz and some illite.

1066-1068 m. No cuttings (Loss of circulation)

1068-1076 m Phonolite: Dark greenish grey fine-grained sanidine porphyritic lava with nepheline occurring as microphenocrysts in fine groundmass. The rock is highly altered and the greenish colouration is mainly due to abundant pyroxene which occurs as slender needles aligned in fine-grained matrix. Alteration minerals: pyrite, calcite, quartz and clays.

1076-1078 m No cuttings (Loss of circulation)

1078-1086 m: Fine-grained trachyte Dark greenish grey fine-grained sanidine and pyroxene porphyritic lava. The rock is highly altered and fractured. Alteration minerals present include, calcite, quartz, pyrite and oxides.

1086-1100 m No cuttings (Loss of circulation)

1100-1102 m Tuff: Light grey poorly crystalline rock with scoracious textures. The rock is vesicular and has glassy matrix. The rock is highly altered with pyrite, calcite and some clays being deposited in vesicles. Alteration minerals present include, pyrite, calcite and clays.

1102-1112 m No cuttings (Loss of circulation)

1112-1154 m Tuff: Brownish grey, poorly crystalline rock. The rock is moderate to highly alter and has minor fractured surfaces. Small quartz veins were noted filled up with quartz and calcite. Epidote, calcite, quartz and clays were noted as the main secondary minerals.

1154-1158 m No cuttings (Loss of circulation)

1158-1160 m Fine-grained trachyte: Dark grey to light grey fine-grained feldspar porphyritic rock. The rock is moderately altered with minor fractured surfaces. Small quartz veins were evidenced. Epidote, calcite, quartz and illite were noted as the main secondary minerals.

1160-1162 m: No cuttings (Loss of circulation).

1162-1178 m Fine-grained trachyte: Dark grey to light grey fine-grained feldspar porphyritic rock. The rock is moderately altered with minor fractured surfaces. Small quartz veins were evidenced. Epidote, calcite, quartz and illite were noted as the main secondary minerals.

1178-1180 m No cuttings (Loss of circulation)

1180-1226 m Fine-grained trachyte: Dark grey to light grey fine-grained feldspar porphyritic rock. The rock is fractured and moderately altered. Minor quartz veins were noted in some cuttings. Epidote, calcite, quartz and clays were noted as the main secondary minerals.

1226-1230 m No cuttings (Loss of circulation)

1230-1252 m Fine-grained trachyte: Light grey, fine-grained feldspar porphyritic rock. The rock is moderately altered with minor fractured surfaces. Pyrite cubes occurs disseminated in fine-grained groundmass. Alteration minerals: pyrite, calcite, illite and quartz.

1252-1254 m No cuttings (Loss of circulation)

1254-1282 m Fine-grained trachyte: Light grey phyric lava with quartz veining. There are phenocrysts of feldspars and Opaque minerals which include pyroxene and some amphiboles. The rock is moderately altered and bleached into whitish clays. Alteration minerals: pyrite, calcite quartz and illite.

1282-1284 m No cuttings (Loss of circulation)

1284-1290 m Fine-grained trachyte: Light grey, fine-grained sanidine and pyroxene phyric lava. The rock is veined with quartz. The rock is moderately altered and bleached into whitish clays. Alteration minerals: pyrite, calcite, illite and quartz.

1290-1292 m No cuttings (Loss of circulation)

1292-1334 m Fine-grained trachyte: Light grey to greenish grey fine-grained feldspar porphyritic lava. Phenocrysts of feldspars and opaque minerals including pyroxene and some amphiboles. The rock is moderately altered and bleached into whitish clays. Alteration minerals: pyrite, calcite, illite and quartz.

1334-1336 m No cuttings (Loss of circulation)

1336-1376 m Fine-grained trachyte: Greenish grey, fine-grained sanidine and pyroxene porphyritic lava. The rock is fractured, moderate to highly altered and veined. Quartz, pyrite and clays filled up the veins and vesicles. Alteration minerals: epidote, chlorite, pyrite and illite are the secondary minerals noted.

1376-1380 m No cuttings (Loss of circulation)

1380-1382 m Medium-grained trachyte: Light grey medium-grained porphyritic lava with phenocrysts of feldspars and mafic minerals (pyroxenes.). The rock is massive and moderately altered. Fractured cuttings were evidenced by highly altered surfaces. The dark minerals are prismatic. Alteration minerals: pyrite, calcite, illite and quartz.

1382-1384 m No cuttings (Loss of circulation)

1384-1424 m Medium-grained trachyte: Light grey medium-grained porphyritic lava with phenocryst of feldspars and mafic minerals (pyroxenes.). The rock is massive and has dark minerals which are prismatic. The rock is highly altered. Alteration minerals: pyrite, calcite, illite and quartz.

1424-1426 m No cuttings (Loss of circulation)

1426-1434 m Tuff: Light grey fine-grained poorly crystalline rock. Some cuttings are fragmental and vesicular. The fragments are small in size and has glassy matrix. Alteration minerals: pyrite, calcite, illite and quartz.

1434-1458 m Medium-grained trachyte: Light grey medium-grained porphyritic lava with phenocryst of feldspars and mafic minerals (pyroxenes.). The groundmass has a trachytic texture, composed mainly of flow aligned acicular alkali feldspars. Alteration minerals: pyrite, calcite, illite and quartz.

1458-1462 m Tuff: Light grey fine-grained poorly crystalline rock. The rock is vesicular, highly altered and has glassy matrix. Alteration minerals: quartz, calcite, pyrite and chlorites.

1462-1470 m Medium-grained trachyte: Light grey medium-grained porphyritic lava with phenocryst of feldspars and mafic minerals (pyroxenes). The rock is fractured and highly altered. Alteration minerals: quartz, calcite, albite, pyrite and illite.

1470-1472 m No cuttings (Loss of circulation)

1472-1478 m Tuff: Light grey, fine-grained poorly crystalline rock. The rock is vesicular and has glassy matrix. Alteration minerals: quartz, illite, pyrite and minor calcite.

1478-1484 m No cuttings (Loss of circulation)

1484-1490 m Pyroclastics: Reddish brownish grey mixed rock fragments. It is fine-grained, ashy and vesicular rock. The rock has vesicle infillings of mafic minerals, quartz, abundant pyrite and chlorites. Alteration minerals: quartz, chlorite, pyrite and minor calcite.

1490-1496 m No cuttings (Loss of circulation)

1496-1508 m Pyroclastics: Highly altered poorly crystalline and vesicular mixed cuttings. The rock appears re-worked with rounded fragments and abundant pyrite cubes disseminated in the groundmass. Alteration minerals: quartz, chlorite, illite, pyrite and minor calcite.

1508-1516 m No cuttings (Loss of circulation)

1516-1518 m Tuff/Pyroclastics: Grey to brownish grey, highly altered poorly crystalline vesicular rock fragments. The vesicles are filled up with quartz, calcite, and abundant pyrite. Alteration minerals: pyrite, calcite, illite and quartz.

1518-1526 m No cuttings (Loss of circulation)

1526-1542 m Pyroclastics: Grey to brownish grey, highly altered poorly crystalline and vesicular fragments. The vesicles are filled up with calcite, wollastonite and abundant pyrite. Alteration minerals: pyrite, illite, calcite, wollastonite and quartz.

1542-1544 m No cuttings (Loss of circulation)

1544-1550 m Tuff: Grey fine-grained poorly crystalline fragmental rock. The rock has fine-grained glassy matrix. The rock is fractured and highly altered. Calcite, pyrite, illite and wollastonite are the secondary minerals present.

1550-1552 m No cuttings (Loss of circulation)

1552-1560 m Medium-grained trachyte: Grey medium-grained sanidine and pyroxene porphyritic lava. Rock fractured and highly altered into clays. Secondary minerals: pyrite, calcite, wollastonite and illite.

1560-1564 m No cuttings (Loss of circulation)

1564-1578 m Medium-grained trachyte: Grey, medium-grained sanidine and pyroxene phyric lava. Minor quartz and pyrite veins were noted at this depth. Fracturing is evident by highly altered cuttings surfaces. Alteration minerals: calcite, pyrite, quartz and illite.

1578-1580 m Pyroclastics: Grey fine-grained ashy, vesicular and mixed rocks debris. The rock is highly altered. Pyrite, quartz illite and chlorite occur as secondary minerals.

1580-1582 m No cuttings (Loss of circulation)

1582-1586 m Medium-grained trachyte: Grey medium-grained phyric lava with phenocrysts of feldspars and mafic minerals. There is quartz veining and pyrite infilling. Fracturing is also evident by, highly altered cuttings surface. Alteration minerals: Pyrite, Quartz, calcite, wollastonite and illite.

1586-1600 m Tuff: Grey fine-grained poorly crystalline fragmental rock. The secondary minerals are mainly clays with some pyrite infilling. The rock is fractured and highly altered. Alteration minerals: Quartz, pyrite, calcite, illite and chlorite.

1600-1604 m No cuttings (Loss of circulation)

1604-1606 m Medium-grained trachyte: Grey medium-grained crystalline rock. The rock is porphyritic with sanidine and pyroxene phenocrysts. It is fractured and highly altered. Alteration minerals: Quartz, pyrite, calcite, illite and chlorite.

1606-1608 m No cuttings (Loss of circulation)

1608-1616 m Tuff: Grey, fine-grained poorly crystalline fragmental rock with glassy matrix. The rock is fractured and, highly altered. Alteration minerals: Quartz, pyrite, calcite, illite and chlorite.

1616-1618 m No cuttings (Loss of circulation)

1618-1650 m medium-grained trachyte: Grey, medium-grained sanidine and pyroxene porphyritic lava. Quartz veining evident in most cuttings. Alteration minerals: Quartz, pyrite calcite, illite and chlorite.

1648-1702 m Medium-grained trachyte: Brownish grey to grey, medium-grained porphyritic lava. The phenocrysts consist mainly of sanidine, pyroxenes and mafic minerals. The rock is fractured and has minor veins with quartz infilling. Alteration minerals: wollastonite, quartz, pyrite and illite.

1702-1722 m Tuff: Grey, fine-grained, poorly crystalline and fragmental rock, with glassy texture. The rock is bleached and highly altered into whitish clays. Alteration minerals: wollastonite, quartz, pyrite, epidote and illite.

1722-1724 m No cuttings (Loss of circulation)

1724-1732 m Medium-grained trachyte: Grey, medium-grained sanidine and pyroxene phyric lava. The rock is fractured and highly altered. Minor veins which are filled up with quartz and calcite were noted. The secondary minerals are mainly illite, quartz, epidote and pyrite.

1732-1734 m No cuttings (Loss of circulation)

1734-1742 m Fine-grained trachyte: Grey, fine-grained lava with phenocrysts of feldspars and mafic minerals. There is also some oxidation, quartz veining and pyrite infilling. Fracturing is also evident, highly altered. Alteration minerals: quartz, pyrite, wollastonite and illite.

1742-1746 m No cuttings (Loss of circulation)

1746-1756 m Syenitic intrusive: Grey, fresh, coarse-grained lava. The rock is porphyritic with phenocrysts of feldspars and mafic minerals. The rock is relatively fresh in a mixture of highly altered cuttings, suggesting a later intrusive activity. Alteration minerals: calcite (minor), wollastonite, pyrite, quartz and chlorite.

1756-1788 m Tuff: Grey, fine-grained poorly crystalline and fragmental rock with phenocrysts of feldspar and mafic minerals. The rock is fractured and highly bleached into whitish clays. Alteration minerals: calcite, pyrite, quartz and illite.

1788-1790 m Syenitic intrusive: Grey, fresh, coarse-grained lava. The rock is porphyritic with sanidine feldspars and mafic minerals. Minor veins were noted filled-up with quartz and pyrite. Alteration minerals: illite, pyrite, wollastonite, actinolite and quartz.

1790-1802 m No cuttings (Loss of circulation)

1802-1830 m Syenitic intrusive: Grey, fresh, coarse-grained lava which is equigranular with phenocrysts of feldspars and mafic minerals. There is also some oxidation, quartz veining and pyrite infilling. Fracturing was evident by highly altered surfaces. Alteration minerals: albite, illite, wollastonite, actinolite and quartz.

1830-1834 m No cuttings (Loss of circulation)

1834-1844 m Tuff: Light grey, poorly crystalline and fragmental rock. The rock is vesicular and highly altered. Vesicles and voids are filled up with calcite and clays. Alteration minerals: calcite, pyrite, wollastonite, quartz and illite.

1844-1850 m No cuttings (Loss of circulation)

1850-1872 m Medium-grained trachyte: Grey, medium-grained sanidine and pyroxene phyric lava. Quartz veins were noted. The rock is fractured and highly altered. Alteration minerals: wollastonite, pyrite quartz, actinolite and chlorite.

1872-1882 m No cuttings (Loss of circulation)

1882-1918 m Medium-grained trachyte: Grey, medium-grained sanidine and pyroxene porphyritic lava. Minor quartz veins were also evidenced in some cuttings. Fracturing was evidenced by highly altered cutting surfaces. Alteration minerals: actinolite, pyrite chlorite, quartz and illite.

1918-1934 m Tuff: Grey, fine-grained poorly crystalline fragmental rock. The rock is fractured, highly altered and has a glassy matrix. Alteration minerals: calcite, illite, epidote wollastonite and pyrite.

1934-1938 m No cuttings (Loss of circulation)

1938-1952 m Tuff: Brownish grey, fine-grained poorly crystalline fragmental rock. The rock is vesicular and has glassy texture. The rock is highly altered and bleached into whitish clays. Alteration minerals: wollastonite, actinolite, illite, epidote and pyrite.

1952-1980 m Syenitic intrusive: Grey, fresh, coarse-grained lava which is equigranular with phenocrysts of sanidine feldspars and mafic minerals. The rock is relatively fresh with minor chilled/fractured surfaces. Alteration minerals: quartz, pyrite, chlorite, illite and wollastonite.

1980-1986 m No cuttings (Loss of circulation)

1986-1992 m Syenitic intrusive: Grey, fresh, coarse-grained lava with phenocrysts of sanidine feldspars and mafic minerals. The rock is generally fresh with minor chilled or fractured surfaces. Alteration minerals: quartz, pyrite, illite, chlorite, wollastonite, albite and epidote.

1992-1998 m No cuttings (Loss of circulation)

1998-2000 m Syenitic intrusive: Grey, fresh, coarse-grained phyric lava. The phenocryst consists mainly of sanidine and mafic minerals. The rock is relatively fresh with minor chilled margins. Alteration minerals: quartz, pyrite, illite, wollastonite and epidote.

2000-2018 m Tuff: Grey fine-grained poorly crystalline rock it's fragmental with grains of previously formed rocks. The secondary minerals are mainly clays with some pyrite infilling. The rock is highly altered. Alteration minerals: pyrite, illite, wollastonite and actinolite.

2018-2024 m No cuttings (Loss of circulation)

2024-2038 m Fine-grained trachyte: Brownish grey, fine-grained sanidine and pyroxene porphyritic lava. The rock is fractured, altered and has minor quartz veins. Alteration minerals: actinolite, wollastonite, illite, chlorite and epidote.

2038-2044 m No cuttings (Loss of circulation)

2044-2080 m Fine-grained trachyte: Grey, fine-grained lava which is equigranular with phenocrysts mainly of sanidine and mafic minerals. The rock is fractured, altered and has minor veins filled with quartz, illite and pyrite. Alteration minerals: actinolite, wollastonite, illite, quartz and adularia.

2080-2082 m No cuttings (Loss of circulation)

2082-2106 m Glassy trachyte: Grey fine-grained poorly crystalline glassy lava. The rock consists of fresh, quenched glass which has minor phenocryst of sanidine and mafic minerals. These cuttings were interpreted to be formed as a result of a shallow magma intrusion. Alteration minerals: actinolite wollastonite, epidote, illite and pyrite.

APPENDIX E: Lithological description and hydrothermal alteration minerals of well MW-06

0-4 m No cuttings (Loss of circulation).

4-6 m Pyroclastics: Brownish grey mixed rock fragments consisting of soils, obsidian glass, and ashy rock debris. Some cuttings are vesicular and highly oxidized into reddish oxides. Alteration minerals: oxides.

6-14 m No cuttings (Loss of circulation)

14-36 m Fine-grained trachyte: Dark grey fine-grained sanidine and pyroxene porphyritic lava. The rock is generally fresh and massive with minor oxidized surfaces due to water-rock interaction. Alteration minerals: Oxides.

36-40 m No cuttings (Loss of circulation)

40-50 m Fine-grained trachyte: Brownish grey fine-grained sanidine and pyroxene porphyritic lava. The rock is generally fresh with minor fractured and oxidized surface. Alteration minerals: Oxides.

50-52 m No cuttings (Loss of circulation)

52-66 m Fine-grained trachyte: Grey fine-grained sanidine porphyritic rock. The pyroxenes are the mafic phenocrysts in groundmass of feldspars the rock is massive and fresh. Alteration minerals: oxides.

66-72 m Pyroclastics: Brownish grey to reddish brown fine-grained lava the rock is vesicular and fresh with medium sized vesicles obsidian fragments are also seen. Alteration minerals: Oxides.

72-80 m Fine-grained trachyte: Dark grey fine-grained sanidine and pyroxene porphyritic rock. The rock is generally fresh with minor fractured and oxidized surfaces. Alteration minerals: Oxides.

80-84 m Pyroclastics: Brownish grey to reddish brown mixed, reworked and ashy fragments. Obsidian fragments constitute some of the cuttings. Alteration minerals: Oxides.

84-134 m Medium-grained trachyte: Brownish grey medium-grained sanidine and pyroxene porphyritic rock with phenocrysts of pyroxenes in fine-grained groundmass of feldspars. The rock is massive and generally fresh, however minor fractured and oxidized surfaces were noted. Alteration minerals: Oxides.

134-136 m Fine-grained trachyte: Light grey fine-grained lava with phenocrysts of sanidine and pyroxene. The rock is massive and slightly oxidized. Alteration minerals: Oxides.

136-150 m No cuttings (Loss of circulation)

150-152 m Fine-grained trachyte: Light grey fine-grained lava with phenocrysts of alkali feldspars and pyroxenes. The rock is massive and slightly oxidized. Alteration minerals: Oxides.

152-156 m No cuttings (Loss of circulation)

156-160 m Medium-grained trachyte: Light grey medium-grained lava with phenocrysts of feldspars and pyroxenes. The rock is massive and slightly oxidized. Alteration minerals: Oxides.

160-166 m No cuttings (loss of circulation)

166-180 m Fine-grained trachyte: Grey fine-grained lava with phenocrysts of feldspars and pyroxenes. The rock is massive and slightly oxidized. Alteration minerals: Oxides.

180-208 m Medium-grained trachyte: Brownish grey, medium-grained sanidine and pyroxene porphyritic rock. The rock is generally fresh though few cuttings are fractured and highly oxidized as a result of surface-water rock interaction. Alteration minerals: Oxides.

208-240 m Pyroclastics: Brownish grey to reddish grey mixed rock fragments; some porphyritic, some vesicular and highly altered. Alteration minerals: Oxides.

240-264 m medium-grained trachyte: Brownish grey medium-grained sanidine and pyroxene porphyritic lava. Massive and oxidized on fractured surfaces. Alteration minerals: Oxides and zeolite (cowlescite).

264-268 m Pyroclastics: highly oxidized reddish brown ashy and mixed debris. Some are vesicular, while others are poorly crystalline fragments. Alteration minerals: Oxide, zeolite and smectite.

268-334 m Phonolite: Brown to brownish grey, medium-grained sanidine and pyroxene porphyritic lava. Rock slightly altered with minor oxidized and fractured surfaces. Alteration minerals: oxides, smectite.

334-366 m Pyroclastics/tuff: Brownish to reddish brown, fine-grained vesicular rock. The rock is porphyritic with phenocrysts of sanidine and pyroxene. The rock is slightly fractured and altered. Alteration minerals: calcite, chalcedony, pyrite and zeolite.

366-386 m Tuff: Brownish grey highly oxidized poorly crystalline and vesicular fragments. The rock has glassy matrix and dark (mafic) microphenocrysts enclosed in fine-grained groundmass. Alteration minerals: calcite, pyrite, and clays.

386-400 m No cuttings (Loss of circulation)

400-402 m Tuff: Brownish grey to reddish brown, poorly crystalline rock with glassy matrix. The rock is slightly oxidized and exhibits slight alteration into clays and minor calcite. Alteration minerals: smectite, calcite, chalcedony, pyrite and zeolite.

402-436 m Medium-grained trachyte: Greenish grey, sanidine and pyroxene porphyritic rock. It is massive with feldspars and dark mafic minerals (pyroxene).as primary minerals. The rock is slightly fractured and moderately altered. Alteration minerals: smectite, calcite, chalcedony, pyrite and zeolite.

436-444 m Tuff: Light grey to brownish grey, vesicular and poorly crystalline rock. The rock is moderately altered and has vesicles filled with clays and pyrite. Minor veins were noted, filled with mainly chalcedony and clays. Alteration minerals: calcite, chalcedony, pyrite and zeolite.

444-456 m Medium-grained trachyte: Grey medium-grained sanidine and pyroxene porphyritic lava. The rock is moderately altered and has minor fractured surfaces. Alteration minerals: calcite, chalcedony, pyrite and zeolite.

456-458 m Pyroclastics: Brownish grey to greenish grey, ashy and vesicular mixed rock debris. The vesicles are filled with clays and calcite. The rock is highly altered. Alteration minerals: calcite, chalcedony, pyrite and zeolite.

458-492 m Medium-grained trachyte: Grey medium-grained sanidine and pyroxene porphyritic lava. It's massive and slightly altered. Minor fractured surfaces were noted. Alteration minerals: calcite, chalcedony, pyrite and zeolite.

492-498 m Pyroclastics: Brown to brownish grey, fine-grained, ashy and vesicular rock debris. The rock is highly oxidized and unsorted. Alteration minerals: oxides, chalcedony, pyrite, smectite and zeolite.

498-600 m Fine-grained trachyte: Brownish grey, fine-grained sanidine and pyroxene porphyritic lava. The rock is massive and moderately altered. It has feldspathic groundmass with mafic minerals present as microphenocrysts. Alteration minerals: oxides, pyrite, calcite, smectite, and zeolite.

600-616 m Medium-grained trachyte: Grey medium-grained sanidine porphyritic rock.it is massive with feldspathic groundmass. The rock is moderately altered and has slightly oxidized surfaces. Alteration minerals: oxides, pyrite, calcite, quartz, smectite, and zeolite.

616-618 m Tuff: Dark grey, fine-grained porphyritic rock. The rock is vesicular and poorly crystalline. It has glassy matrix and is highly altered into reddish brown clays. Alteration minerals: smectite, quartz, pyrite and calcite.

618-630 m Pyroclastics: Brownish grey, fined-grained rock sanidine porphyritic.it is mixture of highly oxidized vesicular rock fragments. The vesicles are filled with calcite and clays. Alteration minerals: oxides, calcite, pyrite and smectite.

630-704 m Tuff: Dark grey fine-grained porphyritic rock. The rock is vesicular and has glassy matrix. It is highly altered into reddish brown clays. Alteration minerals: oxides, smectite, calcite and pyrite.

704-710 m Medium-grained trachyte: Brownish grey, medium-grained lava with phenocrysts of sanidine and pyroxenes. Rock partly massive and partly vesicular; also slightly oxidised and moderately altered. Minor quartz and calcite veins were noted. Alteration minerals: oxides, quartz, calcite, pyrite and clays.

710-712 m No cuttings (Loss of circulation)

712-724 m Tuff: Dark grey fine-grained poorly crystalline and vesicular rock. The rock is highly altered with clays infill in vesicles and voids. Alteration minerals: oxides, smectite, pyrite, calcite and quartz.

724-728 m No cuttings (Loss of circulation)

728-744 m Fine-grained trachyte: Light grey, fine-grained sanidine porphyritic rock its massive feldspar laths aligned in preferred trachoid flow texture. The rock is highly altered. The groundmass is fine-grained and is mainly feldspathic. Alteration minerals: smectite, quartz, calcite and pyrite.

744-748 m No cuttings (Loss of circulation)

748-770 m Medium-grained trachyte: Light grey, medium-grained sanidine and pyroxene porphyritic rock. The rock is massive and has feldspar laths aligned in preferred trachoid flow texture. The groundmass is fine grained and is mainly feldspathic. Few veins were noted, filled up with quartz and calcite. The rock is fractured and highly altered. Alteration minerals: calcite, quartz, pyrite and illite.

770-778 m No cuttings (Loss of circulation)

778-796 m Medium-grained trachyte: Light grey, medium-grained sanidine and pyroxene porphyritic rock. The rock is massive and has feldspar laths aligned in preferred trachoid flow texture. The groundmass is fine grained and is mainly feldspathic. Alteration minerals: smectite, calcite, pyrite, quartz and clays.

796-798 m No cuttings (Loss of circulation)

798-808 m Medium-grained trachyte: Light grey, to brownish grey, medium-grained sanidine and pyroxene porphyritic rock. The rock is fractured and moderately altered. Alteration minerals: calcite, pyrite, quartz and clays.

808-812 m No cuttings (Loss of circulation)

812-816 m Medium-grained trachyte: Light grey, medium-grained sanidine and pyroxene porphyritic rock. The rock is highly altered; evidenced by highly altered cutting surfaces. Alteration minerals: Smectite, calcite, quartz, pyrite and illite.

816-820 m No cuttings (Loss of circulation)

820-830 m Medium-grained trachyte: Light grey to brownish grey, medium-grained sanidine and pyroxene porphyritic rock. The rock is massive and has feldspar laths aligned in preferred trachoid flow texture. The groundmass is fine grained and is mainly feldspathic. Fracturing was evidenced by highly altered surfaces. Alteration minerals: smectite, calcite, pyrite, and clays.

830-834 m No cuttings (Loss of circulation)

834-836 m Medium-grained trachyte: Light grey, medium-grained sanidine and pyroxene porphyritic rock. The rock is massive, fractured and is highly altered. The groundmass is fine grained and is mainly feldspathic. Alteration minerals: calcite, pyrite and clays.

836-840 m No cuttings (Loss of circulation)

840-844 m Medium-grained trachyte: Light grey, medium-grained sanidine and pyroxene porphyritic rock. The rock is massive, fractured and is highly altered. The groundmass is fine grained and is mainly feldspathic. Alteration minerals: calcite, pyrite and illite.

844-846 m No cuttings (Loss of circulation)

846-848 m Medium-grained trachyte: Light grey, medium-grained sanidine and pyroxene porphyritic rock. The rock is massive, fractured and is highly altered. The groundmass is fine grained and is mainly feldspathic. Alteration minerals: calcite, pyrite and illite.

848-860 m No cuttings (Loss of circulation)

860-864 m Medium-grained trachyte: Light grey, medium-grained sanidine and pyroxene porphyritic rock. The rock is massive, fractured and is highly altered. The groundmass is fine grained and is mainly feldspathic. Alteration minerals: calcite, pyrite and smectite.

864-866 m No cuttings (Loss of circulation)

866-884 m Medium-grained trachyte: Light grey, medium-grained sanidine and pyroxene porphyritic rock. The rock is fractured and highly altered. The groundmass is fine grained and is mainly feldspathic. Alteration minerals: smectite, calcite, pyrite and quartz.

884-886 m Syenite intrusion: Light grey, coarse-grained sanidine and pyroxene porphyritic rock. The rock is fresh with slightly altered on some surfaces. It's massive and has feldspar laths aligned in preferred trachoid flow texture. The groundmass is fine grained and is mainly feldspathic. Alteration minerals: calcite, pyrite and illite clays.

886-914 m Medium-grained trachyte: Light grey, medium-grained sanidine and pyroxene porphyritic lava. The rock is massive and has feldspar laths aligned in preferred trachoid flow texture. The groundmass is fine grained and is mainly feldspathic. Alteration minerals: calcite, pyrite and illite.

914-922 m No cuttings (Loss of circulation)

922-930 m Medium-grained trachyte: Light grey, to brownish grey, medium-grained sanidine and pyroxene porphyritic rock. The rock is massive and has feldspar laths aligned in preferred trachoid flow texture. The groundmass is fine grained and is mainly feldspathic. Alteration minerals: calcite, pyrite and clays.

930-938 m No cuttings (Loss of circulation)

938-950 m Medium-grained trachyte: Light grey, medium-grained sanidine and pyroxene porphyritic lava. The rock is has feldspar laths aligned in preferred trachoid flow texture. The rock is fractured and is highly altered. Alteration minerals: calcite, pyrite and clays.

950-956 m No cuttings (Loss of circulation)

956-960 m Medium-grained trachyte: Light grey, to brownish grey, medium-grained sanidine and pyroxene porphyritic lava. The rock is massive and has feldspar laths aligned in preferred trachoid flow texture. The rock is fractured and is highly bleached into whitish clays. Alteration minerals: Quartz, calcite, pyrite and illite.

960-966 m Pyroclastics: Brownish grey to reddish grey, ashy, fined-grained rock debris. The rock is a mixture of highly oxidized vesicular fragments. The vesicles are filled with calcite and clays. Alteration minerals: Smectite, calcite, pyrite, albite, quartz and illite.

966-990 m Medium-grained trachyte: Light grey, medium-grained sanidine and pyroxene porphyritic lava. The rock is massive feldspar laths aligned in preferred trachoid flow texture. The groundmass is fine grained and is mainly feldspathic. Alteration minerals: calcite, pyrite and illite.

990-994 m No cuttings (Loss of circulation)

994-1016 m Medium-grained trachyte: Light grey, medium-grained sanidine and pyroxene porphyritic lava. The rock is massive feldspar laths aligned in preferred trachoid flow texture. The groundmass is fine grained and is mainly feldspathic. Alteration minerals: quartz, calcite, pyrite and illite.

1016-1020 m No cuttings (Loss of circulation)

1020-1040 m Medium-grained trachyte: Light grey, medium-grained sanidine and pyroxene porphyritic lava. The rock is massive feldspar laths aligned in preferred trachoid flow texture. The rock is moderate to highly altered. Alteration minerals: calcite, quartz, pyrite and clays.

1040-1054 m No cuttings (Loss of circulation)

1054-1094 m Medium-grained trachyte: Light grey, medium-grained sanidine and pyroxene porphyritic lava. The rock is massive feldspar laths aligned in preferred trachoid flow texture. The rock is fractured and moderately altered. Alteration minerals: calcite, pyrite and epidote.

1094-1104 m Tuff: Grey fined-grained poorly crystalline rock. The rock is has glassy matrix and is highly altered into clays. It is vesicular, with vesicles filled up with calcite and clays.

1104-1124 m Syenite intrusion: Light grey, coarse-grained sanidine and pyroxene porphyritic rock. The rock is fresh with slightly altered on some faces. Its massive feldspar laths aligned in preferred trachoid flow texture. The groundmass is fine-grained and is mainly feldspathic. Alteration minerals: calcite, pyrite and illite.

1124-1152 m No cuttings **(**Loss of circulation)

1152-1184 m Medium-grained trachyte: Light grey medium-grained sanidine and pyroxene porphyritic lava. The rock is fractured and highly altered. The groundmass is fine grained and is mainly feldspathic. Minor quartz veins were noted in this zone. Alteration minerals: quartz, calcite, pyrite, epidote and illite.

1184-1360 m Fine-grained trachyte: Dark grey fine-grained sanidine and pyroxene porphyritic rock. The rock is fractured and highly altered. The fine-grained feldspar laths in the groundmass have aligned in preferred trachoid flow texture. Alteration minerals: quartz, calcite, albite, epidote, pyrite and illite.

1360-1362 m No cuttings **(**Loss of circulation)

1362-1408 m Fine-grained trachyte: Dark greenish grey, fine- to medium-grained porphyritic rock. The phenocrysts consist mainly of sanidine and pyroxene in a glassy groundmass. The rock is moderately fractured and is completely oxidized from 1472-1480 m depth. Alteration minerals: Pyrite, quartz, calcite, albite, epidote and illite.

1408-1426 m Medium-grained trachyte: Light grey medium-grained sanidine and pyroxene porphyritic lava. The rock is fractured and highly altered. The groundmass is fine grained and is mainly feldspathic. Alteration minerals: calcite, pyrite and clays.

1426-1448 m Tuff: Light grey, fine-grained poorly crystalline rock. The rock is vesicular and has dark microphenocrysts of mafic minerals in fine-grained glassy groundmass. It is highly altered and bleached into whitish clays. The vesicles are filled with calcite and clays. Alteration minerals: calcite, albite, epidote, pyrite and illite.

1448-1464 m Medium-grained trachyte: Light grey, medium-grained sanidine and pyroxene porphyritic rock. The rock is massive and has feldspar laths aligned in preferred trachoid flow texture. The groundmass is fine grained and is mainly feldspathic. Few small veins were noted, filled up with quartz, calcite and clays. Alteration minerals: calcite, quartz, pyrite and illite.

1464-1476 m Tuff: Grey, fine-grained poorly crystalline rock. The rock is vesicular and highly altered. The rock has dark microphenocrysts of mafic minerals in fine-grained glassy groundmass. Fractured surfaces were noted in some cuttings. The vesicles are filled with calcite and clays. Alteration minerals: Quartz, calcite, pyrite and illite.

1476-1482 m Medium-grained trachyte: Light grey, medium-grained sanidine and pyroxene porphyritic rock. The groundmass is fine grained and is mainly feldspathic. The rock is massive and is moderately altered. Alteration minerals: calcite, pyrite and illite.

1482-1502 m Tuff: Grey, fine-grained poorly crystalline rock. It is mixture of highly oxidized vesicular rock fragments. The vesicles are filled with calcite and clays. The rock has dark microphenocrysts of mafic minerals in fine-grained glassy groundmass. Alteration minerals: calcite, pyrite, illite and chlorite.

1502-1536 m Medium-grained trachyte: Brownish grey medium-grained porphyritic lava with phenocrysts of pyroxenes, the ground mass is feldspathic. The rock is highly altered and bleached into whitish clays. Alteration minerals: calcite, pyrite and illite.

1536-1540 m Fine-grained trachyte: Dark grey fine-grained porphyritic rock with phenocrysts of pyroxene. The rock is moderately altered and groundmass is made up, mainly of feldspars. Alteration minerals: calcite, pyrite, quartz and illite.

1540-1556 m Medium-grained trachyte: Light grey medium-grained sanidine and pyroxene porphyritic rock. The rock is moderately to highly altered. It is massive and has feldspar laths aligned in preferred trachoid flow texture. The groundmass is fine-grained and is mainly feldspathic. Alteration minerals: calcite, pyrite, quartz and clays.

1556-1574 m Tuffs: Grey to reddish grey, fined-grained poorly crystalline and vesicular rock. The rock has a dark (mafic) microphenocrysts enclosed in glassy matrix. It is fractured and highly altered. The vesicles are filled with calcite and clays. Alteration minerals: calcite, pyrite, quartz and clays.

1574-1590 m Fine-grained trachyte: Dark grey fine-grained porphyritic rock with phenocrysts of sanidine and pyroxenes. The rock is moderately altered and has groundmass of mainly sanidine feldspars. Alteration minerals: calcite, pyrite, quartz and clays.

1590-1596 m Tuff: Grey to reddish grey, fined-grained poorly crystalline and vesicular rock. The rock has a dark (mafic) microphenocrysts enclosed in glassy matrix. It is fractured and highly altered. The vesicles are filled with calcite and clays. Alteration minerals: calcite, pyrite, quartz and clays.

1596-1614 m Fine-grained trachyte: Dark grey fine-grained porphyritic rock with phenocrysts of sanidine and pyroxenes. The rock is moderately altered and has groundmass of mainly sanidine feldspars. Alteration minerals: calcite, pyrite, quartz and illite.

1614-1644 m Palaeo-soils and tuffaceous sediments: Reddish brown, highly oxidized mixed soils and vesicular rock sediments. Sediments are vesicular, reworked and poorly crystalline. The vesicles are filled with pyrite, calcite and clays. Alteration minerals: calcite, pyrite, quartz and illite.

1644-1678 m Syenitic intrusion: light grey, coarse-grained sanidine and pyroxene porphyritic rock. The rock is fresh indicating later activity. The groundmass is fine grained and is mainly feldspathic. Alteration minerals: calcite, pyrite, quartz and illite.

1678-1702 m Medium-grained trachyte: Light grey medium-grained sanidine porphyritic rock its massive feldspar laths aligned in preferred trachoid flow texture. The groundmass is fine grained and is mainly feldspathic. Alteration minerals: calcite, pyrite, quartz and illite.

1702-1704 m Tuff: Grey to reddish grey, fine-grained poorly crystalline and vesicular rock. The rock has a dark (mafic) microphenocrysts enclosed in glassy matrix. It is fractured and highly altered. The vesicles are filled with calcite and clays. Alteration minerals: calcite, pyrite, quartz and chlorite clays.

1704-1728 m Fine-grained trachyte: Dark grey fine-grained porphyritic rock with phenocrysts of sanidine and pyroxenes. The rock is moderately altered and has groundmass of mainly sanidine feldspars. Alteration minerals: calcite, pyrite, quartz and illite.

1728-1734 m Medium-grained trachyte: Grey medium-grained sanidine porphyritic rock its massive feldspar laths aligned in preferred trachoid flow texture. The groundmass is fine grained and is mainly feldspathic. Alteration minerals: calcite, pyrite, quartz and illite.

1734-1744 m Fine-grained trachyte: Dark grey fine-grained porphyritic rock with phenocrysts of pyroxenes. The rock is moderately altered with minor fractured surfaces. Alteration minerals: Quartz, calcite, pyrite, chlorite and illite.

1744-1754 m Medium-grained trachyte: Light grey to brownish grey, medium-grained sanidine and pyroxene porphyritic rock. It is highly altered and fractured. Minor quartz veins were noted. Alteration minerals: Quartz, calcite, pyrite and illite.

1754-1768 m Fine-grained trachyte: Dark grey fine-grained porphyritic rock with phenocrysts of sanidine and pyroxenes. The rock is moderately altered and has pyrite cubes being disseminated in fine-grained groundmass. Alteration minerals: Pyrite, calcite (minor) and quartz.

1768-1786 m Medium-grained trachyte: Light grey to brownish grey, medium-grained sanidine and pyroxene porphyritic rock. The rock is highly altered and has massive feldspar laths aligned in preferred trachoid flow texture. Pyrite cubes is being disseminated in fine-grained matrix. Alteration minerals: Pyrite, quartz and illite.

1786-2084 m Fine-grained trachyte: Dark grey fine-grained porphyritic rock with phenocrysts of pyroxenes. The rock is moderately to highly altered into greenish grey clays. Alteration minerals: quartz, pyrite, chlorite and illite.

2084-2114 m Medium-grained trachyte: Light grey medium-grained sanidine and pyroxene porphyritic rock. The rock is highly altered, massive and has feldspar laths aligned in preferred trachoid flow texture. Alteration minerals: wollastonite, actinolite, pyrite, and illite.

2114-2124 m No cuttings (Loss of circulation)

2124-2174 m Medium-grained trachyte: Light grey medium-grained Sanidine porphyritic rock its massive highly altered and has feldspar laths aligned in preferred trachoid flow texture. The groundmass is fine-grained and is mainly feldspathic. Alteration minerals: pyrite, wollastonite and actinolite.

2174-2190 m. Chilled fresh glassy cuttings. Dark grey fresh quenched glassy cuttings with microphenocrysts of mafic dark minerals. Epidote, wollastonite, actinolite and illite are the main alteration minerals.

APPENDIX F: Lithological description and hydrothermal alteration minerals of well MW-07

0-10 m No cuttings (Loss of circulation)

10-12 m Pyroclastics: Brownish grey, mixed rock fragments, comprising of glassy, vesicular, ashy and oxidized rock debris. Iron oxides are the only alteration mineral present.

12-20 m No cuttings (Loss of circulation)

20-68 m Fine-grained trachyte: Brownish grey, fine-grained porphyritic rock consisting of sanidine and pyroxene phenocrysts. The rock is generally fresh with minor fractured and oxidized surfaces. Alteration minerals: Oxides.

68-78 m Medium-grained trachyte: Light grey medium-grained sanidine porphyritic rock its massive feldspar laths aligned in preferred trachoid flow texture. The groundmass is fine grained and is mainly feldspathic. Alteration minerals: Oxides.

78-118 m Tuff: Brownish grey, poorly crystalline and vesicular rock fragments. The rock is highly oxidized into reddish brown clays. Alteration minerals: Oxides.

118-156 m Trachy phonolite: light grey, fine-grained sanidine and pyroxene porphyritic lava. The rock is slightly oxidized and becomes intensely oxidized between 124-156 m. Alteration minerals: oxides.

156-290 m *Medium-grained trachyte:* Light grey, medium-grained sanidine and pyroxene phyric rock. The rock is generally fresh, massive and has feldspar laths aligned in preferred trachoid flow texture. The groundmass is fine grained and is mainly feldspathic. Alteration minerals: oxides.

290-322 m Tuff: Brownish grey, poorly crystalline and vesicular rock fragments. The rock is highly oxidized into reddish brown oxides. Oxides and clay minerals are the secondary minerals present

322-368 m Fine-grained trachyte: light to dark grey, fine-grained and porphyritic. Sanidine phenocrysts are elongated and scattered in the rock matrix. The rock is slightly oxidized and becomes intensely. Alteration minerals: Oxides.

368-384 m Pyroclastics: Brownish grey to reddish brown, ashy and mixed rock fragments. The rocks are highly altered and oxidized. Alteration minerals: Oxides.

384-412 m Medium-grained trachyte: Light grey, medium-grained sanidine and pyroxene phyric rock. The rock is massive and has feldspar laths aligned in preferred trachoid flow texture. The groundmass is fine grained and is mainly feldspathic. The rock is moderately altered with minor oxidized fractured surfaces. Alteration minerals: oxides.

412-458 m Tuff: Light grey, poorly crystalline vesicular rock fragments. The rock has fine-grained glassy matrix. The rock is fractured and highly bleached into whitish clays. Alteration: oxides, minor calcites and clays.

458-462 m No cuttings (Loss of circulation)

462-472 m Tuff: Light grey, poorly crystalline vesicular rock fragments. The rock has fine-grained glassy matrix. The rock is fractured and is highly bleached into whitish clays. Alteration: oxides, chalcedony, smectite, calcite and pyrite.

472-526 m Medium-grained trachyte: Light grey to greenish grey, medium-grained sanidine and pyroxene phyric lava. The rock is fractured and moderately altered. Alteration minerals: oxides, chalcedony, smectite, calcite and pyrite.

526-538 m Tuff: Light grey to greenish grey, poorly crystalline and vesicular rock. The rock has fine-grained glassy matrix. The rock is highly altered into greenish clays. Alteration minerals: oxides, smectite, calcite and pyrite.

538-546 m Fine-grained trachyte: Greenish grey, sanidine and pyroxene moderately altered porphyritic lava. Fracturing evident by highly oxidized surfaces. Alteration minerals: oxides, smectite, calcite and pyrite.

546-588 m Tuff: Reddish brown, poorly crystalline and vesicular rock. The rock is fractured and highly altered. Alteration minerals: Smectite, calcite, pyrite and chalcedony.

588-680 m Phonolite: Light grey to greenish grey, fine-gained sanidine and pyroxene porphyritic lava. Rock moderately altered into greenish clays. Alteration minerals calcite, pyrite, chalcedony, smectite.

680-692 m Medium-grained trachyte: Light grey to greenish grey, medium-grained sanidine and pyroxene phyric lava. The rock is moderately altered and oxidized. Alteration minerals: pyrite, calcite and quartz.

692-694m No cuttings (Loss of circulation)

694-704 m Medium-grained trachyte: Light grey, medium-grained sanidine and pyroxene phyric rock. The rock is moderately to highly altered. It is massive and has feldspar laths aligned in preferred trachoid

flow texture in fine-grained matrix. Alteration minerals: pyrite, calcite and chlorite.

704-706 m No cuttings (Loss of circulation)

706-758 m Fine-grained trachyte: Brownish grey, fine-grained sanidine and pyroxene porphyritic lava. The rock is moderately to highly altered. The rock has minor veins filed in with calcite and clays. Calcite, pyrite, clays form the main secondary minerals.

758-802 m Medium-grained trachyte: Light grey medium-grained sanidine and pyroxene phyric rock. The rock is massive and has feldspar laths aligned in preferred trachoid flow texture. The rock has a fine-grained groundmass which is mainly feldspathic. Alteration minerals: quartz, pyrite and calcite.

802-814 m Tuff: Light grey, poorly crystalline and vesicular rock. The rock has glassy matrix which are extensively altered into clays and calcite. Alteration minerals: quartz, albite, pyrite and calcite.

814-820 m No cuttings (Loss of circulation)

820-866 m Phonolite: Brownish grey, fine-grained sanidine and pyroxene porphyritic lava. The rock is highly altered and bleached into whitish clay. Alteration minerals: pyrite, calcite and illite.

866-872 m Syenitic intrusion: Light grey, coarse-grained, sanidine and pyroxene phyric lava. The rock is generally fresh with slightly chilled margins. Alteration minerals: Oxide, calcite, pyrite and illite.

872-892 m Tuff: Light grey, poorly crystalline vesicular rock. The rock is highly altered . The rock has glassy matrix. Alteration minerals: Calcite, pyrite and chlorite

892-950 m Fine-grained trachyte: Brownish grey, fine-grained sanidine and pyroxene porphyritic lava. Rock moderately to highly altered. Minor veins noted, filled in with calcite and clays. Epidote coloration was evidenced in some samples especially from 948m. Alteration minerals: Calcite, pyrite and illite.

950-988 m Tuff: Reddish brown, poorly crystalline, fine gained and vesicular rock. The rock is fractured and is highly altered. Pyrite was noted disseminated in the fine-grained groundmass and in vesicles. Calcite and quartz occurs as infill in vesicles. Secondary minerals: Epidote, quartz, calcite, pyrite.

988-1148 m Rhyolite: Light grey, quartz and feldspar porphyritic rock. The rock is highly altered and has feldspar laths aligned in flow texture. Quartz veining was evidenced. Alteration minerals: quartz, calcite, pyrite and illite.

1148-1176 m Fine-grained trachyte: Light grey, fine-grained sanidine and pyroxene phyric lava. The rock is massive and has feldspar laths aligned in preferred trachoid flow texture. The rock is fractured and highly altered into clays. Minor quartz veining was evidenced. Alteration minerals: quartz, calcite, pyrite and illite.

1176-1192 m Tuff: Brownish grey, poorly crystalline, fine-grained and vesicular rock. The rock is fractured and is highly altered. Pyrite cubes noted disseminated in groundmass and in vesicles. Calcite and quartz occurs as infill in veins and vesicles. Alteration minerals: Calcite, quartz, pyrite and clays.

1192-1224 m No cuttings (Loss of circulation)

1224-1264 m Trachydacite: Brownish grey to greenish grey, fine-grained sanidine and pyroxene phyric lava. The rock is fractured and highly altered. The rock is massive and has feldspar laths aligned in preferred trachoid flow texture. Alteration minerals: Epidote, pyrite, calcite, quartz and chlorite.

1264-1274 m No cuttings (Loss of circulation)

1274-1292 m Tuff: Brownish grey moderate to altered poorly crystalline fine gained and vesicular rock. The rock is fractured and highly altered. Pyrite disseminated in the groundmass. Calcite and quartz occurs as infill in vesicles. Veining was evidenced which were filled in with quartz and calcite. Alteration minerals: Pyrite, quartz, calcite and illite.

1292-1314 m Fine-grained trachyte: Brownish grey, fine-grained lava composed mainly of feldspars and pyroxene phenocrysts. The rock is moderately altered. Few quartz and calcite veins were noted. Pyrite cubes dissemination in fine-grained matrix. Alteration minerals: Pyrite, quartz, calcite and illite.

1314-1322 m Syenitic intrusion: Light grey, coarse-grained massive and porphyritic lava with large phenocrysts of sanidine and pyroxenes. It shows low intensity of alteration and has abundant calcite. Minor highly altered chilled margin were noted. Alteration minerals: Pyrite, epidote, quartz, calcite and illite.

1322-1460 m Fine-grained trachyte: Brownish grey to greenish grey, fine-grained sanidine and pyroxene porphyritic lava. The rock is fractured and is highly altered into greenish clays. Deposition of clays, quartz and calcite on the fractured surfaces was noted. Alteration minerals: Pyrite, epidote, quartz, calcite and illite.

1460-1482 m No cuttings (Loss of circulation)

1482-1486 m Trachy phonolite: Brownish grey, fine-grained lava composed mainly of sanidine feldspars and pyroxenes phenocrysts. The rock is highly altered. Minor quartz veins are present. Pyrite cubes were dissemination in fine-grained groundmass. Alteration minerals: Pyrite, quartz, calcite wollastonite, illite.

1486-1514 m No cuttings (Loss of circulation)

1514-1520 m Fine-grained trachyte: Grey to greenish and brownish grey fine-grained, porphyritic, highly altered trachyte. Plenty of pyrite, chalcopyrite, calcite and wollastonite as secondary minerals.

1520-1534 m No cuttings (Loss of circulation)

1534-1546 m Fine-grained trachyte: Brownish grey, fine-grained lava composed mainly of sanidine feldspars and pyroxene phenocrysts. The rock is highly altered. Few quartz veins are also present. Pyrite dissemination on groundmass is noted. Alteration minerals: Pyrite, quartz, calcite and illite and wollastonite.

1546-1580 m No cuttings (Loss of circulation)

1580-1588 m Tuff: Brownish grey moderate to altered poorly crystalline fine gained and vesicular rock. The rock is fractured and highly altered. Pyrite disseminated in the groundmass. Calcite and quartz occurs as infill in veins and vesicles. Alteration minerals: calcite, quartz and clays.

1588-1610 m Fine-grained trachyte: Brownish grey, fine-grained lava composed mainly of feldspars and pyroxenes phenocrysts. The rock is moderately to highly altered. Minor quartz veins noted. Pyrite cubes dissemination in fine-grained groundmass. Alteration minerals: quartz, calcite, pyrite and clays.

1610-1616 m No cuttings (Loss of circulation)

1616-1678 m Fine-grained trachyte: Brownish grey, fine-grained sanidine and pyroxene porphyritic lava. The rock is moderately altered into greenish clays. Minor fractured surfaces were noted. Alteration minerals: calcite, quartz and clays.

1678-1696 m Syenitic intrusion: Light grey, generally fresh, coarse-grained massive and porphyritic lava with large phenocrysts of sanidine and pyroxenes. It shows low intensity of alteration and has abundant calcite. Alteration minerals: calcite, pyrite quartz and clays.

1696-1712 m Tuff: Brownish grey moderate to altered poorly crystalline fine gained and vesicular rock. The rock is fractured and highly altered. Pyrite disseminated in fine-grained matrix. Calcite and quartz occurs as infill in veins and vesicles. Alteration minerals: calcite, quartz, and clays.

1712-1720 m No cuttings (Loss of circulation)

1720-1724 m Medium-grained trachyte: Brownish grey, fine-grained lava composed mainly of sanidine and pyroxenes phenocrysts. The rock is highly altered and bleached into brownish and whitish clays. Alteration minerals: Pyrite, calcite and illite.

1724-1728 m No cuttings (Loss of circulation)

1728-1734 m Syenitic intrusion: Light grey, coarse-grained, massive and porphyritic syenite with large phenocrysts of sanidine and pyroxenes. It shows low intensity of alteration and has abundant calcite. Alteration minerals: calcite, pyrite and minor illite.

1734-1740 m No cuttings (Loss of circulation)

1740-1756 m Trachy phonolite: Brownish grey to greenish grey medium-grained sanidine and pyroxene porphyritic rock. The rock is massive and has nepheline occurring as microphenocrysts. Pyroxene occurs characteristically as slender needles, often abundant enough to colour the rock into greenish color. Quartz veining was evidenced. Alteration minerals: quartz, pyrite, calcite and illite.

1756-1774 m No cuttings (Loss of circulation)

1774-1778 m Tuff: Brownish grey moderate to altered poorly crystalline fine gained and vesicular rock. The rock is fractured and highly altered. Pyrite disseminated in the groundmass. Calcite and quartz occurs as infill in vesicles. Veining was evidenced which were filled in with quartz and calcite. Alteration minerals: Quartz, calcite, pyrite and illite.

1778-1790 m No cuttings (Loss of circulation)

1790-1808 m Tuff: Brownish grey moderate to altered poorly crystalline fine gained and vesicular rock. The rock is fractured and highly altered. Pyrite disseminated in the groundmass. Calcite and quartz occurs as infill in veins and vesicles. Alteration minerals: Quartz, calcite, pyrite and illite.

1808-1950 m No cuttings (Loss of circulation)

1950-1964 m Syenitic intrusion: Light grey, coarse-grained massive and porphyritic lava with large phenocrysts of sanidine and pyroxenes. It shows low intensity of alteration and has abundant calcite. Alteration minerals: calcite, adularia, quartz, epidote and illite.

1964-2132 m No cuttings (Loss of circulation)

APPENDIX G: Some results of the XRD clay analysis diffractograms

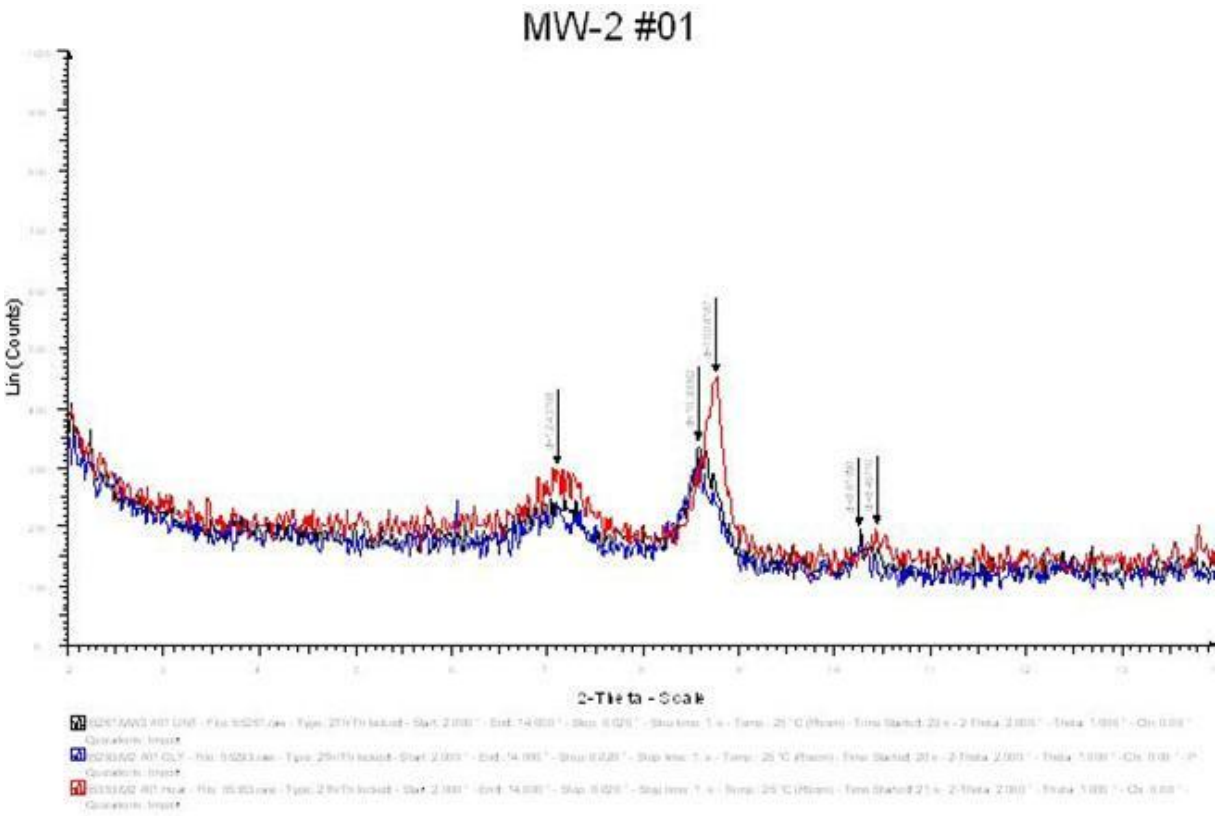

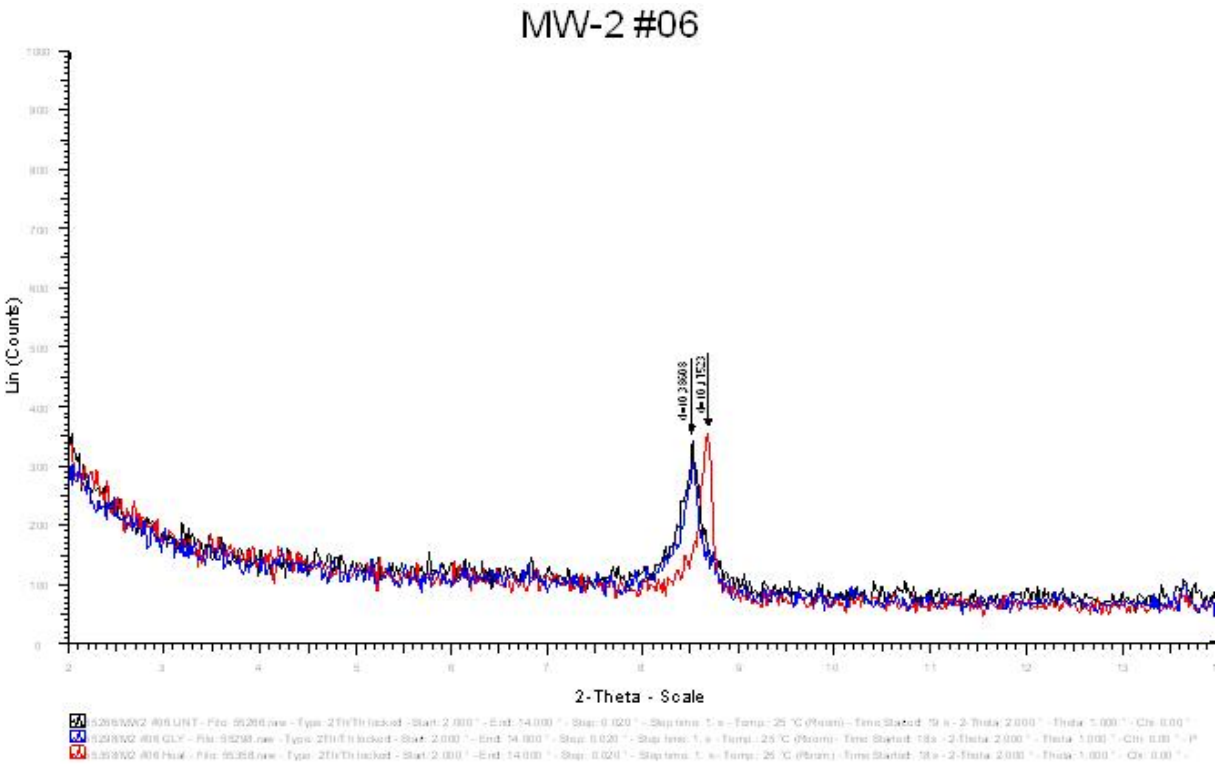

MW-4 #01

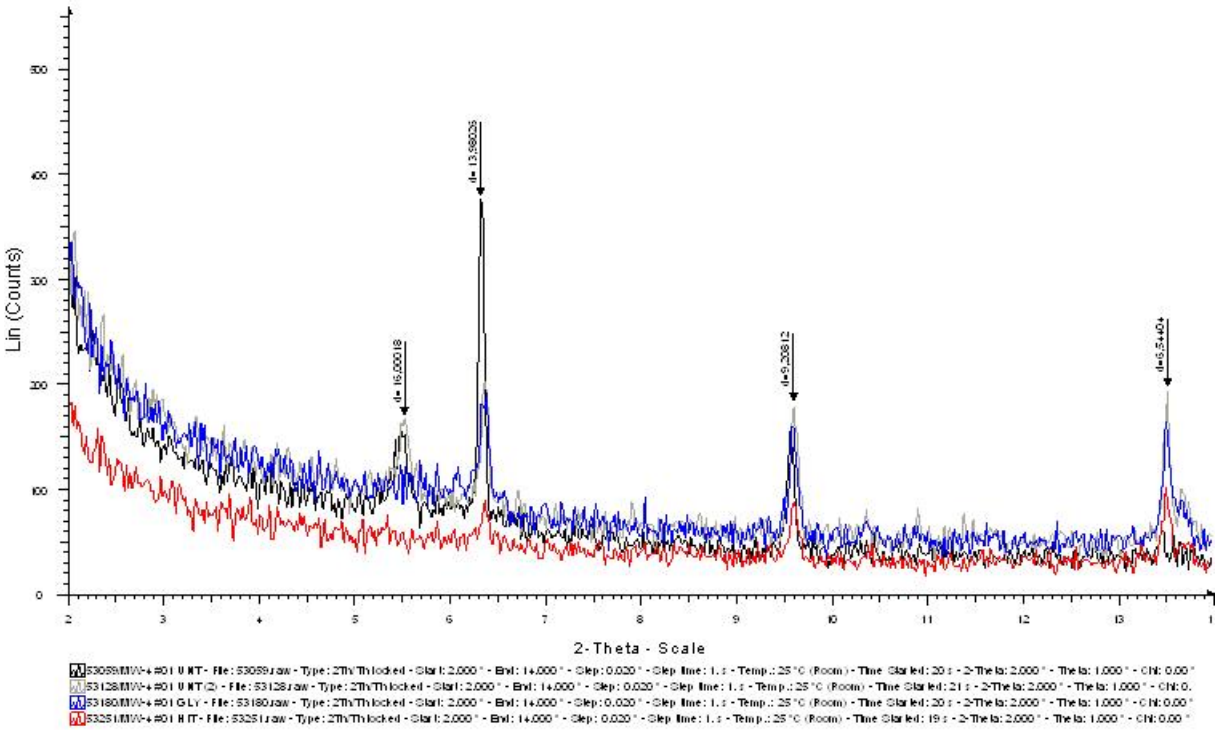
Lin (Counts)
2-Theta - Scale
d= 16.00018
d= 13.98026
d= 9.20812
d= 6.54402
S3059/MW-4 #01 UNT - File: S3059.raw - Type: 2Th/Th locked - Start: 2.000 ° - End: 14.000 ° - Step: 0.020 ° - Step time: 1. s - Temp.: 25 °C (Room) - Time Started: 20 s - 2-Theta: 2.000 ° - Theta: 1.000 ° - Chi: 0.00 °
S3128/MW-4 #01 UNT (2) - File: S3128.raw - Type: 2Th/Th locked - Start: 2.000 ° - End: 14.000 ° - Step: 0.020 ° - Step time: 1. s - Temp.: 25 °C (Room) - Time Started: 21 s - 2-Theta: 2.000 ° - Theta: 1.000 ° - Chi: 0.
S3180/MW-4 #01 GLY - File: S3180.raw - Type: 2Th/Th locked - Start: 2.000 ° - End: 14.000 ° - Step: 0.020 ° - Step time: 1. s - Temp.: 25 °C (Room) - Time Started: 20 s - 2-Theta: 2.000 ° - Theta: 1.000 ° - Chi: 0.00 °
S3251/MW-4 #01 HT - File: S3251.raw - Type: 2Th/Th locked - Start: 2.000 ° - End: 14.000 ° - Step: 0.020 ° - Step time: 1. s - Temp.: 25 °C (Room) - Time Started: 19 s - 2-Theta: 2.000 ° - Theta: 1.000 ° - Chi: 0.00 °

MW-4 #02

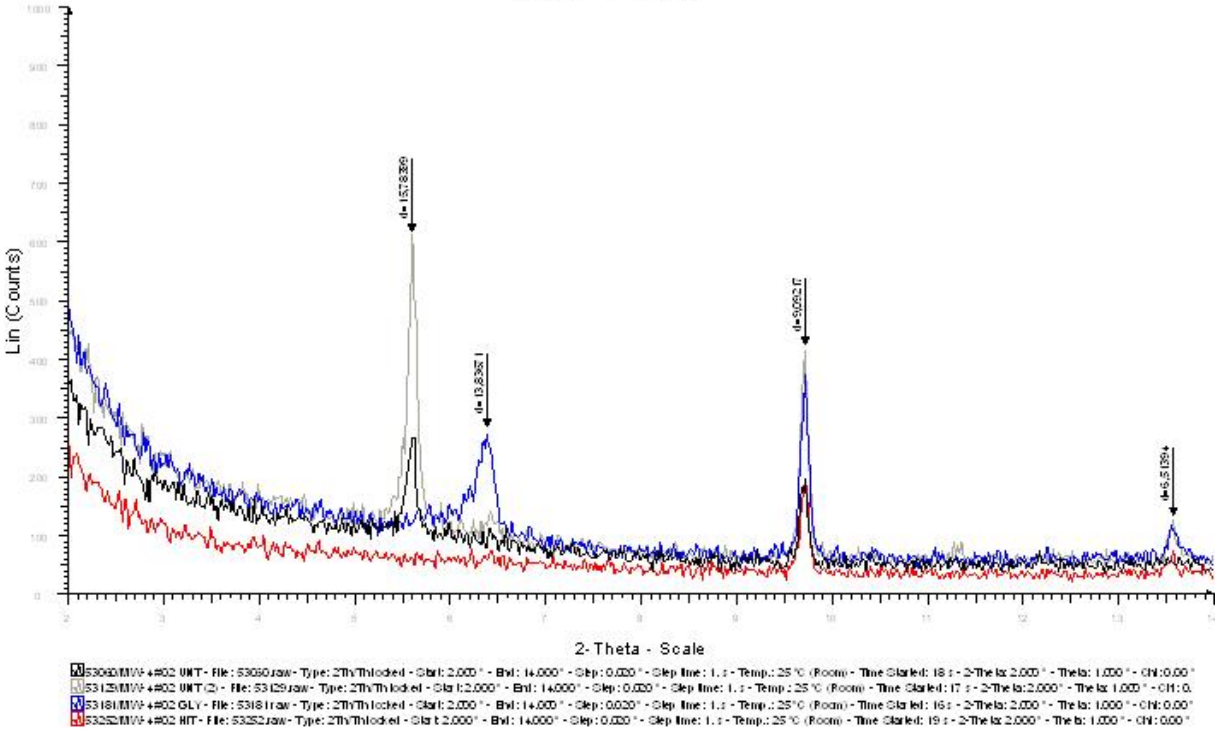
Lin (Counts)
2-Theta - Scale
d= 14.17839
d= 13.83621
d= 9.09621
d= 6.51894
S3060/MW-4 #02 UNT - File: S3060.raw - Type: 2Th/Th locked - Start: 2.000 ° - End: 14.000 ° - Step: 0.020 ° - Step time: 1. s - Temp.: 25 °C (Room) - Time Started: 18 s - 2-Theta: 2.000 ° - Theta: 1.000 ° - Chi: 0.00 °
S3129/MW-4 #02 UNT (2) - File: S3129.raw - Type: 2Th/Th locked - Start: 2.000 ° - End: 14.000 ° - Step: 0.020 ° - Step time: 1. s - Temp.: 25 °C (Room) - Time Started: 17 s - 2-Theta: 2.000 ° - Theta: 1.000 ° - Chi: 0.
S3181/MW-4 #02 GLY - File: S3181.raw - Type: 2Th/Th locked - Start: 2.000 ° - End: 14.000 ° - Step: 0.020 ° - Step time: 1. s - Temp.: 25 °C (Room) - Time Started: 16 s - 2-Theta: 2.000 ° - Theta: 1.000 ° - Chi: 0.00 °
S3252/MW-4 #02 HT - File: S3252.raw - Type: 2Th/Th locked - Start: 2.000 ° - End: 14.000 ° - Step: 0.020 ° - Step time: 1. s - Temp.: 25 °C (Room) - Time Started: 19 s - 2-Theta: 2.000 ° - Theta: 1.000 ° - Chi: 0.00 °

MW-6 #08

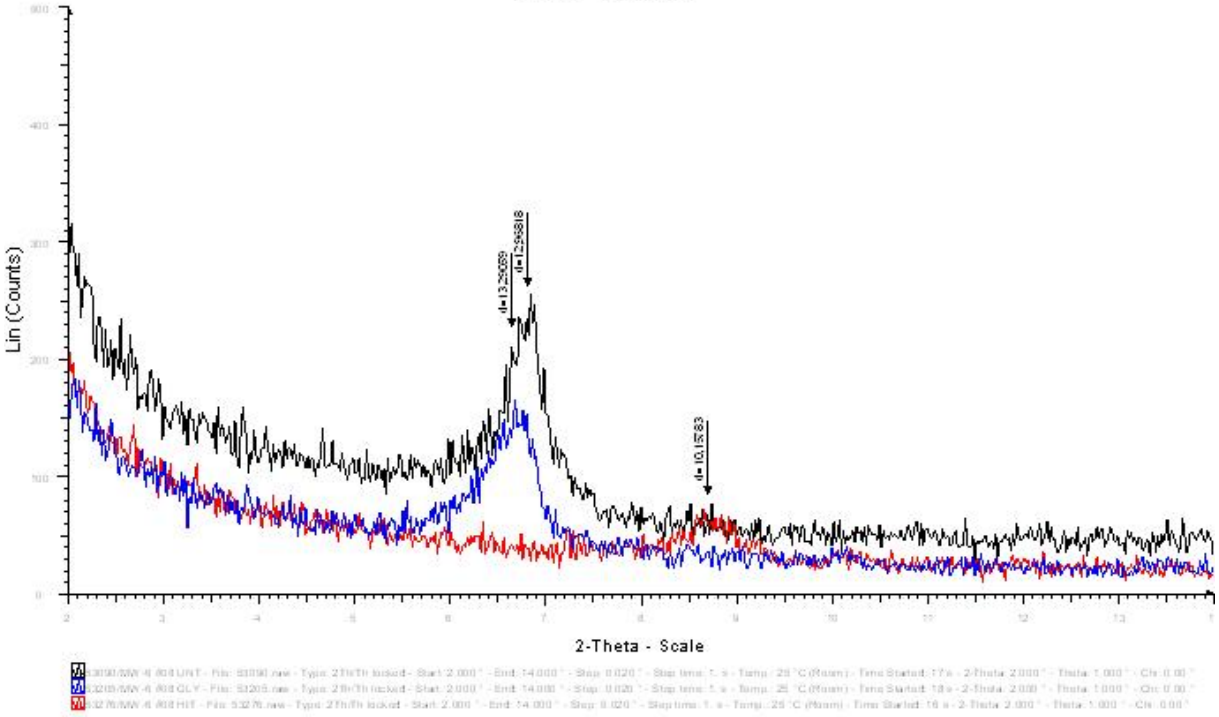
Lin (Counts)
d=13.29689
d=12.96818
d=10.1583
2-Theta - Scale

MW-7 #09

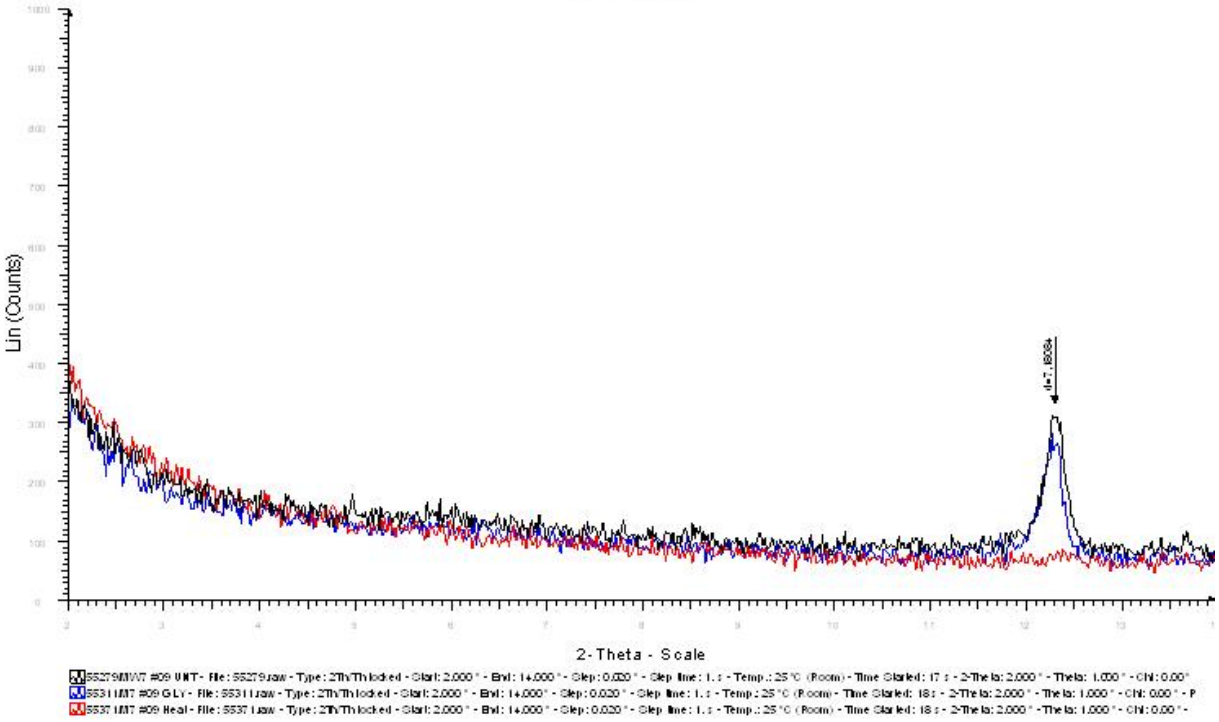
Lin (Counts)
d=7.18884
2-Theta - Scale

MW-4 #07

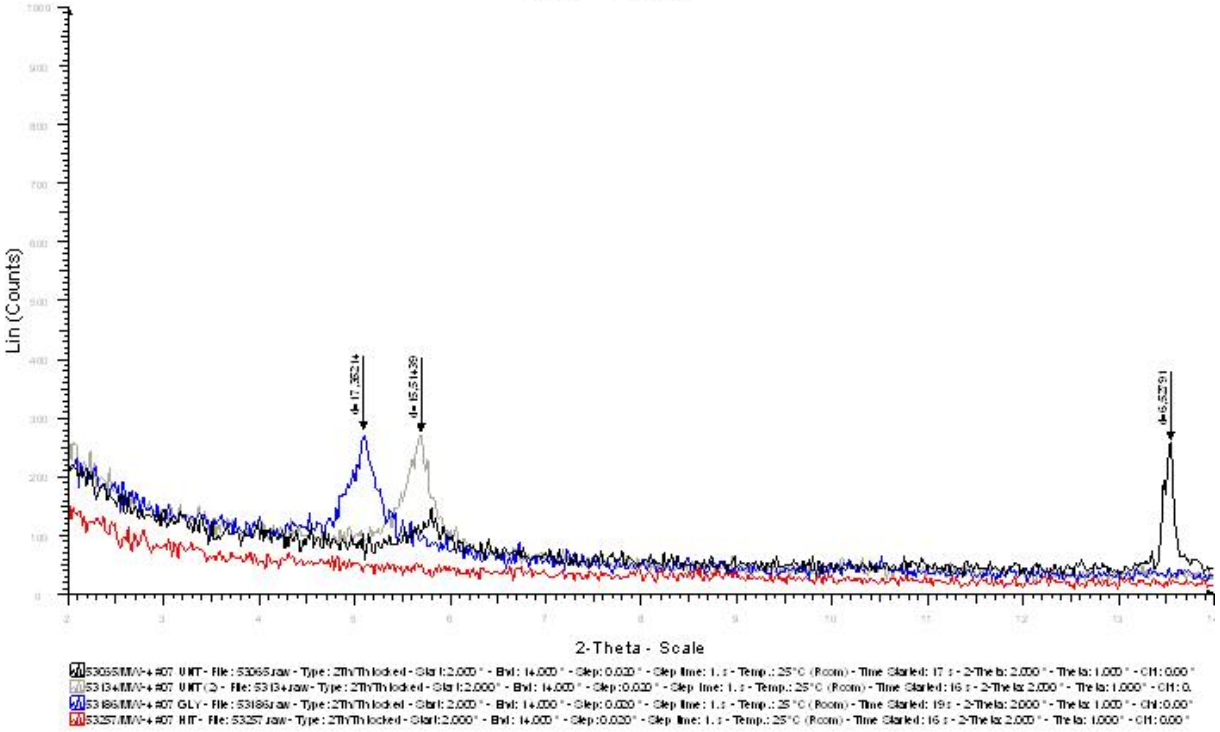
Lin (Counts)
d= 17.35214
d= 15.51439
d= 6.52791
2-Theta - Scale
53065/MW-4 #07 UNT - File: 53065.raw - Type: 2Th/Th locked - Start: 2.000 ° - End: 14.000 ° - Step: 0.020 ° - Step time: 1. s - Temp.: 25 °C (Room) - Time Started: 17 s - 2-Theta: 2.000 ° - Theta: 1.000 ° - Chi: 0.00 °
53134/MW-4 #07 UNT (2 - File: 53134.raw - Type: 2Th/Th locked - Start: 2.000 ° - End: 14.000 ° - Step: 0.020 ° - Step time: 1. s - Temp.: 25 °C (Room) - Time Started: 16 s - 2-Theta: 2.000 ° - Theta: 1.000 ° - Chi: 0.
53186/MW-4 #07 GLY - File: 53186.raw - Type: 2Th/Th locked - Start: 2.000 ° - End: 14.000 ° - Step: 0.020 ° - Step time: 1. s - Temp.: 25 °C (Room) - Time Started: 19 s - 2-Theta: 2.000 ° - Theta: 1.000 ° - Chi: 0.00 °
53257/MW-4 #07 HT - File: 53257.raw - Type: 2Th/Th locked - Start: 2.000 ° - End: 14.000 ° - Step: 0.020 ° - Step time: 1. s - Temp.: 25 °C (Room) - Time Started: 16 s - 2-Theta: 2.000 ° - Theta: 1.000 ° - Chi: 0.00 °

MW-6 #10

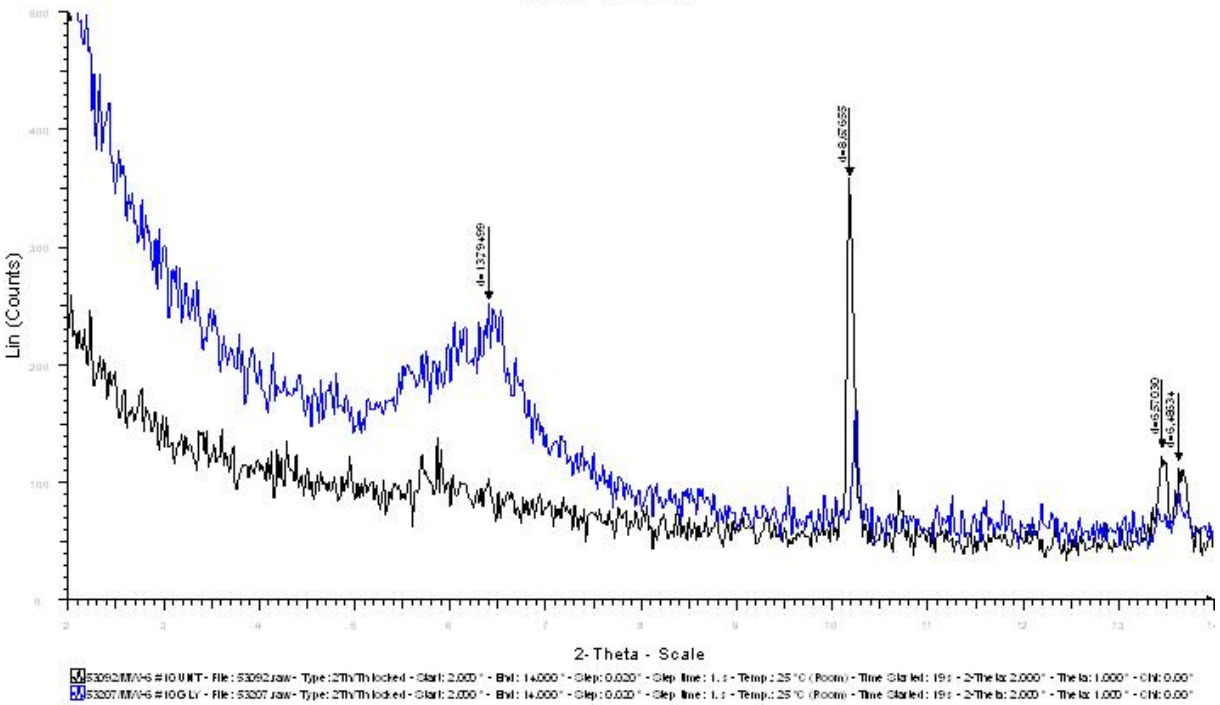
Lin (Counts)
d= 13.79499
d= 8.05035
d= 5.70330
d= 5.48634
2-Theta - Scale
53092/MW-6 #10 UNT - File: 53092.raw - Type: 2Th/Th locked - Start: 2.000 ° - End: 14.000 ° - Step: 0.020 ° - Step time: 1. s - Temp.: 25 °C (Room) - Time Started: 19 s - 2-Theta: 2.000 ° - Theta: 1.000 ° - Chi: 0.00 °
53207/MW-6 #10 GLY - File: 53207.raw - Type: 2Th/Th locked - Start: 2.000 ° - End: 14.000 ° - Step: 0.020 ° - Step time: 1. s - Temp.: 25 °C (Room) - Time Started: 19 s - 2-Theta: 2.000 ° - Theta: 1.000 ° - Chi: 0.00 °